On induced *CPT*-odd Chern–Simons terms in the 3+1 effective action

G. E. Volovik

Helsinki University of Technology, Low Temperature Laboratory, FIN-02015 HUT, Finland; Landau Institute of Theoretical Physics, Russian Academy of Sciences, 117334 Moscow, Russia

(Submitted 31 May 1999)
Pis'ma Zh. Éksp. Teor. Fiz. **70**, No. 1, 3–6 (10 July 1999)

This paper was originally designated as a Comment on the paper by R. Jackiw and V. A. Kostelecký, Phys. Rev. Lett. **82**, 3572 (1999). It gives an example of a fermionic system in which the *CPT*-odd Chern–Simons terms in the effective action are unambiguously induced by chiral fermions: superfluid ^{3}He-A. In this system the Lorentz and gauge invariances are both violated at high energy, but the behavior of the system beyond the cutoff is known. This allows one to construct a *CPT*-odd action which combines the conventional 3+1 CS term and the mixed axial–gravitational CS term discussed by G. E. Volovik and A. Vilenkin, http://xxx.lanl.gov/abs/hep-ph/9905460. The influence of the CS term on the dynamics of the effective gauge field has been observed experimentally in rotating ^{3}He-A. © *1999 American Institute of Physics.* [S0021-3640(99)00113-9]

PACS numbers: 11.15.−q, 11.10.Ef, 11.30.Er, 67.57.−z

Recently the problem of the radiatively induced *CPT*-odd Chern–Simons (CS) term in 3+1 quantum field theory has been addressed in a number of papers.[1–6] The CS term $L_{\rm CS}=\frac{1}{2}k_\mu e^{\mu\alpha\beta\gamma}F_{\alpha\beta}A_\gamma$ in the 3+1 electromagnetic action, where k^μ is a constant 4-vector, is induced by the *CPT*- and Lorentz-violating axial-vector term $b^\mu\gamma_\mu\gamma_5$ in the Dirac Lagrangian for massive fermions. In the limit of small and large b compared with the mass m of the Dirac fermions, it was found that

$$k^\mu=\frac{3}{16\pi^2}b^\mu, \quad b\ll m, \tag{1}$$

$$k^\mu=-\frac{1}{16\pi^2}b^\mu, \quad b\gg m. \tag{2}$$

However it has been concluded that the existence of the CS term depends on the choice of regularization procedure — a ''renormalization ambiguity.'' This means that the result for k_μ depends on physics beyond the cutoff.

The above *CPT*-odd term can result not only from the violation of the *CPT* symmetry in the vacuum. The nonzero density of chiral fermions violates the *CPT* invariance

and thus can also lead to the CS term, with b^0 being determined by the chemical potential μ and temperature T of the fermionic system.[7–9]

Here we provide an example of a fermionic system in which such a CS term is unambiguously induced by fermions. In this system the Lorentz and gauge invariances both are violated at high energy, but the behavior of the system beyond the cutoff is known. This allows the calculation of the CS term in different physical situations. The influence of this CS term on the dynamics of the effective gauge field has been observed experimentally.

The aforementioned example is superfluid ^{3}He-A, where there are two species of fermionic quasiparticles in the low-energy corner: left-handed and right-handed Weyl fermions.[10] The quasiparticles interact with the order parameter, the unit vector $\hat{\mathbf{l}}$ vector of the orbital angular momentum of Cooper pairs, in the same manner as chiral relativistic fermions interact with the vector potential of the $U(1)$ gauge field, $\mathbf{A}\equiv p_F\hat{\mathbf{l}}$, where p_F is the Fermi momentum. The ''electric charges'' — the charges of the left and right quasiparticles with respect to this effective gauge field — are $e_R=-e_L=-1$. The normal component of superfluid ^{3}He-A consists of thermal fermions, whose density is determined by T and by the velocity $\mathbf{v}_n-\mathbf{v}_s$ of the flow of the normal component with respect to the superfluid vacuum. The velocity of the counterflow in the direction of $\hat{\mathbf{l}}$ is equivalent to the chemical potentials for left and right fermions in the relativistic systems:

$$\mu_R=-\mu_L=p_F\hat{\mathbf{l}}\cdot(\mathbf{v}_n-\mathbf{v}_s). \tag{3}$$

As in the relativistic theories, the state of the system of chiral quasiparticles with nonzero counterflow velocity (an analog of the chemical potential) violates Lorentz invariance and *CPT* symmetry and induces the *CPT*-odd CS term. This term can be written in general form, applicable both for the relativistic systems, where it was found in Refs. 7 and 8 and for ^{3}He-A (Ref. 10):

$$\frac{1}{4\pi^2}\left(\sum_L \mu_L e_L^2-\sum_R \mu_R e_R^2\right)\mathbf{A}\cdot(\boldsymbol{\nabla}\times\mathbf{A}). \tag{4}$$

Here sums over L and R mean summation over all the left-handed and right-handed fermionic species respectively; e_L and e_R are charges of left and right fermions with respect to $U(1)$ field (say, hypercharge field in the Standard model).

Translation of Eq. (4) to the ^{3}He-A language gives

$$\frac{p_F^3}{2\pi^2}[\hat{\mathbf{l}}_0\cdot(\mathbf{v}_s-\mathbf{v}_n)][\,\delta\hat{\mathbf{l}}\cdot(\boldsymbol{\nabla}\times\delta\hat{\mathbf{l}})]. \tag{5}$$

Here $\hat{\mathbf{l}}_0$ is the direction of the order parameter $\hat{\mathbf{l}}$ in the homogeneous ground state; and $\delta\hat{\mathbf{l}}=\hat{\mathbf{l}}-\hat{\mathbf{l}}_0$ is the deviation of the order parameter from its ground state direction.

Since for chiral fermions the chemical potential plays the part of the parameter b^0 in the fermionic Lagrangian, the connection between k^0 and b^0 in ^{3}He-A is $k^0=b^0/2\pi^2$. Though it agrees with the result obtained in a relativistic system with nonzero chemical potential for chiral fermions,[7] it does not coincide with Eq. (2) obtained in the massless limit $m/b^0\to 0$.

The instability of the electromagnetic vacuum due to the 3+1 CS term has been discussed by Caroll, Field and Jackiw,[11] Andrianov and Soldati,[12] and Joyce and Shaposhnikov.[11] In the case of a nonzero density of right electrons ($\mu_R \neq 0$) this instability leads to the conversion of the density of right electrons to the hypermagnetic field. This effect was used in the scenario for nucleation of the primordial magnetic field.[9] In ^{3}He-A this phenomenon is represented by the well-known helical instability of the counterflow, which is triggered by the term in Eq. (5).[13] The conversion of the counterflow of the normal component (an analog of μ_R in the Joyce–Shaposhnikov scenario) into a nonuniform $\hat{\mathbf{l}}$ field with $\nabla \times \hat{\mathbf{l}} \neq 0$ (an analog of the hypermagnetic field) due to this instability has been observed in rotating ^{3}He-A.[14,10]

Recently another type of CS term has been found for both systems, ^{3}He-A and chiral relativistic fermions with nonzero μ or/and T. This is the mixed axial–gravitational CS term, which contains both the gauge field and the gravimagnetic field:[15]

$$\frac{1}{8\pi^2}\left(\sum_L \mu_L^2 e_L - \sum_R \mu_R^2 e_R\right)\mathbf{A}\cdot\mathbf{B_g}, \quad \mathbf{B_g} = \nabla \times \mathbf{g}, \quad \mathbf{g} \equiv g_{0i}. \tag{6}$$

Here g_{0i} is the element of the metric in the reference frame of the heat bath (in superfluids it is the element of the effective metric in the frame in which the normal component is at rest). If the heat bath of chiral fermions is rotating in Minkowski space, the ''gravimagnetic field'' is expressed in terms of rotational velocity $\mathbf{\Omega}$:

$$\mathbf{B_g} = \nabla \times \mathbf{g} = 2\frac{\mathbf{\Omega}}{c^2}. \tag{7}$$

Here c is the material parameter, which is the speed of light in a relativistic system, and the initial slope in the energy spectrum of fermionic quasiparticles propagating in the plane transverse to the $\hat{\mathbf{l}}$ vector in ^{3}He-A (Ref. 10). The material parameters do not enter Eq. (6) explicitly: they enter only through the metric. That is why the same equation (6) can be applied to different fermionic systems, including those with a varying speed of light. In a relativistic system this equation describes a macroscopic parity violating effect: rotation of the heat bath (or of a black hole) produces a flux of chiral fermions along the rotation axis.[16]

Comparison of Eqs. (6) and (4) suggests that the two *CPT*-odd terms can be unified if one uses the Larmor theorem and introduces the combined fields:

$$\mathbf{A}_{L(R)} = e_{L(R)}\mathbf{A} + \frac{1}{2}\mu_{L(R)}\mathbf{g}, \quad \mathbf{B}_{L(R)} = \nabla \times \mathbf{A}_{L(R)}. \tag{8}$$

Then the general form of the CS *CPT*-odd term is

$$\frac{1}{4\pi^2}\left(\sum_L \mu_L \mathbf{A}_L \cdot \mathbf{B}_L - \sum_R \mu_R \mathbf{A}_R \cdot \mathbf{B}_R\right). \tag{9}$$

Note that in the Standard Model, nullification of the *CPT*-odd term in Eq. (9) occurs if the ''gyromagnetic'' ratio e/μ is the same for all fermions. This happens because of the anomaly cancellation. For the *CPT*-odd term induced by the vacuum fermions, the

anomaly cancellation was discussed in Refs. 6 and 2. In ^{3}He-A the ''gyromagnetic ratio'' is the same for two fermionic species, $e_L/\mu_L = e_R/\mu_R$, but the CS terms survive, since there is no anomaly cancellation in this system.

In ^{3}He-A there are also subtle points related to gauge invariance of the CS term, as discussed by Coleman and Glashow,[17] and to the reference frame. They are determined by the physical situations.

(i) The reference frame for superfluid velocity $\mathbf{v}_s$ is the heat bath frame — the frame of the normal component moving with velocity $\mathbf{v}_n$. At $T=0$ this frame disappears: thermal fermions are frozen out. To avoid uncertainty in determination of the counterflow velocity $\mathbf{v}_s - \mathbf{v}_n$, and thus of the chemical potential of the chiral fermions, the limit $T \rightarrow 0$ must be taken after all other limits.

(ii) The leading terms in the low-energy effective action for the ''electrodynamics'' of ^{3}He-A are gauge invariant, because the main contributions to the effective action are induced by the low-energy fermions, which are ''relativistic'' and obey the gauge invariant Lagrangian. Equation (9) is an example of such a gauge invariant term in the low-energy action. It is gauge invariant if the b^0 parameter (or μ_R) is constant, i.e., if the background counterflow and $\hat{\mathbf{l}}_0$ field are uniform. The nonuniform corrections, which correspond to the inhomogeneous b^0, violate the gauge invariance. This is natural, since these corrections are determined by the higher-energy fermions, which do not obey the gauge invariance from the very beginning. This is in agreement with the conclusion made in Ref.1, that for existence of the CS term the ''weak condition'' — gauge invariance at zero 4-momentum — is required.

I thank Alex Vilenkin for discussions. This work was supported in part by Grant 96-02-16072 from the Russian Fund for Fundamental Research and by the European Science Foundation.

[1] R. Jackiw and V. Alan Kostelecký, Phys. Rev. Lett. **82**, 3572 (1999).
[2] D. Colladay and V. Alan Kostelecký, Phys. Rev. D **58**, 116002 (1998).
[3] C. D. Fosco and J. C. Le Guillou, http://xxx.lanl.gov/abs/hep-th/9904138.
[4] A. A. Andrianov, R. Soldati, and L. Sorbo, Phys. Rev. D **59**, 025002/1-13 (1998).
[5] J.-M. Chung, http://xxx.lanl.gov/abs/hep-th/9905095.
[6] M. Perez-Victoria, http://xxx.lanl.gov/abs/hep-th/9905061.
[7] A. Vilenkin, Phys. Rev. D **22**, 3080 (1980).
[8] A. N. Redlich and L. C. R. Wijewardhana, Phys. Rev. Lett. **54**, 970 (1985).
[9] M. Joyce and M. Shaposhnikov, Phys. Rev. Lett. **79**, 1193 (1997).
[10] G. E. Volovik, Physica B **255**, 86 (1998).
[11] S. M. Caroll, G. B. Field, and R. Jackiw, Phys. Rev. D **41**, 1231 (1990).
[12] A. A. Andrianov and R. Soldati, Phys. Lett. B **435**, 449 (1998).
[13] D. Vollhardt, P. and P. Wölfle, *The Superfluid Phases of Helium 3*, Taylor and Francis, London–New York–Philadelphia, 1990.
[14] V. M. H. Ruutu, J. Kopu, M. Krusius *et al.*, Phys. Rev. Lett. **79**, 5058 (1997).
[15] G. E. Volovik and A. Vilenkin, http://xxx.lanl.gov/abs/hep-ph/9905460.
[16] A. Vilenkin, Phys. Rev. D **20**, 1807 (1979); Phys. Rev. D **21**, 2260 (1980).
[17] S. Coleman and S. Glashow, http://xxx.lanl.gov/abs/hep-ph/9812418.

Published in English in the original Russian journal. Edited by Steve Torstveit.

Fermionic atom laser

K. G. Petrosyan
Department of Theoretical Physics, Yerevan Physics Institute, Alikhanian Br.-2, Yerevan 375036, Armenia

(Submitted May 12, 1999)
Pis'ma Zh. Éksp. Teor. Fiz. **70**, No. 1, 13–17 (10 July 1999)

An output coupling of a magnetically trapped two-species Fermi gas to a untrapped species is considered which can be implemented using rf or optical Raman transitions. The process can be used to produce an intense output beam of fermionic atoms once the device reaches a threshold in the zero-temperature case. For finite temperatures there is no threshold, as the output current grows smoothly. This behavior, which is reminiscent of conventional optical and cavity-QED lasers, suggests the name *fermionic atom laser* for this device. © *1999 American Institute of Physics.* [S0021-3640(99)00313-8]

PACS numbers: 03.75.Fi, 39.10.+j

Since the experimental realization of Bose–Einstein condensation (BEC)[1] there has been much interest in the properties of trapped degenerate gases.[2] Although most of the attention is being paid to alkali bosons, recently some work, both experimental and theoretical, has been done on Fermi gases.[3–5] Another research topic of current interest is the atom laser, or boser, an idea which has been the subject of a number of proposals[6] and which has been shown to be realizable experimentally.[7] The idea is to couple out the condensates which have formed to produce a coherent output beam of atoms. Other bosers proposed are the excitonic[8] and exciton–polariton[9] lasers. An atomic parametric oscillator which produces correlated atomic beams was proposed in Ref. 10.

Up till now almost all of the attention has been paid to bosonic atom lasers. That is obviously due to the great progress that has been made in the BEC area. However, there exists yet another interesting possibility for getting coherent atomic waves. Recently in a series of papers Stoof, Houbiers, *et al.*[4] and Baranov *et al.*[5] have discussed the possibility of formation of BCS states and of superfluidity in atomic ^{6}Li in a magnetic trap. Although the formation of Cooper pairs has not yet been observed experimentally, their estimates show that the process is quite possible. If one accepts the possibility of formation of fermionic pairs (in momentum space), one might wonder what would happen if they were coupled out of the trap.

In this paper we present a simple scheme for the output coupling. We will show that the problem is akin to the case of electron tunneling between a superconductor and a normal metal and will find that the device possesses a threshold at zero temperature but is thresholdless at finite temperatures. We then point out an analogy between the device and cavity-QED lasers.[11]

Some of the boser proposals have used the Born–Markov approximation, which has been shown to fail for the case of an atom laser.[12] Very recently a non-Markovian stochastic Schrödinger equation has been derived[13] that opens up the way for further investigation of atom lasers as open quantum systems coupled to a finite number of output oscillators, as is in fact the case. Although a detailed microscopic theory, which should include the presence of quantum fluctuations, would provide a deeper understanding of the process, here we present a simple theory without taking quantum fluctuations fully into account in order to get an idea of what is going on in the case of the fermionic atom laser. However, in the present paper we do not make the Markovian approximation but just work within a Hamiltonian approach that has been applied to the superconductive tunneling problem.[14] Another simplification we make is to consider the problem in a homogeneous approximation, assuming that the magnetic trap fields are uniform, so that the particles are simply placed in a potential-well box. We will trace out an analogy between our case and electron tunneling[15] and will also consider finite temperatures.[16,17]

Let us consider two species of fermions which are confined in a trap and interact with one another by two-body collisions (s-wave scattering). The Hamiltonian with one output channel reads

$$H=\sum_{\sigma=+,-}\int d^3\mathbf{r}\Bigg(\psi_\sigma^\dagger(\mathbf{r})\Bigg[-\frac{\hbar^2}{2M}\nabla^2+V_\sigma(\mathbf{r})-\mu_\sigma\Bigg]\psi_\sigma(\mathbf{r})$$
$$-\frac{g}{2}\psi_\sigma^\dagger(\mathbf{r})\psi_{-\sigma}^\dagger(\mathbf{r})\psi_{-\sigma}(\mathbf{r})\psi_\sigma(\mathbf{r})\Bigg)+\int d^3\mathbf{r}\Bigg(\psi_o^\dagger(\mathbf{r})\Bigg[-\frac{\hbar^2}{2M}\nabla^2$$
$$+V_o(\mathbf{r})-\mu_o\Bigg]\psi_o(\mathbf{r})+\sum_\sigma\lambda_\sigma(\psi_o^\dagger(\mathbf{r})\psi_\sigma(\mathbf{r})+\text{h.c.})\Bigg). \tag{1}$$

Here $\psi_\sigma^\dagger(\mathbf{r})$ and $\psi_\sigma(\mathbf{r})$ are the creation and annihilation field operators for the two fermionic species ($\sigma=\pm$), $\psi_o(\mathbf{r})$ describes the output field with chemical potential μ_o and coupling constants λ_σ; $V_\sigma(\mathbf{r})$ are the trapping potentials, $V_o(\mathbf{r})$ is the repulsive potential, μ_σ are the chemical potentials, M is the mass of the particles, and g is the interaction parameter.

The Hamiltonian describes, e.g., a trapped atomic ^{6}Li (fermion) gas. The two trapped levels are the $|6\rangle$ and $|5\rangle$ levels,[4] and we choose transitions to the $|3\rangle$ untrapped level as the output channel. The transitions from the trapped levels to the untrapped level can be provided, e.g., by rf fields, which have been used for the output coupling of bosons.[7]

We now expand the annihilation and creation operators for the second-quantized field in trap eigenfunctions as

$$\psi_\sigma(\mathbf{r})=\sum_n v_{n\sigma}(\mathbf{r})a_{n\sigma},\quad \psi_o(\mathbf{r})=\sum_k v_{ko}(\mathbf{r})b_k \tag{2}$$

and after a linearization which introduces a gap Δ, and assuming the functions $v_{n\sigma}(\mathbf{r})$ and $v_{ko}(\mathbf{r})$ are known, we write the Hamiltonian of our model in the form

$$H=\sum_{\sigma=+,-}\theta_{n\sigma}a^{\dagger}_{n\sigma}a_{n\sigma}+\sum_{k}\theta_{ko}b^{\dagger}_{k}b_{k}+\sum_{nn'}(\delta_{nn'o}a^{\dagger}_{n+}a^{\dagger}_{n'-}+\delta^{*}_{nn'o}a_{n+}a_{n'-})$$

$$+\sum_{nk\sigma}(T_{nk\sigma}a^{\dagger}_{n\sigma}b_{k}+\text{h.c.}), \tag{3}$$

where

$$\theta_{n\sigma}=\int d^{3}\mathbf{r}v^{*}_{n\sigma}(\mathbf{r})\left[-\frac{\hbar^{2}}{2M}\nabla^{2}+V_{\sigma}(\mathbf{r})-\mu_{\sigma}\right]v_{n\sigma}(\mathbf{r}),$$

$$\theta_{ko}=\int d^{3}\mathbf{r}v^{*}_{ko}(\mathbf{r})\left[-\frac{\hbar^{2}}{2M}\nabla^{2}+V_{o}(\mathbf{r})-\mu_{o}\right]v_{ko}(\mathbf{r}),$$

$$T_{nk\sigma}=\lambda_{\sigma}\int d^{3}\mathbf{r}v^{*}_{n\sigma}(\mathbf{r})v_{ko}(\mathbf{r}),\quad \delta_{nn'o}=\Delta\int d^{3}\mathbf{r}v^{*}_{n+}(\mathbf{r})v^{*}_{n'-}(\mathbf{r}). \tag{4}$$

After the diagonalization procedure the Hamiltonian takes the form

$$H=\sum_{n\sigma=+,-}\omega_{n\sigma}c^{\dagger}_{n\sigma}c_{n\sigma}+\sum_{k}\theta_{ko}b^{\dagger}_{k}b_{k}+\sum_{nk\sigma}(\alpha_{nk\sigma}b^{\dagger}_{k}c_{n\sigma}+\beta^{*}_{nk\sigma}b^{\dagger}_{k}c^{\dagger}_{-n,-\sigma}+\text{h.c.}). \tag{5}$$

where we have defined

$$\alpha_{nk\sigma}=u_{n}T^{*}_{nk\sigma},\quad \beta_{nk\sigma}=v_{n}T_{nk\sigma},\quad \omega_{n\sigma}=\theta_{n\sigma}(|u_{n}|^{2}+|v_{n}|^{2})+2\delta_{nno}(u^{*}_{n}v_{n}+\text{c.c.}), \tag{6}$$

and

$$a_{n,+}=u_{n}c_{n,+}+v^{*}_{n}c^{\dagger}_{-n,-},\quad a^{\dagger}_{-n,-}=-v_{n}c_{n,+}+u^{*}_{n}c^{\dagger}_{-n,-}. \tag{7}$$

For the model under consideration one has[4]

$$|u_{n}|^{2}=\frac{1}{2}\left(1+\frac{\xi_{n}}{\sqrt{\xi^{2}_{n}+|\Delta|^{2}}}\right),\quad |u_{n}|^{2}+|v_{n}|^{2}=1. \tag{8}$$

Here $\xi_{n}=\epsilon_{n}-\epsilon_{F}$ is the energy difference from the ''mean'' Fermi level, defined as $\epsilon_{F}=(\mu_{+}+\mu_{-})/2$, where $\mu_{\pm}$ are the Fermi levels of the two species; the Cooper particles have the dispersion relation $\omega_{n\sigma}=-m_{\sigma}\delta\epsilon_{F}+\sqrt{\xi^{2}_{n}+|\Delta|^{2}}$ with $m_{\pm}=\pm\frac{1}{2}$, and $\delta\epsilon_{F}=\mu_{+}-\mu_{-}$ is the difference between the Fermi levels of the species.

For the fermionic output coupler we distinguish two different cases, one in with the chemical potentials two species are equal to each other ($\mu_{+}=\mu_{-}\equiv\mu$), and one in which they are unequal ($\mu_{+}\neq\mu_{-}$). Here we consider only the case of equal chemical potentials, which gives the highest critical BCS temperature.[4]

We now proceed with the Hamiltonian (5) to calculate the output intensity or current of the fermionic beam, i.e., the mean value of the derivative of the number of fermions coupled out, $\langle\dot{N}_{o}\rangle$, where $N_{o}\equiv\Sigma_{k}b^{\dagger}_{k}b_{k}$. One can carry out the standard procedure[14,15] to calculate this quantity and will arrive at the formula

$$\langle \dot{N}_o \rangle \propto \sum_{nk} |T_{nk}|^2 \{ u_n^2 [N_F(E_{n\sigma}) - N_F(E_k)] \delta(E_{n\sigma} - E_k - \delta E) + v_n^2 [N_F(-E_{n\sigma}) - N_F(E_k)] \delta(E_{n\sigma} + E_k + \delta E) \}, \quad (9)$$

where $N_F(E_k) = [\exp(\beta E_k) + 1]^{-1}$ is the Fermi distribution for noninteracting particles with energy spectrum E_k and inverse temperature $\beta = 1/k_B T$. Here n runs over the trap level states, with the dispersion relation $E_{n\sigma} = \sqrt{\xi_n^2 + |\Delta|^2}$ ($\delta\epsilon_F = 0$), and k runs over the output free particle dispersion $E_k = (\hbar k)^2/(2M)$ (we assume the potentials $V_+(\mathbf{x})$ and $V_-(\mathbf{x})$ to be space-independent, so they just shift the chemical potentials $\mu_\pm$). δE is the difference (''bias'') between the Fermi levels of in-trap and out-of-trap fermions, which is proportional to the magnetic field. Note that here $\delta E > 0$, so that the second term in the braces vanishes.

Equation (9) can be regarded as the Fermi golden rule applied to the transitions from the trap states to the output, so that $N_F(E_{n\sigma})[1 - N_F(E_k)] - [1 - N_F(E_{n\sigma})] N_F(E_k) = N_F(E_{n\sigma}) - N_F(E_k)$ accounts for the probability of a particle to undergo a transition from the occupied trap level $E_{n\sigma}$ to the unoccupied output level E_k, and the summation includes all possible transitions. Equation (9) accounts for transitions of both the particles and ''antiparticles'' (holes) with energies $\pm E_{n\sigma}$, respectively. Note that $N_F(-E_{n\sigma}) = 1 - N_F(E_{n\sigma})$.

Let us first consider the zero-temperature case. In this case the Fermi distribution $N_F(E)$ becomes a step function, being equal to unity below the Fermi level and to zero above that level. The case with equal chemical potentials is very similar to the superconductor–normal-metal electron tunneling process.[15–17] For that case Eq. (9) simplifies to become

$$\langle \dot{N}_o \rangle \propto \sqrt{(\delta E)^2 - |\Delta|^2} \cdot \theta(\delta E - |\Delta|). \quad (10)$$

Here $\theta(\delta E - |\Delta|)$ is the Heaviside step function.

There is a threshold here, corresponding to the gap value $\delta E = |\Delta|$. It can be explained as the value of the energy difference equal to the ''bound energy'' of the fermionic pair: to effect the output coupling, one of the paired particles must acquire sufficient energy that the partner particle can surmount the gap. The value of the gap for the trapped fermions is of the order of the BCS transition temperature T_c, which is about 30 nK.[4] The value of δE, which is the difference between the two Fermi levels, can in principle be adjusted to the value of the gap, but this requires the two species to be trapped by an extremely weak magnetic field. A lower limit on the magnetic field has been estimated to be $B \gg a_{\rm hf}/\mu_e \simeq 0.011$ T (Ref. 4), where $a_{\rm hf}$ is the hyperfine constant and μ_e is the electron magneton. On the other hand, the energy difference that can be achieved is about $\delta E \sim 10^{-5} - 10^{-4}$ K. So the possibility of observing the threshold is questionable, but it does exist in principle. Once a higher transition temperature is achieved, the device will possess a threshold.

In the case of finite temperatures Eq. (9) gives a smooth dependence of the output current on the applied field (see Fig. 1). There is no threshold here, since the current grows smoothly as the field increases. The reason is that for finite temperatures there always exist particles at the excited levels, so that unpaired fermions at the Fermi level can be coupled out for any value of the bias. This case is reminiscent of cavity-QED

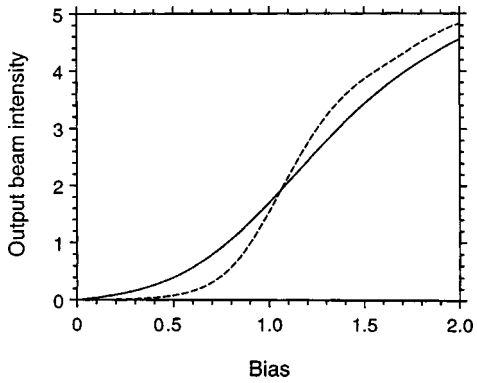

FIG. 1. Fermionic atom laser's output $\langle \dot{N}_o \rangle$ (arbitrary units) as a function of the bias δE (scaled in units of the gap Δ) at temperatures $T/T_c = 0.5$ (solid curve) and $T/T_c = 0.25$ (dashed curve) for the case of equal chemical potentials of the trapped species, $\mu_+ = \mu_-$: the mass of the ^{6}Li atom is $M = 10^{-26}$ kg, the Fermi momentum $k_F = 0.42 \times 10^6\ \mathrm{m}^{-1}$, the trap size $L = 15\ \mu$m, and the gap $\Delta = 0.9 \times 10^{-30}$ J.

lasers with spontaneous photons being emitted into a cavity mode.[11] Thus the thermal fluctuations at finite temperatures, which create particles at the upper levels in the trapped Fermi gas, play the same role as spontaneous-emission-induced noise in the case of cavity-QED lasers, resulting in thresholdless lasing.

This treatment can be extended to the case in which both traps contain fermions in BCS states, which would be an analog of superconductor–superconductor electron tunneling,[15–17] or to the case of traps containing noninteracting Fermi gases without pairing, which is the normal-metal–normal-metal tunneling case. Imagine also a case of two traps when one of the traps contains Cooper pairs and the other contains two species of interacting fermions. The process of particle exchange between the traps would be similar to a model describing an Anderson impurity embedded in a superconductor, which has recently been solved exactly for the zero-temperature case.[18] All these processes can serve as tests of fundamental quantum physical phenomena. Actually, there exists an interesting possibility of obtaining Schrödinger-cat states for the case of two trapped BCS Fermi gases, in direct analogy with the Josephson junction case proposed in Ref. 19.

In conclusion, we have considered the output coupling of trapped fermionic pairs. For the zero-temperature case we have found a threshold, a critical value of the trapping magnetic field above which the output current of fermions begins to grow. At finite temperatures the output beam grows smoothly without a threshold transition. Both threshold and thresholdless behaviors are reminiscent of optical lasers: conventional lasers and cavity-QED lasers or microlasers, and we have therefore named the device the fermionic atom laser.

[1] M. H. Anderson, J. R. Ensher, M. R. Matthews, C. E. Wieman, and E. A. Cornell, Science **269**, 198 (1995); K. B. Davis, M.-O. Mewes, M. R. Andrews, N. J. van Druten, D. S. Durfee, D. M. Kurn, and W. Ketterle, Phys. Rev. Lett. **75**, 3969 (1995); C. C. Bradley, C. A. Sackett, J. J. Tollett, and R. G. Hulet, Phys. Rev. Lett. **75**, 1687 (1995); **79**, 1170 (1997).

[2] For an extensive list of references, see the BEC on-line bibliography maintained by M. Edwards at: http://amo.phy.gasou.edu/bec.html/bibliography.html.

[3] B. DeMarco, J. L. Bohn, J. P. Burke, Jr., M. Holland, and D. S. Jin, http://xxx.lanl.gov/abs/cond-mat/9812350; F. S. Cataliotti, E. A. Cornell, C. Fort, M. Inguscio, F. Marin, M. Prevedelli, L. Ricci, and G. M. Tino, Phys. Rev. A **57**, 1136 (1998); E. R. I. Abraham, W. I. McAlexander, J. M. Gerton, R. G. Hulet, R. Cote, and A. Dalgarno, Phys. Rev. A **55**, R3299 (1997).
[4] H. T. C. Stoof, M. Houbiers, C. A. Sackett, and R. G. Hulet, Phys. Rev. Lett. **76**, 10 (1996); M. Houbiers, R. Ferwerda, H. T. C. Stoof, W. I. McAlexander, C. A. Sackett, R. G. Hulet, Phys. Rev. A **56**, 4864 (1997); M. Houbiers and H. T. C. Stoof, Phys. Rev. A **59**, 1556 (1999); M. Houbiers, H. T. C. Stoof, W. I. McAlexander, R. G. Hulet, Phys. Rev. A **57**, R1497 (1998); G. Bruun, Y. Castin, R. Dum, and K. Burnett, http://xxx.lanl.gov/abs/cond-mat/9810013.
[5] M. A. Baranov, Yu. Kagan, M. Yu. Kagan, JETP Lett. **64**, 301 (1996); M. A. Baranov and D. S. Petrov, Phys. Rev. A **58**, R801 (1998); M. A. Baranov, http://xxx.lanl.gov/abs/cond-mat/9801142; M. A. Baranov and D. S. Petrov, http://xxx.lanl.gov/abs/cond-mat/9901108.
[6] H. M. Wiseman and M. J. Collett, Phys. Lett. A **202**, 246 (1995); R. J. C. Spreeuw, T. Pfau, U. Janicke, M. Wilkens, Europhys. Lett. **32**, 469 (1995); M. Olshanii, Y. Castin, and J. Dalibard, *Proceedings of the 12th International Conference on Laser Spectroscopy*, edited by M. Inguscio, M. Allegrini, and A. Lasso (World Scientific, Singapore, 1995); M. Holland, K. Burnett, C. Gardiner, J. I. Cirac, P. Zoller, Phys. Rev. A **54**, R1757 (1996); A. M. Guzman, M. Moore, P. Meystre, Phys. Rev. A **53**, 977 (1996); H. Wiseman, A. Martins, and D. Walls, Quantum Semiclassic. Opt. **8**, 737 (1996); G. M. Moy, J. J. Hope, and C. M. Savage, Phys. Rev. A **55**, 3631 (1997); M. Naraschewski, A. Schenzle, and H. Wallis, Phys. Rev. A **56**, 603 (1997); H. Steck, M. Naraschewski, and H. Wallis, Phys. Rev. Lett. **80**, 1 (1998); B. Jackson, J. F. McCann, and C. S. Adams, http://xxx.lanl.gov/abs/cond-mat/9804038.
[7] M.-O. Mewes, M. R. Andrews, D. M. Kurn, D. S. Durfee, C. G. Townsend, and W. Ketterle, Phys. Rev. Lett. **78**, 582 (1997).
[8] A. N. Oraevskiĭ, JETP Lett. **65**, 459 (1997).
[9] A. Imamoglu, R. J. Ram, S. Pau, and Y. Yamamoto, Phys. Rev. A **53**, 4250 (1996).
[10] N. S. Ananikian and K. G. Petrosyan, Phys. Lett. A **236**, 84 (1997).
[11] P. R. Rice and H. J. Carmichael, Phys. Rev. A **50**, 4318 (1994); and references therein.
[12] G. M. Moy, J. J. Hope, and C. M. Savage, Phys. Rev. A **59**, 667 (1999).
[13] L. Diosi, N. Gisin, and W. T. Strunz, Phys. Rev. A **58**, 1699 (1998); W. T. Strunz, L. Diosi, N. Gisin, Phys. Rev. Lett. **82**, 1801 (1999).
[14] M. H. Cohen, L. M. Falicov, and J. C. Phillips, Phys. Rev. Lett. **8**, 316 (1962).
[15] G. D. Mahan, *Many-Particle Physics* (Plenum Press, New York, 1981).
[16] R. P. Feynman, *Statistical Mechanics* (Addison-Wesley, Reading, Mass., 1998).
[17] M. Tinkham, *Introduction to Superconductivity* (McGraw-Hill, New York, 1975).
[18] V. I. Rupasov, Phys. Rev. Lett. **80**, 3368 (1998); Phys. Lett. A **237**, 80 (1997).
[19] C. C. Gerry, Phys. Rev. B **57**, 7474 (1998).

Published in English in the original Russian journal. Edited by Steve Torstveit.

Collective braking mechanism in plasma and the momentum-transfer distribution function

S. N. Gordienko

L. D. Landau Institute of Theoretical Physics, Russian Academy of Sciences, 142432 Chernogolovka, Moscow Region, Russia; Kurchatov Institute Russian Science Center, 123182 Moscow, Russia

(Submitted 12 April 1999; resubmitted 3 June 1999)
Pis'ma Zh. Éksp. Teor. Fiz. **70**, No. 1, 18–23 (10 July 1999)

It is shown that the lower limit in the Coulomb logarithm is determined by the collective behavior of the plasma and not binary collisions with small impact parameters. For this reason, the assumption that the ''largest'' momentum transfer is determined by binary collisions results in a factor of two overestimation of the numerical coefficient in the second moment of the momentum transfer, i.e., the multiparticle nature of the lower limit in the Coulomb logarithm affects not only the logarithm itself but also the numerical coefficient multiplying it. Correctly taking into account fluctuational electric fields with scales less than or of the order of the Debye radius (multiple nature of collisions in plasma) substantially changes the physics of Coulomb collisions and results in the appearance of a new characteristic scale in plasma theory, $(r_D r_{\min})^{1/2}$, which has no analog in kinetic problems with a non-Coulomb interaction potential. © *1999 American Institute of Physics.* [S0021-3640(99)00413-2]

PACS numbers: 52.20.Hv, 52.20.Fs

There is an enormous literature on the problem of momentum and energy losses due to Coulomb collisions of a charged particle moving in plasma (see, for example, Refs. 1 and 2). At the same time, taking the multiplicity of the scattering into account reveals a number of new fundamental features in the process of momentum transfer to a plasma particle. It turns out that if the multiplicity of the interaction in plasma is neglected, then it is impossible not only to establish correctly the value of the argument of the Coulomb logarithm but also to calculate correctly the numerical factor in front of the logarithm.

1. Let us consider the statistical properties of the momentum increment imparted to a particle with charge Z_0 and velocity v in a plasma over a time interval τ by its interaction with other plasma particles. The formulation of the problem will be similar to that in Ref. 3. We shall study time intervals τ in which the change in the velocity of the test particle itself and of the plasma particles can be assumed to be small, i.e., the motion of the particles can be assumed to be uniform and rectilinear in these time intervals. According to Newton's second law, the increment to the momentum of a test particle over time τ is

$$\Delta \mathbf{p}_\tau = Z_0 e \int_t^{t+\tau} \mathbf{E}(t')\, dt', \tag{1}$$

where $\mathbf{E}(t')$ is the electric field produced by plasma particles at the location of the test particle at time t'. Since we are confining ourselves only to time intervals in which the motion of the particles can be assumed to be uniform and rectilinear,

$$\mathbf{E}(t') = -\sum e \frac{\mathbf{r}+\mathbf{v}(t'-t)-\mathbf{r}_i-\mathbf{v}_i(t'-t)}{|\mathbf{r}+\mathbf{v}(t'-t)-\mathbf{r}_i-\mathbf{v}_i(t'-t)|^3} + \sum Ze \frac{\mathbf{r}+\mathbf{v}(t'-t)-\mathbf{R}_i-\mathbf{V}_i(t'-t)}{|\mathbf{r}+\mathbf{v}(t'-t)-\mathbf{R}_i-\mathbf{V}_i(t'-t)|^3}, \tag{2}$$

where the summation in the first sum extends over all plasma electrons and the summation in the second sum extends over all plasma ions; $\mathbf{r}$, $\mathbf{r}_i$ and $\mathbf{v}$, $\mathbf{v}_i$ are, respectively, the coordinates and velocity of the test particle and the ith electron at time t, and $\mathbf{R}_i$ and $\mathbf{V}_i$ are the coordinates and velocity of the ith ion at time t.

The generating function (Fourier transform of the distribution function) corresponding to the random quantity $\Delta \mathbf{p}_\tau$ can be written, by definition, as

$$p(\mathbf{u}) = \langle \exp(i(\mathbf{u}, \Delta \mathbf{p}_\tau)) \rangle, \tag{3}$$

where the brackets denote an ensemble average, and $(\mathbf{a},\mathbf{b})$ and $[\mathbf{a},\mathbf{b}]$ will denote, respectively, the scalar and vector products of the vectors $\mathbf{a}$ and $\mathbf{b}$.

2. Assuming the plasma to be in thermal equilibrium and neglecting interparticle correlations, i.e., taking into account only terms of zeroth order in the parameter $e^2 n^{1/3}/T$ in the statistical weight, we rewrite expression (3) as

$$p(\mathbf{u}) = \left(\frac{1}{V}\right)^{N_e} \int \left\langle \exp\left[i\left(\mathbf{u}, \int_0^\tau \sum Z_0 e^2 \frac{(\mathbf{v}-\mathbf{v}_i)t' - \mathbf{r}_i}{|(\mathbf{v}-\mathbf{v}_i)t' - \mathbf{r}_i|^3} dt' \right) \right] \right\rangle_m \prod_{i=1}^{N_e} d\mathbf{r}_i$$
$$\times \left(\frac{1}{V}\right)^{N_i} \int \left\langle \exp\left[-i\left(\mathbf{u}, \int_0^\tau \sum ZZ_0 e^2 \frac{(\mathbf{v}-\mathbf{v}_i)t' - \mathbf{R}_i}{|(\mathbf{v}-\mathbf{v}_i)t' - \mathbf{R}_i|^3} dt' \right) \right] \right\rangle_m \prod_{i=1}^{N_i} d\mathbf{R}_i, \tag{4}$$

where the index m denotes averaging over a Maxwellian distribution, V is the volume of the plasma, and N_e and N_i are, respectively, the number of electrons and ions.

To calculate the generating function explicitly we introduce

$$U_e = \int \left[\left\langle \exp\left(i\left(\mathbf{u}, \int_t^{t+\tau} Z_0 e^2 \frac{\mathbf{r}+\mathbf{v}(t'-t)-\mathbf{v}_i(t'-t)}{|\mathbf{r}+\mathbf{v}(t'-t)-\mathbf{v}_i(t'-t)|^3} dt' \right) \right) \right\rangle_m - 1 \right] d\mathbf{r}, \tag{5}$$

$$U_i = \int \left[\left\langle \exp\left(-i\left(\mathbf{u}, \int_t^{t+\tau} Z_0 Z e^2 \frac{\mathbf{r}+\mathbf{v}(t'-t)-\mathbf{V}_i(t'-t)}{|\mathbf{r}+\mathbf{v}(t'-t)-\mathbf{V}_i(t'-t)|^3} dt' \right) \right) \right\rangle_m - 1 \right] d\mathbf{r}, \tag{6}$$

where the Maxwellian average in Eq. (5) extends over the velocities $\mathbf{v}_i$ of the plasma electrons and in Eq. (6) over the ion velocities $\mathbf{V}_i$.

Simple calculations give the following expression for the generating function of interest to us:

$$p(\mathbf{u}) = \exp(nU_e)\exp(nU_i/Z), \tag{7}$$

3. We shall now examine the generating function (7). We shall be interested in the braking of a test particle moving with velocity v. We shall study the distribution function $f(\Delta\mathbf{p}_\tau)$ of the random quantity $\Delta\mathbf{p}_\tau$ at times τ for which

$$B_e = n(v^*\tau)^3 \gg 1 \quad \text{and} \quad B_i = n(V^*\tau)^3 \gg Z,$$

where $v^* = \max(v, v_T)$ and $V^* = \max(v, V_T)$. Changing to the variables $\mathbf{r}' = \mathbf{r}/v^*\tau$, it is easy to show that the quantities B_e and B_i are large parameters in the theory that we shall use to construct the asymptotic expansion of the distribution function. Since the real parts of the exponents in Eqs. (7) are nonpositive, and the parameters B_e and B_i are large, the neighborhood of a point in $\mathbf{u}$ space where the real parts of the exponents in Eq. (7) are maximum will make the main contribution to the distribution function

$$f(\Delta\mathbf{p}_\tau) = \int \exp[-i(\mathbf{u}, \Delta\mathbf{p}_\tau)]p(\mathbf{u})\frac{d\mathbf{u}}{(2\pi)^3}. \tag{8}$$

Compared with the indicated neighborhood, the contribution of the rest of $\mathbf{u}$ space to the distribution function is exponentially small because of the large values of the parameters B_i and B_e. It is easy to see that the real part of the exponent in Eq. (7) is not positive, and to find the distribution function it is necessary to study the functions U_e and U_i near the point $\mathbf{u} = 0$. After the calculations we find, to terms of lowest order in the large quantity $\ln(1/|\mathbf{u}|)$,

$$U_e = \left\langle -\frac{2\pi Z_0^2 e^4 \tau}{|\mathbf{x}|^3}(\mathbf{u},\mathbf{x})^2 - \frac{\pi Z_0^2 e^4 \tau}{|\mathbf{x}|^3}[\mathbf{u},\mathbf{x}]^2 \ln\left(\frac{|\mathbf{x}|^6\tau^2}{e^4 Z_0^2 [\mathbf{u},\mathbf{x}]^2}\right)\right\rangle_m, \tag{9}$$

$$U_i = \left\langle -\frac{2\pi Z_0^2 Z^2 e^4 \tau}{|\mathbf{X}|^3}(\mathbf{u},\mathbf{X})^2 - \frac{\pi Z_0^2 Z^2 e^4 \tau}{|\mathbf{X}|^3}[\mathbf{u},\mathbf{X}]^2 \ln\left(\frac{|\mathbf{X}|^6\tau^2}{Z^2 Z_0^2 e^4 [\mathbf{u},\mathbf{X}]^2}\right)\right\rangle_m, \tag{10}$$

where $\mathbf{x} = \mathbf{v} - \mathbf{v}_i$ and $\mathbf{X} = \mathbf{v} - \mathbf{V}_i$. The averaging, denoted by the brackets, with respect to a Maxwellian velocity distribution affects only $\mathbf{x}$ and $\mathbf{X}$ and has no effect on the functional dependence on $\mathbf{u}$ of interest to us. The indicated averaging can be performed explicitly and will lead to the appearance of an error function in expressions (9) and (10).

4. We note that since the functions U_e and U_i possess only a finite number of smooth derivatives because of the logarithmic singularity at $\mathbf{u} = 0$, the distribution function for large momentum transfers decreases no more rapidly than as a power law. For this reason, the moments of the momentum transfer should diverge starting at some particular moment. We shall show below that the divergence occurs already at the second moment.

The moments diverge because rectilinear particle trajectories were assumed in the calculation of the momentum transfer. For this reason, a large momentum transfer that is physically meaningless occurs if particles pass close to one another. We note that these unphysical momentum transfers can be avoided by calculating the distribution function using Eqs. (9) and (10) in the limit of an infinitely large Coulomb logarithm Λ. Let us

illustrate this for the example of an electron moving with thermal velocity in plasma. In this case, there are of the order of $r_{\min}^2\lambda_{st}n\sim 1/\Lambda$ particles on the mean free path λ_{st} at distance $r_{\min}=e^2/T$ from an electron, i.e., an additional smallness $1/\Lambda$ is associated with the unphysical momentum transfers. Therefore, to avoid these fictitious momentum transfers, only the leading term in $1/\Lambda$ should be retained in the calculation (for $\Lambda=+\infty$ there is simply not enough time for impact parameters responsible for the unphysical momentum transfers to play a role, since no particles lie at a distance less than $r_{\min}$ from the test particle during the free-flight time). It can be shown that for this it is sufficient to use in expression (7) instead of U_e and U_i the expressions

$$U_e^*=\left\langle -\frac{2\pi Z_0^2e^4\tau}{|\mathbf{x}|^3}(\mathbf{u},\mathbf{x})^2-\frac{\pi Z_0^2e^4\tau}{|\mathbf{x}|^3}[\mathbf{u},\mathbf{x}]^2\ln\left(\frac{|\mathbf{x}|^4\tau^2}{e^4Z_0^2}\xi_e\right)\right\rangle_m, \tag{11}$$

$$U_i^*=\left\langle -\frac{2\pi Z_0^2Z^2e^4\tau}{|\mathbf{X}|^3}(\mathbf{u},\mathbf{X})^2-\frac{\pi Z_0^2Z^2e^4\tau}{|\mathbf{X}|^3}[\mathbf{u},\mathbf{X}]^2\ln\left(\frac{|\mathbf{X}|^4\tau^2}{Z^2Z_0^2e^4}\xi_i\right)\right\rangle_m, \tag{12}$$

where $\xi_e=\min[A_e,\ A_e^2/(\Delta\mathbf{p}_\tau)^2]$, $\xi_i=\min[A_i,\ A_i^2/(\Delta\mathbf{p}_\tau)^2]$, $A_e=\pi Z_e^2e^4\tau/|\mathbf{x}|$, and $A_i=\pi Z_0^2Z^2e^4\tau/|\mathbf{X}|$.

5. The nearly Gaussian structure of the distribution function (a Gaussian function with a deformed ''tail'') following from Eqs. (11) and (12) permits reducing the calculation of the second moment of the momentum transfer to the calculation of the trace of the corresponding matrix and to write

$$\langle(\Delta\mathbf{p}_\tau)^2\rangle=4n\pi Z_0^2e^4\tau\left\langle\frac{1}{|\mathbf{x}|}\right\rangle_m\ln(n(v^*\tau)^3)+4n\pi ZZ_0^2e^4\tau\left\langle\frac{1}{|\mathbf{X}|}\right\rangle_m\ln(n(V^*\tau)^3/Z). \tag{13}$$

To understand the qualitatively new physical content of expression (13), let us shall calculate the second moment under the assumption that the momentum transfer producing the curvature of the trajectory is due to binary collisions with small impact parameters. The second moment is calculated in Ref. 3 on the basis of this plausible assumption. To calculate the second moment it is necessary to calculate the second derivatives of the generating function at $\mathbf{u}=0$, i.e.,

$$\langle(\Delta\mathbf{p}_\tau)^2\rangle=\left.\frac{\partial^2p(\mathbf{u})}{\partial\mathbf{u}\partial\mathbf{u}}\right|_{\mathbf{u}=0}. \tag{14}$$

Substituting expression (7) into Eq. (14) we find

$$\langle(\Delta\mathbf{p}_\tau)^2\rangle=8\pi Z_0^2e^4n\tau\left\langle\frac{1}{|\mathbf{x}|}\int_1^{+\infty}\frac{d\mu}{\mu^2-1}\right\rangle_m+8\pi Z_0^2Ze^4n\tau\left\langle\frac{1}{|\mathbf{X}|}\int_1^{+\infty}\frac{d\mu}{\mu^2-1}\right\rangle_m. \tag{15}$$

The integrals in Eq. (15), which arise after integrating over t', can be calculated in elliptical coordinates with centers a and b at the points $(0,0,0)$ and $(0,0,-|\mathbf{x}|\tau)$ for the first term and, correspondingly, at $(0,0,0)$ and $(0,0,-|\mathbf{X}|\tau)$ for the second term in Eq. (15), where $\mu=(r_a+r_b)/2$, $\nu=(r_a-r_b)/2$, and the angle ϕ is the angle of rotation around the z axis. The integrations over the angle ϕ and over ν are elementary, and the remaining integrals over μ are indicated in Eq. (15). The integrals in Eq. (15) diverge

logarithmically at $\mu=1$. On the assumption that maximum momentum transfer occurs in binary collisions with small impact parameters, expression (15) must be integrated not up to $\mu=1$, but rather $\mu_1=1+(r_{\min}^{(e)}/|\mathbf{x}|\tau)^2$ and $\mu_2=1+(r_{\min}^{(i)}/|\mathbf{X}|\tau)^2$, where $r_{\min}^{(e)}=Z_0e^2/\min[Mv^{*2},m_ev^{*2}]$ and $r_{\min}^{(i)}=Z_0Ze^2/\min[MV^{*2},m_iV^{*2}]$, must be taken as the lower limits in the first and second terms in Eq. (15), respectively, since the curvatures of the trajectories of the colliding particles become substantial precisely at such impact parameters. After the indicated change is made in the lower limits, we find to logarithmic accuracy

$$\langle(\Delta\mathbf{p}_\tau)^2\rangle_P=8\pi Z_0^2e^4n\tau\left\langle\frac{1}{|\mathbf{x}|}\right\rangle_m\ln\left(\frac{v^*\tau}{r_{\min}^{(e)}}\right)+8\pi ZZ_0^2e^4n\left\langle\frac{1}{|\mathbf{X}|}\right\rangle_m\ln\left(\frac{V^*\tau}{r_{\min}^{(i)}}\right), \tag{16}$$

where the subscript P signifies that the quantity so labeled is calculated in the binary (pair) collision approximation.

The assumption of momentum transfer resulting in a large curvature of the trajectory due to a head-on binary collision of particles alters the structure of the Coulomb logarithm and the factor in front of the logarithm as compared with the correct value (it leads to a factor of 2 error for $\tau\sim1/\omega_{pe}$ according to Eqs. (13) and (16)). Therefore before a binary collision with a large momentum transfer occurs the trajectory is curved appreciably because of the interaction of a particle with the collective electric fields present in the plasma. Thus, we have shown that scattering by collective plasma fields and not binary collisions determines not only the upper limit but also the lower limit in the Coulomb logarithm.

6. We shall now present the computational results for the second moment with allowance for the permittivity of the plasma (Debye screening). In this case, for $\tau\max[v^*,V^*]\leqslant r_D$ expressions (13) and (16) remain in force, while for $\tau\min[v^*,V^*]\geqslant r_D$

$$\langle(\Delta\mathbf{p}_\tau)^2\rangle=4n\pi Z_0^2e^4\tau\left\langle\frac{1}{|\mathbf{x}|}\right\rangle_m\ln(nr_D^3)+4n\pi ZZ_0^2e^4\tau\left\langle\frac{1}{|\mathbf{X}|}\right\rangle_m\ln(nr_D^3/Z), \tag{17}$$

and, correspondingly,

$$\langle(\Delta\mathbf{p}_\tau)^2\rangle_P=8\pi Z_0^2e^4n\tau\left\langle\frac{1}{|\mathbf{x}|}\right\rangle_m\ln\left(\frac{r_D}{r_{\min}^{(e)}}\right)+8\pi ZZ_0^2e^4n\left\langle\frac{1}{|\mathbf{X}|}\right\rangle_m\ln\left(\frac{r_D}{r_{\min}^{(i)}}\right), \tag{18}$$

where r_D is the Debye radius. In the case at hand, the expressions in the arguments of the logarithms are essentially identical, but the numerical coefficients in front of the logarithm differ by a factor of 2.

Of course, the correct value of the second moment of the momentum transfer can also be obtained from Eq. (18), choosing an appropriate distance at which the diverging integrals are cut off at small scales. Comparing Eqs. (17) and (18) we find that the ''cutoff'' in Eq. (15) must be made at $\lambda_e=\sqrt{1/nr_D}$ and $\lambda_i=Z^{1/2}\lambda_e$ — the distances of closest approach of electrons and ions to a test particle as it traverses a distance equal to the Debye length. We note that the scale λ_e is approximately $N_D^{1/6}$ times smaller than the interparticle distance and $N_D^{1/2}$ times greater than $r_{\min}$, where $N_D=nr_D^3$ is the number of particles in the Debye sphere.

7. Expression (18) follows from the binary-collision approximation.[2] The binary approach used to describe the interaction in the derivation of the Boltzmann equation with a short-range interaction potential presumes that the particles are statistically independent and that there exists a time interval Δt during which the test particle undergoes no more than one collision but which is also long compared with the collision duration τ_{int}. However, in plasma τ_{int} depends on the impact parameter r as $\tau_{\text{int}} \sim r/v^*$ and, say, in the time of one collision with $r \sim r_D$ there occur $N_D^{2/3}$ collisions with impact parameter less than the interparticle distance. Therefore the conditions of applicability of the binary-collision approximation are not satisfied. In other words, there is enough time for the momentum of a particle to change strongly because of a large number of collisions with large impact parameters even before collisions with small impact parameters and large momentum transfers start to play a role. This is what gives rise to the new characteristic scale λ_e. The physical meaning of this becomes clear if one takes into account that for interparticle interaction potentials $U(r) \sim 1/r^k$, $k>1$ the momentum transfer processes are determined by head-on collisions of particles (small impact parameters), while for potentials $U(r) \sim 1/r^k$, $k<1$ the momentum transfer is associated with large distances, and the intermediate situation $k=1$ is a special case.

It is also interesting to note that when the method set forth in the present work is used to analyze everywhere nonsingular weak interaction potentials with finite range r_0, in that case no new scale of the type $\sqrt{1/nr_0}$ actually arises in the problem, although dimensional considerations do not preclude such a scale. This finding demonstrates that even though a formal interpretation from the ''naive'' point of view is possible, the new spatial scale arising in the problem with a Coulomb interaction has a deep dynamical meaning. The new scale λ_e can also be rewritten as $\lambda_e = (r_D r_{\min})^{1/2}$, which, possibly, better demonstrates its relation with the physics of the Coulomb interaction.

Taking the multiplicity of the scattering in a plasma into account also changes the numerical values of the coefficients in other expressions containing the Coulomb logarithm, for example, in the expression for polarization losses in plasma.[4] From this standpoint the problem studied in this letter is only an illustration of the fundamental role of small-scale fluctuational electric fields. Justification is always required to neglect these fields or to switch to a binary-collision description.[1,2]

I am deeply grateful to S. I. Anisimov and É. I. Yurchenko for a discussion of the method and the results obtained in this work, to V. D. Shafranov for explaining the significance of the results obtained and for proposing the idea and form of this letter, and to V. I. Kogan for pointing out the deep physical meaning of the Coulomb logarithm.

[1] Trubnikov, in *Reviews of Plasma Physics*, Vol. 1, edited by M. A. Leontovich (Consultants Bureau, New York, 1963) [Russian original, Gosatomizdat, Moscow, 1961].
[2] D. V. Sivukhin, in *Reviews of Plasma Physics*, Vol. 4, edited by M. A. Leontovich (Consultants Bureau, New York, 1968) [Russian original, Gosatomizdat, Moscow, 1964].
[3] V. I. Kogan, Dokl. Akad. Nauk SSSR **135**, 1374 (1960) [Sov. Phys. Dokl. **5**, 1316 (1961)].
[4] V. D. Shafranov, in *Reviews of Plasma Physics*, Vol. 3, edited by M. A. Leontovich (Consultants Bureau, New York, 1967) [Russian original, Gosatomizdat, Moscow, 1963].

Translated by M. E. Alferieff

On the instability of the *p*-electron subsystem of anions in the CuO_2 planes in high-T_c superconductors

I. I. Amelin
Mordovia State University, 430000 Saransk, Russia

(Submitted 14 April 1999; resubmitted 20 May 1999)
Pis'ma Zh. Éksp. Teor. Fiz. **70**, No. 1, 24–29 (10 July 1999)

Calculations of the electronic structure of a cluster of the crystal $YBa_2Cu_3O_7$ are performed in the CNDO approximation. It is established that the hybridized d–p band of the planes consists of an nearly filled d subband of width 3 eV and an unfilled p subband of width 0.8 eV. The computed band structure agrees satisfactorily with experimental investigations. It is shown that the Shubin–Vonsovskiĭ inequality holds in the planes. These conditions are the reason why a charge density wave forms in the p subsystem. In this approximation the formation energy of local pairs is estimated to be kT^*.
 [S0021-3640(99)00513-7]

PACS numbers: 74. 72.Bk, 74.25.Jb

In 1934 Shubin and Vonsovskiĭ showed[1] that a polar state (termed in the literature a state with a charge-density wave (CDW)) with order parameter $m=2$ forms in a narrow half-filled metallic band with one electron per center if

$$ZV>I, \tag{1}$$

where Z is the number of nearest neighbors, I is the electrostatic interaction energy of two collectivized (previously valence) electrons at one lattice site, and V is the same energy between two collectivized electrons of two neighboring lattice sites. The parameter m is the difference of the electron density on neighboring centers. The value $m=2$ corresponds to the formation of local electron pairs in the system. Subsequent investigations have established[2] that a state with a CDW in narrow bands is insulating and is characterized by a band gap $\Delta E=(ZV-I)m$. In ordinary metals the condition (1) holds for intercenter distances $r_0 \leqslant 1-2$ Å. But, as was shown in Ref. 3, for such values of r_0 the insulating state does not occur because of the presence of a wide band (high carrier kinetic energy). However, the condition (1) will be satisfied for large values of r_0 (the case of narrow bands) because of a decrease in the parameter I. As the band widens, the parameters m and ΔE decrease rapidly.[3]

Cluster calculations of a $YBa_2Cu_3O_{6+\delta}$ crystal by the CNDO method have established[4] that in the planes segregated into a separate quantum system the p subsystem is unstable and a CDW forms in it. In Ref. 4 it was assumed that because of the condition (1) instability arises in the narrow p subband of the planes. In the present work, to

confirm this conjecture the parameters V are estimated and the electron density of states $N(E)$ of planes of a $YBa_2Cu_3O_7$ crystal cluster is calculated.

Analyzing the results of x-ray emission and x-ray electron spectroscopy as well as band calculations, it is concluded in Ref. 5 that in $La_{1.83}Sr_{0.17}CuO_4$, for which $T_c = 40$ K, the contribution of d states predominates in the high-energy part of the band near the Fermi level. Conversely, in $YBa_2Cu_3O_7$, with $T_c = 92$ K, the d states are concentrated mainly at low low energies and the $2p$ states predominate near the Fermi level. Band calculations show that in $YBa_2Cu_3O_7$ strong hybridization with the $3d$ states and splitting of the density of $2p$ states into two subbands are observed. This is explained by the fact that in this structure each oxygen atom is bonded with two copper atoms.

In Ref. 6 it is noted that the difference of the energies of the electronic states of the Cu^{+2} and O^{-2} ions is very small compared with other pairs M^{+2}–O^{-2}. For this reason, when the position of the O_z ion, which in the compound $La_{2-x}Sr_xCuO_4$ lies above the Cu ion, changes, a substantial flow of charge occurs in the plane between the Cu and O ions. The results concerning the charge flow have also been confirmed in Refs. 7 and 8. A similar result should also be observed in $YBa_2Cu_3O_{6+\delta}$ on doping. In addition, doping with oxygen will give rise in the crystal to a negligible screening of the parameter I_{Cu}. It has been established that the transition from antiferromagnetic insulator (AFI) to metal with increasing δ is due to the formation of holes on oxygen anions in the planes.[9] Using the photoelectron spectra of thin films of $YBa_2Cu_3O_6$, it has been established that the density of d states of copper is higher and the density of p states of oxygen is lower near the Fermi level than in $YBa_2Cu_3O_7$ films.[10] Therefore the experimental data indicate that on doping, the oxygen in the planes tends to an unusual degree of oxidation, O^{-1}, while the copper ions tend to the configuration Cu^{+1}.

In Ref. 1 the structure of the $3d$ band of copper in a $YBa_2Cu_3O_7$ film was determined at two temperatures (300 and 80 K). It was found that the $3d$ band narrows and the effective hole repulsion potential for copper decreases at low temperature. At 80 K the density of states has a narrow peak with a width of less than 1 eV and a bump separated from the narrow peak by 2 eV. Therefore the width of the $3d$ band of the crystal is estimated to be of the order of 3 eV. The curve of the density of states in this case is close to the density of states obtained by photoelectron spectroscopy for pure copper, where the $3d$ band is localized. The presence of band broadening at 300 K attests to a quite strong overlap of the Cu–O orbitals, resulting in delocalization of the $3d$ electrons. In Ref. 11 the observed narrowing of the $3d$ band with decreasing T is attributed to structural distortions of the CuO_2 planes, where displacements of oxygen atoms occur. Apparently, in that case the phenomenon should be observed in all high-T_c superconductors (HTSCs), but experimental investigations show that it is observed only in $YBa_2Cu_3O_7$. From our point of view,[4] the increase in the width of the d–p band of the $YBa_2Cu_3O_7$ planes from 3 eV (Ref. 12) to 9 eV (the computed value of the d–p band of the crystal as a single quantum system[13]) is due to the appearance of a chemical bond between the planes and chains, transfer of electron density from chains to planes, vanishing of the CDW, and an increase of the copper charges ($z > 1$) in the chains. Apparently, this restructuring of the band explains the broadening of the copper band of the crystal for $\delta = 1$ with increasing temperature and the sharp decrease of T_c in the superstoichiometric compound with $\delta > 1$. Thus calculations have confirmed[13] that for a wide d–p band of the crystal, just as

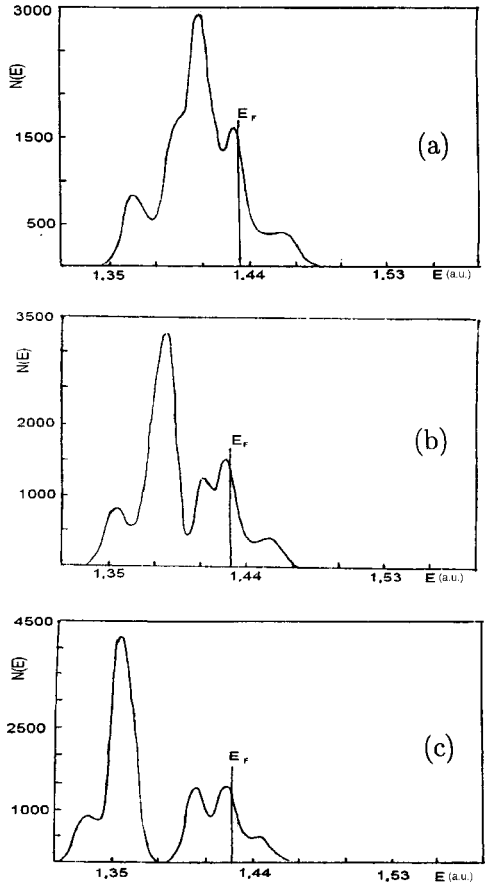

FIG. 1. Electronic density of states $N(E)$ for the CuO_2 planes of the cluster $[Cu_{12}O_{18}]^{-12}$: a) $I_{Cu}=6.39$ eV, b) $I_{Cu}=6.34$ eV, and c) $I_{Cu}=6.26$ eV.

in ordinary metals, a CDW does not form in the p subsystem of the anions O^{-k} ($k<2$).

Calculations of the curves $N(E)$ for a $YBa_2Cu_3O_7$ crystal were performed for various values of I_{Cu} to obtain the band structure of the planes. In Ref. 11 the effective repulsive potential of holes in the d band for copper was determined to be 4.5 eV. This value is close to the well-known value for copper (5 eV). In our calculations we chose I_{Cu} in the range 6.39–6.26 eV to obtain the curves $N(E)$. This value is comparable to the estimates obtained from calculations by other authors as well as from experimental investigations. Fluoroscopic and photoelectron spectroscopy investigations[14] give $I_{Cu}\approx 6-12$ eV. Cluster and band calculations give[14] $I_{Cu}\approx 6-11$ eV. The $N(E)$ curves for $I_{Cu}=6.39$, 6.34, and 6.26 eV are presented in Fig. 1. The parameters, obtained by the CNDO method, for the planes of a crystal cluster $[Cu_{12}O_{18}]^{-12}$ are given in Ref. 4.

The theoretical local density of states in the plane of the copper atoms was obtained in Ref. 15 (see also Ref. 11). It can be noted that for $I_{Cu}=6.26$ eV the curve $N(E)$ is close in form to the curves presented in Refs. 11 and 15. In Fig. 1c the left-hand peak,

less than 1 eV wide, corresponds to the *d* states of the copper ions, and the three peaks on the right-hand side, separated from the left-hand peak by 2 eV, correspond to hybridized *d*–*p* states of the O and Cu ions, the *p* subband, lying near the Fermi level, being split into two peaks. It follows from Fig. 1c that the *d* subband has a width of the order of 3 eV, and the width of the split *p* subband is 0.8 eV. As the parameter I_{Cu} decreases from 6.39 eV to 6.26 eV, the *d* and *p* subbands move apart. Therefore our computed band structure of the planes agrees with the experimental results and the theoretical calculations performed by other authors.

Comparing the results of Ref. 4 and the shapes of the curves obtained, we can draw the following conclusions. In the planes, as the parameter I_{Cu} decreases from 6.39 eV to 6.26 eV, charge flows between the Cu and O atoms, as was also noted in Refs. 5–10, and the parameter *m* increases from $m=0.37$ to $m=1.31$ with the gap ΔE of the cluster decreasing at the same time from 0.35 eV to 0.1 eV. For $I_{Cu}=6.39$ eV in the planes the charges of the Cu ions and the average charges of the O anions are $+1.66$ and -1.17, respectively. For $I_{Cu}=6.26$ eV these charges are $+1.28$ and -0.79. The decrease of the gap with increasing *m* is due to the motion of free *d* states to the Fermi level as I_{Cu} decreases.[4] For $I_{Cu}<6.26$ eV the parameter *m* increases to $m=2$, the copper charges decrease, and ΔE decreases to 0.02 eV.[4] Apparently, a transition of the *p* subsystem to a state with $m\sim 0$ and $\Delta E\sim 0$ is possible at high *T*.

It follows from cluster calculations[4] that for $I_{Cu}=6.26$ eV in the planes there is a very small number of unoccupied 3*d* states near the Fermi level. From this it follows that the 3*d* electrons essentially do not participate in covalent bonds. The distance between the O anions in the planes lies in the range 2.69–3.81 Å . In this case the *p* subband has a negligible width of the order of 0.8 eV because of the weak overlap of the wave functions of the anions. A CDW does not arise in the 3*d* subsystem because the appropriate conditions are not present. When a CDW forms, an energy gap forms in the *p* subband, but the presence of a very small number of unoccupied *d* states near the Fermi level gives a metallic state of the *d*–*p* band in the planes.[4]

The reason why a CDW forms in the 0.8 eV wide *p* subband is that the condition (1) is satisfied. One reason that this is so is that the quantity I_O decreases upon the transition from O to O^{-k}. It follows from atomic calculations that for the O atom the Coulomb interaction energy of two *p* electrons is $I_O=20.873$ eV, for the O^{-1} anion $I_O=17.982$ eV, and for the O^{-2} anion $I_O\sim 13.46$ eV. Ohno's formula,[16] which is used in quantum mechanical CNDO calculations, was used to obtain a rough estimate of the Coulomb interaction energy V_{AB} between electrons located on the atoms A and B:

$$V_{AB}(R_{AB})=14.3986/(R_{AB}^2+\mathbf{c}^2)^{1/2}(\text{eV}), \tag{2}$$

where $\mathbf{c}=14.3986/2^{-1}(\mathbf{I}_A+\mathbf{I}_B)$ and R_{AB} is the internuclear distance between the atoms A and B, in Å . In a CuO_2 plane the O^{-1} ion has two neighboring Cu ions at distances $R_{Cu-O}=1.89$ Å , four neighboring O^{-1} anions at distances $R_{O-O}=2.69$ Å , and two neighboring O^{-1} anions at distances $R_{O-O}=3.81$ Å . For the copper ion I_{Cu} was taken to be 6.26 eV. The calculations give the following estimates for the parameter *V*: $V_{CuO}(1.89)=6.45$ eV, $V_{OO}(3.81)=3.70$ eV, and $V_{OO}(2.69)=5.13$ eV. Formula (2) neglects the spatial arrangement of the *d* and *p* electron clouds. Taking the spatial distribu-

tion of the p electron density into account should result in a decrease in $V_{OO}(2.69)$. With allowance for the specific distribution of the p electron density in the CuO_2 planes, we can set $V_{OO}(2.69) \approx V_{OO}(3.81) \approx 3.70$ eV.

In Ref. 17 it is shown that the transition from a state with $m<2$ to a state with $m=2$ in the p subsystem of the planes can occur with a negligible displacement of the Cu ions, and this transition is accompanied by a decrease of the gap of the crystal cluster. This suggests that vibrations of atoms can participate in the formation of electron pairs in HTSCs. The negligible difference between the parameters a and b of the unit cell of the crystal and the low degree of degeneracy of the orbitals of the planes likewise favors the formation of local pairs.

Apparently, the instability of the p subsystem favors the formation of a superconducting state with high $T_c \sim n$ and relatively low density n in the HTSCs. At present, experimental investigations of HTSCs indicate that the carriers are local electron pairs satisfying Bose–Einstein statistics.[18,19] Local-pair formation occurs for $T^* > T_c$ and is accompanied by the appearance of a pseudogap in the electron spectrum. In Ref. 20 it is shown that in a planar square lattice with $m=2$ the energy $E_1 = ZV - I$ is identical to the formation energy of an electron pair. It is well known that in metals the Coulomb potential is described by the screened potential $\varphi = q \cdot \exp(-\lambda r)/r$. Then the quantities I and $V(R)$ must be multiplied by $\exp(-\lambda \mathbf{r})$. Taking for the density $n \sim 10^{21}$ cm^{-3} for the metallic CuO_2 planes in the HTSC, we obtain $1/\lambda \sim 1$ Å .[21] The diameter of the p shell of the $O^{-1}$and O^{-2} anions varies in the range 2–2.92 Å . For the screening of the parameter I_0, an intermediate value $R=2.55$ Å can be used. In the presence of holes, $t<1$ in the d shell and $t_1<1$ in the p shell, we have

$$E_1 = t_1(t_1 6 V_{OO}(3.81) \cdot \exp(-3.81\lambda) + 2tV_{CuO}(1.89) \cdot \exp(-1.89\lambda)) - I_0 \cdot \exp(-2.55\lambda). \quad (3)$$

Apparently, a state of the system with $m<2$ will also favor pair formation. In this case the contribution of the electron–electron interaction to the pairing energy can be estimated as $E = E_1 m/2$. In all probability, a contribution of the order of $T_{ef} \sim 20$ K from the participation of the electron–phonon interaction in the formation of pairs can be added to this energy.

In a $YBa_2Cu_3O_{6+\delta}$ crystal, t_1 increases and t decreases as δ increases. An estimate of the temperature $T^* \sim E/k + T_{ef}$ for $t_1=0.83$, $t=0.66$, and $m=0.37$ (Ref. 17) gives 25 K (the parameters correspond to a cluster with $I_{Cu}=6.39$ eV),[17] and for $t_1=0.91$, $t=0.59$, and $m=0.43$ one gets $T^* \approx 145$ K. For $I_{Cu}=6.34$ eV the parameters are $m=0.54$, $t_1=0.99$, and $t=0.50$,[17] and the temperature $T^* \approx 155$ K. For $t_1=1.0$, $t=0.47$, and $m=0.72$ one gets $T^* \approx 35$ K. Thus a bell-shaped curve $T^*(\delta)$ corresponding to the experimental dependence $T_c(\delta)$ is obtained.

[1] S. P. Shubin and S. V. Vonsovskii, Proc. R. Soc. **145**, 159 (1934).
[2] R. Bary, Phys. Rev. B **3**, 2662 (1971).
[3] S. P. Ionov, I. I. Amelin, V. S. Lubimov *et al.*, Phys. Status Solidi B **77**, 441 (1976).
[4] I. I. Amelin, Fiz. Nizk. Temp. **22**, 539 (1996) [Low Temp. Phys. **22**, 415 (1996)].
[5] V. I. Anisimov, V. R. Galakhov, V. A. Gubanov *et al.*, Fiz. Met. Metalloved. **65**, 204 (1987).
[6] R. E. Cohen, W. E. Pickett, H. Krakauer *et al.*, Physica B **150**, 61 (1988).
[7] C. O. Rodriguez, A. I. Lichtenstein, I. I. Mazin *et al.*, Phys. Rev. B **42**, 2692 (1990).
[8] T. Jarlborg, Solid State Commun. **71**, 663 (1989).

[9] G. S. Grader, P. K. Gakkagher, and A. T. Fiory, Phys. Rev. B **38**, 844 (1988).
[10] E. R. Likhachev, S. I. Kurganskiĭ, O. I. Dubrovskiĭ *et al.*, Fiz. Tverd. Tela (St. Petersburg) **39,** 437 (1997) [Phys. Solid State **39**, 378 (1997)].
[11] V. G. Babaev, V. V. Khvostov, and P. V. Shibaev, JETP Lett. **49**, 191 (1989).
[12] I. I. Amelin, Sverkhprovodimost' (KIAE) **5,** 1971 (1992) [Supercond., Phys. Chem. Technol. **5**, 1877 (1992)].
[13] I. I. Amelin, Sverkhprovodimost' (KIAE) **5,** 802 (1992) [Supercond., Phys. Chem. Technol. **5**, 803 (1992)].
[14] V. P. Lukin, *Electronic Structure and Magnetic Properties of High-Temperature Superconductors* [in Russian], Vol. 2 of High-Temperature Superconductivity (Topical Problems), edited by A. A. Kiselev (Leningrad State University Press, Leningrad, 1989), p. 160.
[15] W. M. Temmerman *et al.*, J. Phys. C **21**, L867 (1988).
[16] K. Ohno, Adv. Quantum Chem. **3**, 240 (1967).
[17] I. I. Amelin, Sverkhprovodimost: Fiz., Khim., Tekh. **7**, 788 (1994).
[18] Y. J. Uemura, Physica C **282–287**, 194 (1997).
[19] N. V. Anshukova, A. I. Golovashkin, L. I. Ivanova *et al.*, Usp. Fiz. Nauk **167,** 887 (1997).
[20] V. I. Spitsyn, G. V. Ionova, S. V. Vonsovskiĭ *et al.*, *Electron Dynamics and Charge-Ordered Crystals* [in Russian] (Chernogolovka, 1985, p. 121).
[21] C. Kittel, *Introduction to Solid-State Physics*, 5th edition (Wiley, New York, 1976) [Russian translation, Nauka, Moscow, 1978, p. 293].

Translated by M. E. Alferieff

Experimental solution of the local-field problem in discotic liquid crystals

E. M. Aver'yanov*) and V. A. Gunyakov
L. V. Kirenskiĭ Institute of Physics, Siberian Branch of the Russian Academy of Sciences, 660036 Krasnoyarsk, Russia

A. Ya. Korets
Krasnoyarsk State Technical University, 660036 Krasnoyarsk, Russia

O. B. Akopova
Ivanovo State University, 153025 Ivanovo, Russia

(Submitted 20 May 1999)
Pis'ma Zh. Éksp. Teor. Fiz. **70**, No. 1, 30–35 (10 July 1999)

Polarized light-absorption spectra are obtained for single-domain planar-oriented samples of the discotic D_{ho}. Previously predicted spectral effects induced by resonant dipole–dipole interactions of the molecules are observed. New methods for determining the parameters of the local field in the D_{ho} phase are developed which take into account the mixing of the molecular excitations. It is shown that the two-dimensional crystalline ordering of the molecular columns decreases the anisotropy of the local field for this phase. © *1999 American Institute of Physics.* [S0021-3640(99)00613-1]

PACS numbers: 61.30.Eb, 78.40.Dw

1. Experimental data on the anisotropy of the local electric field in liquid crystals (LCs) with disk-shaped molecules are important for analyzing a variety of questions which are being actively discussed: the possibility of a ferroelectric state in discoidal nematics N_D (Refs. 1 and 2), the polarity of molecular columns and their antiferroelectric ordering in the discotics $D_{h(0,d)}$ (Refs. 3 and 4) the quasi-one-dimensional electric and photoelectric conductivity of the $D_{h(0,d)}$ phases,[5] the qualitative difference of the characteristic features in the polarized absorption spectra of calamitic and discoidal LCs,[6] and the effect of two-dimensional crystalline ordering of columns on the anisotropy of the dipole–dipole interaction of the molecules. However, such data have been lacking thus far. To determine the local-field parameters in discotics by spectral methods[7] these methods needed to be modified to take into account the mixing of molecular excitations,[8] and single-domain planar-oriented samples needed to be obtained for polarized spectral investigations. These problems are solved in the present work.

2. The object of investigation was the discotic liquid crystal THE7 with the indicated temperatures (°C) of the phase transitions between crystal, discotic D_{ho}, and isotropic liquid (C–D_{ho}–I).

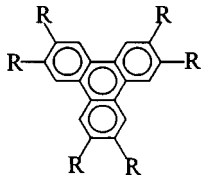

The uniaxial phase of D_{ho} is a two-dimensional hexagonal lattice of molecular columns, which are perpendicular to this lattice and parallel to the director **n**.[5] The molecular cores are translationally ordered along the axes of the columns. The orientational order of the molecular axes **l** (perpendicular to the plane of the core) relative to **n** is characterized by the order parameter $S=\langle 3\cos^2\theta_{\ln}-1\rangle/2$.

Single-domain films of the discotic D_{ho} with an area of several square centimeters, thickness $d=10$–20 μm, and uniform orientation of **n** parallel to the substrates were obtained in NaCl, KBr, CaF_2, and Ge cells using a modification of the method of Ref. 9. Polished substrates were cleaned by conventional chemical methods without using surfactants. The initial uniform homeotropic orientation of the LCs with the optic axis normal to the substrates was obtained by capillary filling of the cell in the isotropic phase followed by slow cooling and lowering of the temperature of the LC to the working range. Next, for a monitored plane-parallel arrangement of the substrates and fixed d, unidirectional stepped displacements of one substrate relative to the other were performed in 15-min intervals using a micrometric screw, with visual and spectral monitoring of the orientation of the sample at the end of each interval. Spectral monitoring consisted of measuring the dependence $D_e(\nu_k,l)$ of the optical density of the IR absorption bands for the extraordinary light wave, polarized in the **Ns** plane, as a function of the shift l of the substrate. Here **N** is the normal to the cell surface and is parallel to the direction of propagation of the light wave, and **s** is the direction of the relative displacement of the substrates. The dependences $D_e(\nu_k,l)$ are presented in Fig. 1 for a number of absorption bands. Saturation of these dependences, which corresponds to a planar orientation of the director **n** and the equality $D_e(\nu_k,l_c)=D_{\parallel}(\nu_k)$, is observed for $l_c\approx 50d$. For orthoscopic observation in crossed prisms, such a sample with an area of several square centimeters is a uniformly colored domain, a fragment of which is displayed in Fig. 2. For an ordinary light wave polarized in a direction normal to the plane **Ns**, the position and optical density $D_{\perp}(\nu_k,l)$ of the IR absorption bands do not change in the process of orienting the LC and are identical to those for the initial homeotropic and final planar orientations. This is illustrated in Fig. 3. The spectra were obtained on an automated Specord M82-57 spectrophotometer with multiscanning and subsequent averaging.

For $d=10$–20 μm the planar orientation of the discotic remains stable for many hours. As d decreases or the temperature approaches the D_{ho}–I transition temperature, the relaxation time of the planar-oriented sample in an unoriented state decreases rapidly. With increasing $d>20$ μm, the uniformity of the initial homeotropic sample and of the planar-oriented sample obtained from it degrades. The results presented below are for temperature $\Delta T=T_{ID}-T=22.3$ K, far from the $D_{ho}-I$ transition.

3. The displacement of the maxima ν_{mj} of the IR absorption bands of the LC, polarized parallel ($j=\parallel$) and perpendicular ($j=\perp$) to the director, relative to their positions ν_{mi} in the isotropic phase is determined by the order parameter S of the molecules, the anisotropy $\tau=(L_{\parallel}-L_{\perp})/3$ of the Lorentz tensor **L** of the LC, and the angle β

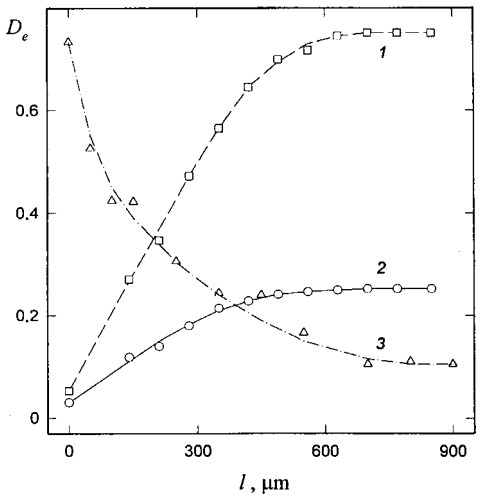

FIG. 1. Optical density $D_e(\nu)$ of the LC THE7 at $T=70.2°$ for the extraordinary light wave as a function of the relative shift l of the substrates for $\nu=830$ and 865 cm^{-1} (*1* and *2*, KBr cell, $d=12.4$ μm) and $\nu=1616$ cm^{-1} (*3*, CaF_2 cell, $d=17.6$ μm). The curves are interpolations.

between the transition dipole moment **d** and the molecular axis **I**. For all isolated absorption bands of THE7 the expected inequality $\nu_{m\perp}>\nu_{mi}$ is satisfied[6] irrespective of the value of β. The bands presented in Fig. 4, $\nu_{mi}^{(1)}=780$, $\nu_{mi}^{(2)}=811$, $\nu_{mi}^{(3)}=836$, $\nu_{mi}^{(4)}=869.5$, and $\nu_{mi}^{(5)}=908$ cm^{-1}, are characterized by different values of β, where for the strongest bands $\beta_2>54.7°>\beta_4>\beta_3\approx 0$. These inequalities correspond to the ratios

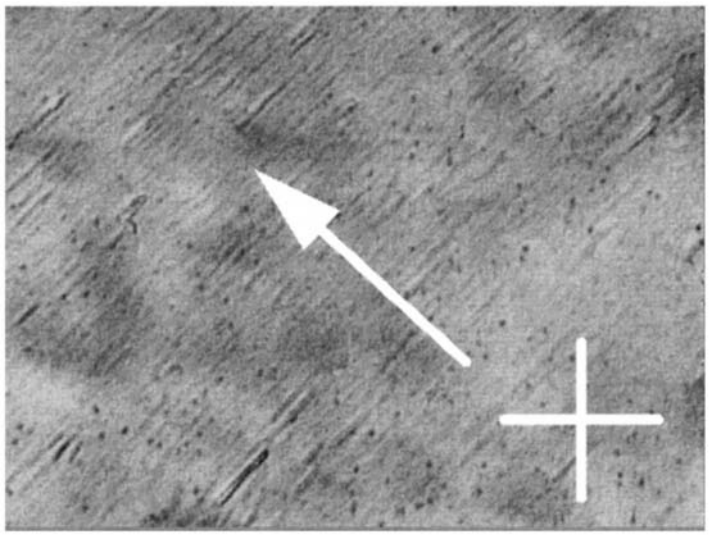

FIG. 2. Texture of the planar-oriented discotic THE7 in crossed prisms, indicated by the cross. The arrow shows the direction of the relative shift of the substrates $\mathbf{s}\parallel\mathbf{n}$.

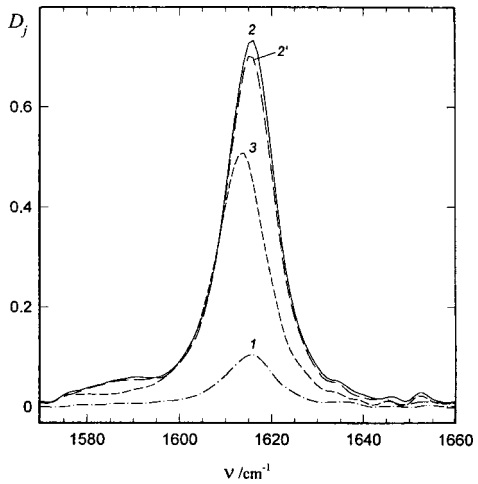

FIG. 3. Polarized components $D_j(\nu)$ of the absorption band of the LC THE7 with $j=\parallel$ (*1*), $\perp$ (*2,2′*) for a sample with planar (*1,2*) and homeotropic (*2′*) orientation and in the isotropic phase (*3*, CaF_2 cell, $d=17.6$ μm).

$\nu_{mi}^{(n)} > \nu_{m\parallel}^{(n)}$ for $n=2-4$ and $\Delta\nu^{(3)} > \Delta\nu^{(4)}$, which are expected for a discoidal LC.[6] Here $\Delta\nu^{(n)} = \nu_{mi}^{(n)} - \nu_{m\parallel}^{(n)}$. The values $\Delta\nu^{(3)} = 6.6$ and $\Delta\nu^{(4)} = 4.2$ cm^{-1} demonstrate the first reliable observation of the splitting of polarized intrinsic absorption bands of a LC as a result of resonant dipole–dipole intermolecular interactions. This splitting is similar in nature to the Davydov splitting of polarized excitonic-absorption bands in molecular crystals.[7,10] High values of S and low values of β in discoidal LCs is optimal for observing this effect in uniaxial LCs,[6] as the present experiment confirms.

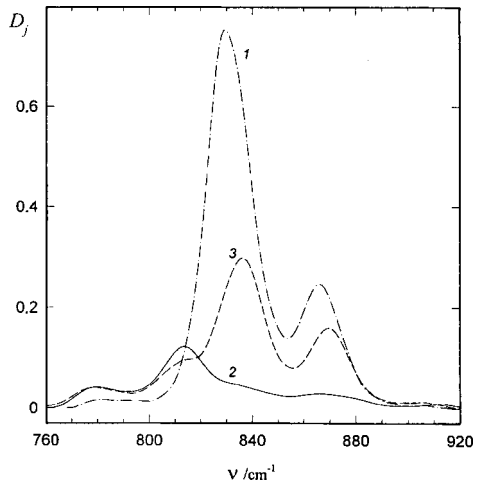

FIG. 4. Polarized components $D_j(\nu)$ of the absorption bands of the LC THE7 (KBr cell, $d=12.4$ μm). The labels are the same as in Fig. 3.

It is seen in Fig. 3 that another unusual relation $\nu_{m\parallel}=\nu_{m\perp}>\nu_{mi}$, possible in discoidal LCs for $\beta\leqslant 90°$ and high values of S and τ,[6] is satisfied. The absorption band $\nu_{mi}^{(6)}=1613.5\ \mathrm{cm}^{-1}$ corresponds to vibrations of the molecular core of THE7 with $\beta\approx 90°$ and is optimal for observing this effect; in addition, the inequality $\Delta\nu^{(3)}\approx|\Delta\nu^{(6)}|$ agrees with expectations.[6]

Thus, polarized absorption of a planar-oriented discotic D_{ho} demonstrates some highly characteristic spectral features which qualitatively distinguish uniaxial discoidal LCs from uniaxial calamitic LCs (formed by rod-shaped molecules) and are due to the difference of the local symmetry of these objects.[6] The relations $\nu_{m\perp}>\nu_{mi}>\nu_{m\parallel}$ and $\nu_{mj}>\nu_{mi}$ observed for the two-dimensional crystal D_{ho} correct the widely held belief that the absorption bands undergo a ''red'' Lorentz shift when the liquid crystallizes.

4. The isolated group of bands $\nu^{(1)}-\nu^{(5)}$ noted above and the band $\nu^{(6)}$ were used to determine the components L_j. The transition from a dilute solution of THE7 in CCl_4 to the isotropic phase of the LC is accompanied by a low-frequency shift of the bands $\nu^{(1)}-\nu^{(5)}$ and by a change in their relative intensities and half-widths. This attests to the presence of mixing of the corresponding molecular vibrations in the LC as a result of local-field effects.[8] With this mixing taken into account, the components L_j can be found from the system of equations[8]

$$\mathrm{Tr}\,\mathbf{L}=1,\quad N_2g_2(N_1g_1+2)=3, \tag{1}$$

where $N_1=D_\parallel/D_\perp$ and $N_2=D_\perp/D_i$ are the dichroic ratios of the integrated optical densities D_j of the entire group of bands $\nu^{(1)}-\nu^{(5)}$,

$$g_1=\frac{n_{b\parallel}}{n_{b\perp}}\left(\frac{f_{b\perp}}{f_{b\parallel}}\right)^2,\quad g_2=\frac{\rho_i n_{b\perp}}{\rho n_{bi}}\left(\frac{f_{bi}}{f_{b\perp}}\right)^2, \tag{2}$$

n_{bj} are the background refractive indices for the group of bands under study, $f_{bj}=1+L_j(n_{bj}^2-1)$ are the background components of the local-field tensor f_b, and ρ and ρ_i are the densities of the liquid-crystal and isotropic phases. The values $n_{b\parallel}=1.452$, $n_{b\perp}=1.527$ ($\Delta T=22.3$ K) and $n_{bi}=1.487$ ($\Delta T=-10$ K) were measured in the transmission region of the LC, $\nu=1900-2500\ \mathrm{cm}^{-1}$, by an interference method using a Ge cell. The ratio $\rho/\rho_i=1.026$ was measured for the same values of ΔT. The parameters in system (1) are $L_\parallel=0.679$, $L_\perp=0.161$, $g_1=0.457$, and $g_2=1.338$.

The components L_j for the band $\nu^{(6)}$ were determined by three different methods. The first method uses the system of equations (1) with the parameters $N_1^*=\delta_1N_1$ and $N_2^*=\delta_2N_2$, where the corrections[8]

$$\delta_1=\frac{1+D_\parallel^{(7)}/D_\parallel^{(6)}}{1+D_\perp^{(7)}/D_\perp^{(6)}}\quad\text{and}\quad\delta_2=\frac{1+D_\perp^{(7)}/D_\perp^{(6)}}{1+D_i^{(7)}/D_i^{(6)}} \tag{3}$$

take into account the mixing of the $\nu^{(6)}$ band with the intense $\nu_{mi}^{(7)}=1507\ \mathrm{cm}^{-1}$ band, for which $\beta_7=\beta_6$. The values $\delta_1\approx 1$ and $\delta_2=0.8$ were obtained for the experimental conditions corresponding to Fig. 3. Using these parameters in Eq. (1) gives the following values: $L_\parallel=0.642$, $L_\perp=0.179$, $g_1=0.498$, $g_2=1.285$, and $SS_\beta=-0.447$. For $\beta_6=90°$ we obtain hence $S=0.894$ and $\tau_0=\tau(S=1)=0.173$.

The local-field parameters presented above are very sensitive to the mixing of the bands $\nu^{(6)}$ and $\nu^{(7)}$. The approximation $\delta_{1,2}=1$ gives almost isotropic values

$L_{\parallel}=0.391$, $L_{\perp}=0.305$, $g_1=0.915$, and $g_2=0.997$ and strongly underestimated values $S=0.809$ and $\tau_0=0.035$. The latter two values correspond to the inequalities $\nu_{m\parallel}^{(6)} > \nu_{mi}^{(6)} > \nu_{m\perp}^{(6)}$ (Ref. 6), which contradict Fig. 3.

The second method of determining the components L_j uses the equality $\nu_{m\parallel} = \nu_{m\perp}$, which is equivalent to the equation[6]

$$N_1^* \frac{n_{b\perp} f_{b\perp}}{n_{b\parallel} f_{b\parallel}} = \frac{L_\perp (3n_{b\perp}^2+1)-1}{L_\parallel (3n_{b\parallel}^2+1)-1} \tag{4}$$

or

$$\frac{n_{b\perp}^2 f_{b\parallel}(3-2N_2^* g_2)}{n_{b\parallel}^2 f_{b\perp} N_2^* g_2} = \frac{L_\perp (3n_{b\perp}^2+1)-1}{L_\parallel (3n_{b\parallel}^2+1)-1}, \tag{5}$$

since equating the left-hand sides of Eqs. (4) and (5) gives the second of Eqs. (1). The condition Tr $\mathbf{L}=1$, taken together with Eq. (4), gives $L_{\parallel}=0.645$, $L_{\perp}=0.177$, $g_1=0.495$, $g_2=1.290$, $SS_\beta=(N_1^* g_1-1)/(N_1^* g_1+2)=-0.447$, and $\tau_0=0.175$. Replacing Eq. (4) with Eq. (5) gives close values: $L_{\parallel}=0.640$, $L_{\perp}=0.180$, $g_1=0.501$, $g_2=1.282$, $SS_\beta=1-N_2^* g_2=-0.444$, and $\tau_0=0.173$. In the approximation $N_2^*=N_2$ the system of equations comprising the relation Tr $\mathbf{L}=1$ and Eq. (5) has no physical roots L_j, which likewise signifies the need to take into account the mixing of the bands $\nu^{(6)}$ and $\nu^{(7)}$.

The third method of determining the components L_j is to use the second equation from Eqs. (1) and Eq. (4) or (5), which makes it possible to avoid the *a priori* assumption that Tr $\mathbf{L}=1$. The results are $L_{\parallel}=0.663$, $L_{\perp}=0.179$, Tr$\mathbf{L}=1.021$, $g_1=0.485$, $g_2=1.285$, $S=0.894$, and $\tau_0=0.180$. Thus one finds that the condition Tr $\mathbf{L}=1$ holds within the limits of experimental accuracy; this has been a matter of dispute in the molecular-statistical theory.[7]

5. The results presented above, which were obtained on planar-oriented samples in cells consisting of different materials and by different methods and for different groups of bands give nearly the same values: $L_{\parallel}=0.66\pm0.02$, $L_{\perp}=0.17\pm0.01$, $g_1=0.48\pm0.02$, and $g_2=1.31\pm0.03$. The quantity $S=0.890\pm0.004$ agrees with the NMR data $S=0.88\pm0.92$ (Refs. 5 and 11) for the homolog THE6 for the same value of ΔT. The ratio of the components $f_{b\parallel}=1.73$ and $f_{b\perp}=1.23$ of the local-field tensor corresponds to a higher electric conductivity of the discotic D_{ho} along the columns[5] and is opposite to the ratio of these components in uniaxial calamitic LCs.[7] The experimental value $\tau_0=0.18\pm0.01$ is greater than the estimated values of this parameter[1] which admit the possibility of a polar phase of the discoidal nematic, and it lowers the corresponding minimum required value of the constant molecular dipole moment along the **I** axis. However, the value of τ_0 obtained is less than the theoretical value $\tau_0^*=0.227$ calculated for THE7 using Eq. (4) of Ref. 12, with allowance for the orientational ordering of the molecules and the experimental values[13] of the column diameter $2a_t=21.94$ Å and the intermolecular distance in the column $2a_l=3.59$ Å. Since the value of τ_0^* neglects the translational ordering of the molecules in the columns and the two-dimensional ordering of the columns themselves, the relation $\tau_0^* > \tau_0$ indicates that the anisotropy of the tensor **L** is lower in the D_{ho} phase on account of the difference of the discotic and nematic ordering of the molecules.

The method proposed here for obtaining and monitoring planar-oriented samples of a discotic LCs greatly expands the possibilities of investigating the structure and properties of these objects by polarized absorption spectroscopy, Raman scattering, and luminescence methods.

This work was supported by the Russian Fund for Fundamental Research (Grant 97-03-33719) and the State Scientific and Technical Program ''Fundamental Spectroscopy'' (Grant 2.3).

*)e-mail: aver@iph.krasnoyarsk.su

[1] P. Palffy-Muhorray, V. A. Lee, and R. G. Petschek, Phys. Rev. Lett. **60**, 2303 (1988).
[2] C. Ayton and G. N. Patey, Phys. Rev. Lett. **76**, 239 (1996).
[3] J. J. Weis, D. Levesque, and G. J. Zarragoicoechea, Phys. Rev. Lett. **69**, 913 (1992).
[4] C. Ayton, D. Q. Wei, and G. N. Patey, Phys. Rev. E **55**, 447 (1997).
[5] S. Chandrasekhar, Handb. Liq. Cryst. B **2**, 749 (1998).
[6] E. M. Aver'yanov, JETP Lett. **66**, 847 (1997); Opt. Zh. **65**(7), 5 (1998).
[7] E. M. Aver'yanov and M. A. Osipov, Usp. Fiz. Nauk **160**(5), 89 (1990); **160**(10), 206 (1990) [Sov. Phys. Usp. **33**, 365, 880 (1990)].
[8] E. M. Aver'yanov, Zh. Éksp. Teor. Fiz. **108**, 258 (1995) [JETP **81**, 139 (1995)].
[9] M. Ghabria, M. Cagnon, and G. Durand, J. Phys. (France) Lett. **46**, L-683 (1985).
[10] V. M. Agranovich, Usp. Fiz. Nauk **112**, 143 (1974) [Sov. Phys. Usp. **17**, 103 (1974)].
[11] X. Shen, R. Y. Dong, N. Boden *et al.*, J. Chem. Phys. **108**, 4324 (1998).
[12] E. M. Aver'yanov, Zh. Éksp. Teor. Fiz. **110**, 1820 (1996) [JETP **83**, 1000 (1996)].
[13] A. M. Levelut, J. Phys. (France) Lett. **40**, L-81 (1981).

Translated by M. E. Alferieff

Piezomagnetism and stress-induced paramagnetic Meissner effect in mechanically loaded high-T_c granular superconductors

S. A. Sergeenkov

Theoretische Physik, ETH–Hönggerberg, 8093 Zürich, Switzerland; Bogoliubov Laboratory of Theoretical Physics, Joint Institute for Nuclear Research, 141980 Dubna, Russia

(Submitted 24 May 1999)
Pis'ma Zh. Éksp. Teor. Fiz. **70**, No. 1, 36–41 (10 July 1999)

Two novel phenomena in a weakly coupled granular superconductor under an applied stress are predicted on the basis of a recently suggested piezophase effect (a macroscopic quantum analog of the piezoelectric effect). Namely, the existence of a stress-induced paramagnetic moment in zero applied magnetic field (piezomagnetism) is considered, and its influence on the low-field magnetization (leading to a mechanically induced paramagnetic Meissner effect) is investigated. The conditions under which these effects can be experimentally measured in high-T_c granular superconductors are discussed.
 [S0021-3640(99)00713-6]

PACS numbers: 74.80.Bj, 74.72.−h, 74.25.Ha

Despite the fact that granular superconductors have been actively studied for decades, they continue to contribute to the variety of intriguing and peculiar phenomena (both of fundamental interest and important for potential applications), while at the same time providing a useful tool for testing new theoretical ideas.[1] To give just a few recent examples, it is sufficient to mention paramagnetic Meissner effect (PME),[2,3] which originates from cooperative behavior of weak-link-mediated orbital moments in high-T_c granular superconductors (HTGS). Among others are the recently introduced thermophase[4,5] and piezophase[6] effects, suggesting, respectively, a direct influence of a thermal gradient and an applied stress on the phase difference between adjacent grains. Besides, two dual effects in HTGS, the formation of magnetic-field-induced electrical polarization (magnetoelectric effect)[7] and the existence of electric-field-induced magnetization (inverse magnetoelectric effect)[8] have been predicted.

In this letter we discuss the possibility of two other interesting effects which are expected to occur in a granular material under mechanical loading. Specifically, we predict the existence of a stress-induced paramagnetic moment in zero applied magnetic field (piezomagnetism) and its influence on the low-field magnetization (leading to a mechanically induced PME).

The possibility of observing tangible piezoeffects in mechanically loaded grain-boundary Josephson junctions (GBJJs) is based on the fact that under plastic deformation,

grain boundaries (GBs) (which are the natural sources of weak links in HTGS), move rather rapidly via the movement of the grain boundary dislocations (GBDs) comprising these GBs.[9–11] Using the above evidence, Ref. 6 considered the *piezophase* response to an applied stress of a single GBJJ (created by the GBD strain field ϵ_d, acting as an insulating barrier of thickness l and height U in a SIS-type junction with the Josephson energy $J \propto e^{-l\sqrt{U}}$). To understand how piezoeffects manifest themselves through GBJJs, let us invoke an analogy with the so-called *thermophase effect*[4,5] (a quantum mechanical alternative for the conventional thermoelectric effect) in JJs. In essence, the thermophase effect assumes a direct coupling between an applied temperature drop ΔT and the resulting phase difference $\Delta\phi$ across a JJ. When a rather small temperature gradient is applied to a JJ, an entropy-carrying normal current $I_n = L_n \Delta T$ (where L_n is the thermoelectric coefficient) is generated through the junction. To satisfy the constraint dictated by the Meissner effect, the resulting supercurrent $I_s = I_c \sin[\Delta\phi]$ (with $I_c = 2eJ/h$ being the Josephson critical current) develops a phase difference across a weak link. The normal current is locally canceled by a counterflow of supercurrent, so that the total current through the junction $I = I_n + I_s = 0$. As a result, supercurrent $I_c \sin[\Delta\phi] = -I_n = -L_n \Delta T$ generates a nonzero phase difference leading to the linear thermophase effect[4,5] $\Delta\phi \simeq -L_{tp}\Delta T$ with $L_{tp} = L_n / I_c(T)$.

By analogy, we can introduce a *piezophase effect* (as a quantum alternative for the conventional piezoelectric effect) across a JJ.[6] Indeed, the linear conventional piezoelectric effect relates the induced polarization P_n to an applied strain ϵ as $P_n = d_n \epsilon$, where d_n is the piezoelectric coefficient.[12] The corresponding normal piezocurrent density is $j_n = dP_n/dt = d_n \dot{\epsilon}$, where $\dot{\epsilon}(\sigma)$ is the rate of plastic deformation, which depends on the number of GBDs of density ρ and a mean dislocation velocity v_d as follows:[13] $\dot{\epsilon}(\sigma) = b\rho v_d(\sigma)$ (where b is the absolute value of the appropriate Burgers vector). In turn, $v_d(\sigma) \simeq v_0(\sigma/\sigma_m)$. To meet the requirements imposed by the Meissner effect, in response to the induced normal piezocurrent, a corresponding Josephson supercurrent of density $j_s = dP_s/dt = j_c \sin[\Delta\phi]$ should emerge within the contact. Here $P_s = -2enb$ is the induced polarization of the Cooper pair, where n is the pair number density and $j_c = 2ebJ/\hbar V$ is the critical current density. The neutrality conditions ($j_n + j_s = 0$ and $P_n + P_s = \text{const}$) will then lead to a linear piezophase effect $\Delta\phi \simeq -d_{pp}\dot{\epsilon}(\sigma)$ (with $d_{pp} = d_n/j_c$ being the piezophase coefficient) and a concomitant change of the pair number density under an applied strain, viz., $\Delta n(\epsilon) = d_{pn}\epsilon$, with $d_{pn} = d_n/2eb$.

Given the markedly different mechanisms and scales of stress-induced changes in defect-free thin films[14] and weak-link-ridden ceramics,[15] it should be possible to register experimentally the piezophase effects suggested here (see below).

To describe adequately the magnetic properties of a granular superconductor, we employ a model of a *random* three-dimensional (3D) overdamped (JJ) array, which is based on the well-known tunneling Hamiltonian[16,17]

$$\mathscr{H} = \sum_{ij}^{N} J(r_{ij})[1 - \cos\phi_{ij}], \tag{1}$$

where $\{i\} = \mathbf{r}_i$ is a 3D lattice vector, N is the number of grains (or weak links), $J(r_{ij})$ is

the Josephson coupling energy, with $\mathbf{r}_{ij}=\mathbf{r}_i-\mathbf{r}_j$ the separation between the grains; the gauge-invariant phase difference is defined as $\phi_{ij}=\phi_{ij}^0-A_{ij}$, where $\phi_{ij}^0=\phi_i-\phi_j$, with ϕ_i being the phase of the superconducting order parameter, and

$$A_{ij}=\frac{2\pi}{\Phi_0}\int_i^j \mathbf{A}(\mathbf{r})\cdot d\mathbf{l}$$

being the frustration parameter, with $\mathbf{A}(\mathbf{r})$ the electromagnetic vector potential, which involves both external fields and possible self-field effects (see below).

In the present paper, we consider a long-range interaction between grains[5,7,8,16,17] (with $J(r_{ij})=J$) and model the true short-range behavior of a HTGS sample through the randomness in the position of the superconducting grains in the array (see below).

According to the above-discussed scenario, under mechanical loading the superconducting phase difference will acquire an additional contribution $\delta\phi_{ij}(\sigma)=-B\boldsymbol{\sigma}\cdot\mathbf{r}_{ij}$, where $B=d_n\dot{\epsilon}_0/\sigma_m j_c b$, with $\dot{\epsilon}_0=b\rho v_0$ being the maximum deformation rate and the other parameters as defined earlier. If, in addition to the external loading, the network of superconducting grains is under the influence of an applied frustrating magnetic field $\mathbf{H}$, the total phase difference across the contact reads

$$\phi_{ij}(\mathbf{H},\boldsymbol{\sigma})=\phi_{ij}^0+\frac{\pi}{\Phi_0}(\mathbf{r}_{ij}\wedge\mathbf{R}_{ij})\cdot\mathbf{H}-B\boldsymbol{\sigma}\cdot\mathbf{r}_{ij}, \tag{2}$$

where $\mathbf{R}_{ij}=(\mathbf{r}_i+\mathbf{r}_j)/2$.

To be able to neglect the influence of the self-field effects[7,8,17] in a real material, the corresponding Josephson penetration length λ_J must be much larger than the junction (or grain) size. Specifically, this condition will be satisfied for short junctions with the size $d\ll\lambda_J$, where $\lambda_J=\sqrt{\Phi_0/4\pi\mu_0 j_c\lambda_L}$, with λ_L being the grain London penetration depth and j_c its Josephson critical current density. In particular, since $\lambda_L\simeq 150\,\mathrm{nm}$ in HTGS, the above criterion will be well met for $d\simeq 1\ \mu\mathrm{m}$ and $j_c\simeq 10^4\,\mathrm{A/m^2}$, which are typical parameters for HTGS ceramics.[1] Likewise, to ensure the uniformity of the applied stress σ, we also assume that $d\ll\lambda_\sigma$, where λ_σ is a characteristic length over which σ is kept homogeneous.

When the Josephson supercurrent $I_{ij}^s=I_c\sin\phi_{ij}$ circulates around a set of grains, it induces a random magnetic moment $\boldsymbol{\mu}_s$ of the Josephson network[16]

$$\boldsymbol{\mu}_s\equiv-\frac{\partial\mathscr{H}}{\partial\mathbf{H}}=\sum_{ij} I_{ij}^s(\mathbf{r}_{ij}\wedge\mathbf{R}_{ij}), \tag{3}$$

which results in a stress-induced net magnetization

$$\mathbf{M}_s(\mathbf{H},\boldsymbol{\sigma})\equiv\frac{1}{V}\langle\boldsymbol{\mu}_s\rangle=\int_0^\infty d\mathbf{r}_{ij}d\mathbf{R}_{ij}f(\mathbf{r}_{ij},\mathbf{R}_{ij})\boldsymbol{\mu}_s, \tag{4}$$

where V is the volume of the sample and f is the joint probability distribution function (see below). To capture the essence of the superconducting piezomagnetic effect, in what follows we assume for simplicity that an *unloaded sample* does not possess any spontaneous magnetization at zero magnetic field (that is $M_s(0,0)=0$) and that its Meissner

response to a small applied field H is purely diamagnetic (that is $M_s(H,0)\simeq -H$). According to Eq. (2), this condition implies $\phi_{ij}^0=2\pi m$ for the initial phase difference, with $m=0,\pm 1,\pm 2,...$

In order to obtain an explicit expression for the piezomagnetization, we consider a site positional disorder that allows for small random radial displacements. Namely, the sites in a 3D cubic lattice are assumed to move from their equilibrium positions according to the normalized distribution function $f(\mathbf{r}_{ij}\mathbf{R}_{ij})\equiv f_r(\mathbf{r}_{ij})f_R(\mathbf{R}_{ij})$. For simplicity we assume an exponential distribution law for the distance between grains, $f_r(\mathbf{r})=f(x)f(y)f(z)$ with $f(x_j)=(1/d)e^{-x_j/d}$ (which reflects the short-range character of the Josephson coupling in granular superconductors)[5] and some short-range distribution for the dependence of the center-of-mass probability $f_R(\mathbf{R})$ (around some constant value D).

Taking the applied stress to be along the x axis, $\boldsymbol{\sigma}=(\sigma,0,0)$, normal to the applied magnetic field $\mathbf{H}=(0,0,H)$, we get finally

$$M_s(H,\sigma)=-M_0(\sigma)\frac{H_{\rm tot}(H,\sigma)/H_0}{[1+H_{\rm tot}^2(H,\sigma)/H_0^2]^2}, \tag{5}$$

for the induced transverse magnetization (along the z axis), where $H_{\rm tot}(H,\sigma)=H-H^*(\sigma)$ is the total magnetic field, with $H^*(\sigma)=[\sigma/\sigma_0(\sigma)]H_0$ being the stress-induced contribution. Here, $M_0(\sigma)=I_c(\sigma)SN/V$, where $S=\pi dD$ is the projected area around the Josephson contact, $H_0=\Phi_0/S$, and $\sigma_0(\sigma)=\sigma_m[j_c(\sigma)/j_d](b/d)$, with $j_d=d_n\dot{\epsilon}_0$ and $\dot{\epsilon}_0=b\rho v_0$ being the maximum values of the dislocation current density and the plastic deformation rate, respectively. According to the recent experiments[15] the tunneling-dominated critical current I_c (and its density j_c) in HTGS ceramics was found to increase exponentially under compressive stress, viz., $I_c(\sigma)=I_c(0)e^{\beta\sigma}$, with $\beta\simeq 1/\sigma_m$. Specifically, the critical current at $\sigma=9$ kbar was found to be three times higher than its value at $\sigma=1.5$ kbar, clearly indicating a weak-link-mediated origin of the phenomenon (in the best defect-free thin films this ratio is controlled by the stress-induced modifications of the carrier number density and practically never exceeds a few percent).[14] Strictly speaking, the critical current will also change (decrease) with applied magnetic field. However, for the fields under discussion (see below) this effect can be neglected to a first approximation. In view of Eq. (5), the dependence of I_c on σ will lead to rather strong piezomagnetic effects. Indeed, Fig. 1 shows the changes of the initial stress-free diamagnetic magnetization M_s/M_c (solid line) under an applied stress σ/σ_c. Here $M_c\equiv M_0(0)$ and $\sigma_c\equiv\sigma_0(0)$ (see below for estimates). As we see, even relatively small values of an applied stress render the low-field Meissner phase strongly paramagnetic (dotted and dashed lines), simultaneously increasing the maximum of the magnetization and shifting it towards higher magnetic fields. According to Eq. (5), the initially diamagnetic Meissner effect turns paramagnetic as soon as the piezomagnetic contribution $H^*(\sigma)$ exceeds the applied magnetic field H. To see whether this can actually happen in a real material, let us estimate a magnitude of the piezomagnetic field H^*. Typically[2,3,18] for HTGS ceramics one has $S\approx 10\ \mu\text{m}^2$, leading to $H_0\simeq 1$G. To estimate the needed value of the dislocation current density j_d, we turn to the available experimental data. According to Ref. 10, a rather strong polarization under compressive pressure $\sigma/\sigma_m\simeq 0.1$ was observed in YBCO ceramic samples at $T=77$ K yielding $d_n=10^2\ \text{C/m}^2$ for the piezoelectric coefficient. Usually[6,9,11] for GBJJs one has

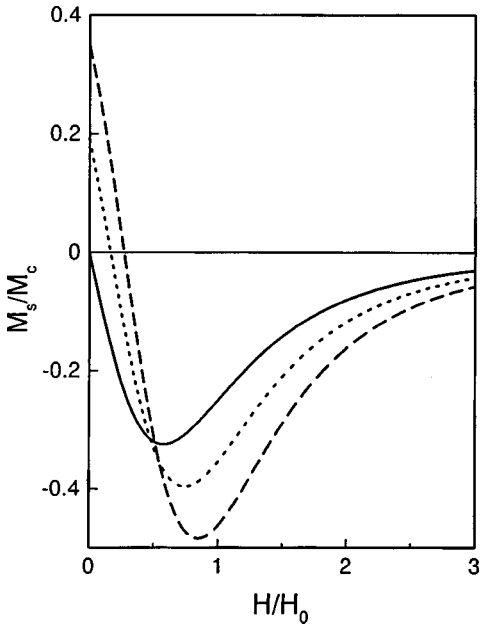

FIG. 1. The reduced magnetization M_s/M_c as a function of the reduced applied magnetic field H/H_0, according to Eq. (5) for different values of reduced applied stress: $\sigma/\sigma_c=0$ (solid line), $\sigma/\sigma_c=0.01$ (dotted line), and $\sigma/\sigma_c=0.05$ (dashed line) .

$\dot{\epsilon}_0 \simeq 10^{-2}\,\mathrm{s}^{-1}$ and $b \simeq 10\,\mathrm{nm}$, leading to $j_d = d_n \dot{\epsilon}_0 \simeq 1\,\mathrm{A/m}^2$ for the maximum dislocation current density. Using the typical values of the critical current density $j_c(\sigma) = 10^4\,\mathrm{A/m}^2$ (found Ref. 15 for $\sigma/\sigma_m \simeq 0.1$) and grain size $d \simeq 1\,\mu\mathrm{m}$, we arrive at the following estimate of the piezomagnetic field: $H^* \simeq 10^{-2} H_0$. Thus the predicted stress-induced paramagnetic Meissner effect should be observable for applied magnetic fields $H \simeq 10^{-2} H_0 \simeq 0.01\,\mathrm{G}$, which correspond to the region where the original PME was first registered.[2,3]

In turn, the piezoelectric coefficient d_n is related to a charge Q in the GBJJ as $d_n = (Q/S)(d/b)^2$ (Ref. 18). Given the above-obtained estimates, we get $Q \simeq 10^{-13}\,\mathrm{C}$ for the effective charge accumulated by the GBs. Notice that the above values of the applied stress σ and the resulting effective charge Q correspond (via the so-called electroplastic effect)[18] to an equivalent applied electric field $E = b^2\sigma/Q \simeq 10^7\,\mathrm{V/m}$ at which rather pronounced electric-field-induced effects in HTGS have recently been observed.[1,8]

Besides, according to Ref.15 the Josephson projected area S decreases slightly under pressure, thus leading to some increase of the characteristic field $H_0 = \Phi_0/S$. In view of Eq. (5), it means that a smaller compressive stress is needed to actually reverse the sign of the induced magnetization M_s. Furthermore, if an unloaded granular superconductor already exhibits the PME, due to the orbital-current-induced spontaneous magnetization resulting from an initial phase difference $\phi_{ij}^0 = 2\pi r$ in Eq. (2) with fractional r (in particular, $r=1/2$ corresponds to the so-called[2,3] π-type state), then according to our scenario this effect will either be further enhanced by applying a compression (with $\sigma > 0$) or will disappear under a strong enough extension (with $\sigma < 0$). Though the par-

ticular form of $M_s(H,\sigma)$ obtained in this paper may change slightly (due mainly to effects neglected here, viz., the field dependence of the critical current and self-field effects), the above-estimated range of accessible parameters still suggests quite an optimistic possibility of observing the predicted effects experimentally in HTGS ceramics.

This work was done during my stay at ETH-Zürich and was funded by the Swiss National Science Foundation. I thank Professor T. M. Rice for hospitality and stimulating discussions on the subject.

[1] For recent reviews on the subject, see, e.g., *Mesoscopic and Strongly Correlated Electron Systems*, edited by. V. F. Gantmakher and M. V. Feigel'man, Phys. Usp. **41**, N2 (1998).
[2] F. V. Kusmartsev, Phys. Rev. Lett. **69**, 2268 (1992).
[3] M. Sigrist and T. M. Rice, Rev. Mod. Phys. **67**, 503 (1995).
[4] G. D. Guttman, B. Nathanson, E. Ben-Jacob *et al.*, Phys. Rev. B **55**, 12691 (1997).
[5] S. Sergeenkov, JETP Lett. **67**, 680 (1998).
[6] S. Sergeenkov, J. Phys.: Condens. Matter **10**, L265 (1998).
[7] S. Sergeenkov, J. Phys. I France **7**, 1175 (1997).
[8] S. A. Sergeenkov and J. V. José, Europhys. Lett. **43**, 469 (1998).
[9] E. Z. Meilikhov and R. M. Farzetdinova, JETP Lett. **65**, 32 (1997).
[10] T. J. Kim, E. Mohler, and W. Grill, J. Alloys Compd. **211/212**, 318 (1994).
[11] V. N. Kovalyova, V. A. Moskalenko, V. D. Natsik *et al.*, Fiz. Nizk. Temp. **17**, 24 (1991) [Sov. J. Low Temp. Phys. **17**, 46 (1991)].
[12] L. D. Landau and E. M. Lifshitz, *Electrodynamics of Continuous Media*, Pergamon Press, New York, 1984.
[13] A. H. Cottrell, *Dislocations and Flow in Crystals*, Clarendon Press, Oxford, 1953.
[14] G. L. Belenky, S. M. Green, A. Roytburd *et al.*, Phys. Rev. B **44**, 10117 (1991).
[15] A. I. D'yachenko, V. Yu. Tarenkov, A. V. Abalioshev *et al.*, Physica C **251**, 207 (1995).
[16] V. M. Vinokur, L. B. Ioffe, A. I. Larkin *et al.*, Zh. Éksp. Teor. Fiz. **93**, 343 (1987) [Sov. Phys. JETP **66**, 198 (1987)].
[17] G. Blatter, M. V. Feigel'man, V. B. Geshkenbein *et al.*, Rev. Mod. Phys. **66**, 1125 (1994).
[18] Yu. A. Osip'yan, V. F. Petrenko, A. V. Zaretskij *et al.*, Adv. Phys. **35**, 115 (1986).

Published in English in the original Russian journal. Edited by Steve Torstveit.

Polarization kinetics of a ferroelectric with complex modulated structure

V. V. Gladkiĭ and V. A. Kirikov
Institute of Crystallography, Russian Academy of Sciences, 117333 Moscow, Russia

(Submitted 27 May 1999)
Pis'ma Zh. Éksp. Teor. Fiz. **70**, No. 1, 42–47 (10 July 1999)

Anomalous changes of the spontaneous polarization, the coercive field, and the spectrum of the distribution of polarization relaxation times in an electric field are detected in the ferroelectric TMA-$ZnCl_4$ at uniaxial pressures in the range where a transition arises to a nonuniform state with several coexisting waves of structural modulation. The anomalies are observed only in quasistatic and weak static fields and are due to a pressure-induced decrease of large potential barriers separating different metastable states of the structure.
 [S0021-3640(99)00813-0]

PACS numbers: 77.84.Jd, 77.22.Ej

$\{N(CH_3)_4\}ZnCl_4$ (TMA-$ZnCl_4$) crystals undergo at atmospheric pressure a sequence of structural phase transitions $Pmcn \rightarrow$ incommensurate phase $\rightarrow P2_1cn \rightarrow P112_1/n \rightarrow P12_1/c1 \rightarrow P2_12_12_1$ at 20, 6.6, 3.3, -92, and $-112\,^{\circ}C$, respectively. Hydrostatic pressure p shifts the temperature of all transitions, and at the critical value $p_c = 1000$ bar the single polar phase $P2_1cn$ with spontaneous polarization P_s along the $a(X)$ crystallographic axis vanishes.[1] Uniaxial pressures σ_{yy} and σ_{zz} perpendicular to the polar X axis completely (and reversibly) suppress ferroelectricity at low (compared with p_c) critical values $\sigma_c \approx 30$ bar, while σ_{xx} has virtually no effect on the temperature of the phase boundaries.[2] The effect is not only sharply anisotropic but it is also strongly nonlinear.[3] X-ray investigations have shown that in the process of suppression of the polar phase at uniaxial pressures $\sigma > 10$ bar a complicated nonuniform state in which several waves of structural modulation coexist, arises in the crystal.[4]

In Refs. 2 and 3 the polarization of the crystal was measured in an ac electric field. Because of long-lived metastable states of the domain structure there is time for only a portion of the volume of the crystal to participate in the polarization, and the measurement data are not the equilibrium values. In the present letter we report the results of an investigation of the polarization and its slow evolution in quasistatic and weak static electric fields for various values of the uniaxial pressure σ_{yy}. Such investigations give an idea of the spectra of the relaxation time distribution in the widest possible range of uniaxial pressures. The investigations were performed in a pressure range where states with multiwave structural modulation arise.

The electric polarization of the crystal and the relaxation of this polarization were measured by a compensation electrometric method using an equal-arm bridge. The volt-

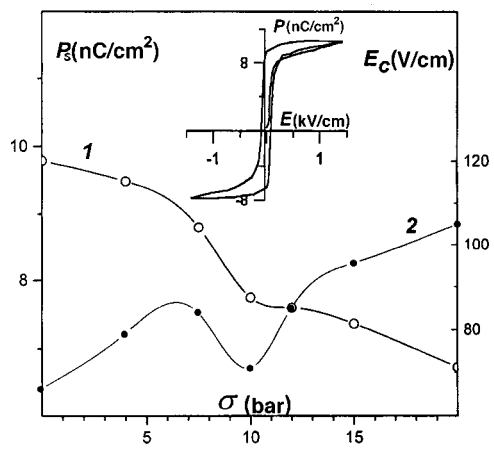

FIG. 1. Spontaneous polarization P_s (*1*) and coercive field E_c (*2*) versus the uniaxial pressure σ for a TMA-$ZnCl_4$ crystal. $T=+5.85$ °C. Inset: Dielectric hysteresis loop for $\sigma=10$ bar.

age sensitivity was 0.1 mV and the charge sensitivity was 10^{-8} μC. Balancing of the voltage across the diagonal of the bridge and detection of the polarization were performed automatically using an electronic arrangement that permits viewing the electric-field and time dependences of the polarization on the monitor screen of a personal computer of the IBM-PC type.[5]

The crystal samples consisted of rectangular bars, whose edges were parallel to the $a(X)$, $b(Y)$, and $c(Z)$ crystallographic axes and were 2, 2.5, and 3.5 mm long, respectively. The faces of a bar which are perpendicular to the polar X axis were polished and coated with an electrically conducting silver paste. The sample was placed in a cryostat with temperature stabilized to within 0.01 K. A uniaxial pressure σ was transferred through a shaft into the cryostat to the sample faces perpendicular to the Y axis.

The spontaneous polarization and coercive field were estimated from the dielectric hysteresis loops with slow, stepped variation of the field. The recording time for one loop was 1.5 h. Recording of the polarization relaxation commenced immediately after a weak static electric field $E=15$ V/cm, a value chosen to be less than the coercive field, was switched on. All measurements were performed at constant temperature $T=5.85$ °C in the existence region of the polar phase, from $+3$ to $+7$ °C. The relaxation was recorded for 3 h, which corresponds to the lower limit of the frequency range of the dispersion of the polarizability, 10^{-5} Hz.

The quasistatic dielectric hysteresis loops of the polarization P versus the electric field E have a clearly expressed rectangular shape with reliably determined values of the spontaneous polarization P_s and coercive field E_c. The hysteresis loop for pressure $\sigma=15$ bar and the curves of P_s and E_c versus σ are presented in Fig. 1. The value $P_s=9.8$ nC/cm^2 at $\sigma=0$ is somewhat higher than the value measured in Ref. 2 in ac fields. As σ increases in the range of low and high values, P_s decreases monotonically but E_c increases. This behavior is, generally speaking, completely understandable. Indeed, the field E decreases the potential barriers U for centers of polarization to the values[6]

$$U = U_0 - 2V_a P_s E, \tag{1}$$

where U_0 are the initial barrier energies (for $E=0$), which in general can also depend on E and σ, and V_a is the activation volume. If the dependence of U_0 on E and σ is weak, i.e., it can be assumed that $U_0 = \text{const}$, then for large $E = E_c$, so that $U = 0$ and a rapid above-barrier polarization process occurs, $P_s E_c = U_0/2V_a = \text{const}$, i.e., the lower P_s, the greater E_c. It is easy to see from Fig. 1 that, indeed, the value $P_s E_c = 6.5$ ergs/cm^3 is the same for $\sigma = 0$ and $\sigma = 20$ bar.

Both dependences $P_s(\sigma)$ and $E_c(\sigma)$, however, have anomalies in the range $\sigma^* = 10$–12 bar: P_s has an inflection point, and E_c has a minimum. It should be noted that new waves of modulation of the structure, corresponding to the two phases adjacent to the polar phase[4] and with amplitudes increasing with σ, appear in the crystal in the same pressure range. This coincidence is probably not accidental, and the anomalies in P_s and E_c are due to a change in the modulation state of the crystal and the interaction energy U of the centers of polarization with one another, defects, and the electric field. Some information about this energy can be obtained by analyzing the experimental data on polarization relaxation in weak fields.

Figure 2 shows the measurement results for the slow relaxation of the polarization $P(t)$ and the dimensionless quantity $y(t) = \Delta P/(P_s - P_0)$ with a weak field $E = 15$ V/cm switched on and for several values of the pressure σ. Here $\Delta P = P_s - P(t)$, $P(t)$ is the measured polarization, and P_0 is the initial polarization (at time $t=0$). A phenomenological analysis of the experimental data was performed just as in Ref. 5, assuming the centers of relaxation to be independent of one another (center nuclei with the direction of P_s corresponding to the applied field). In this case

$$y(t) = \int_0^\infty f(\tau)\exp(-t/\tau)\,d\tau,$$

where $f(t)$ is the normalized distribution function of the relaxation time τ in the crystal, $\int_0^\infty f(\tau)\,d\tau = 1$. If the analytical form of the function $y(t)$ is known, then $f(\tau)$ can be easily found, since $y(t)$ and $\tau^2 f(\tau)$ are, respectively, the Laplace transform and inverse Laplace transform.[5]

The experimental curves $y(t)$ can be described satisfactorily by a power-law function with two parameters a and n:

$$y(t) = 1/(1 + t/a)^n, \tag{2}$$

which, apparently, is a universal empirical temporal law of slow thermally activated relaxation, which we observed previously in other polydomain ferroelectrics (triglycine sulfate[5] and rubidium tetrachlorozincate). Its universality is also indicated by the fact that certain dependences established previously are particular cases of Eq. (2) (see Ref. 5). In Fig. 2 the computed curves $y(t) = \Delta P/P_s$ are drawn using solid lines, and the dots show the experimental data. The relative error $\delta y/y$ of the fit of the function (2) to the data does not exceed 0.5%. The errors in determining the parameters a and n are, respectively, $|\delta a/a| = (1 + t/a)|\delta y/y|/n(t/a) = 2.5\%$ and $|\delta n/n| = |\delta y/y|/n\ln(1 + t/a) = 1\%$.[5] The computational results for a and n for various values of σ and E are presented in Table I.

The law (2) corresponds to the distribution function $f(\tau)$ of the form[5]

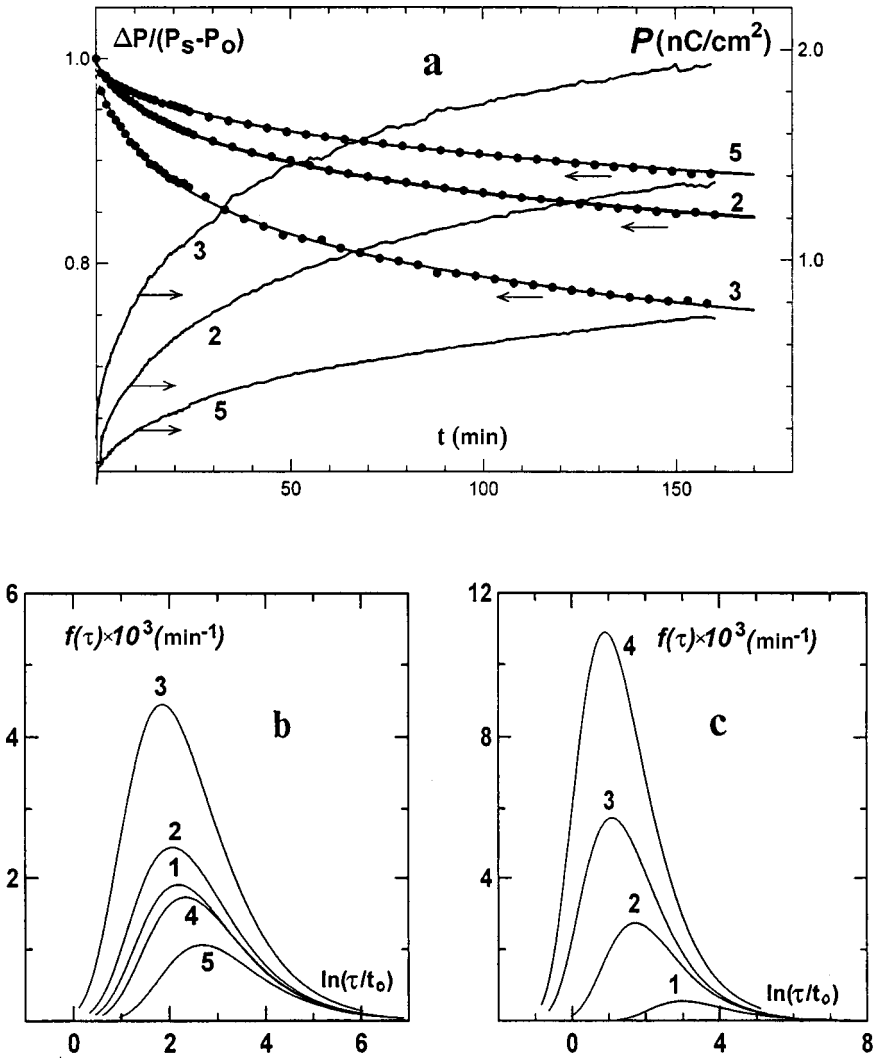

FIG. 2. Relaxation of the polarization $P(t)$ (a) and the spectra $f(\tau)$ of the distribution of the relaxation times of P for various pressures σ (b) and electric fields E (c) for a TMA-$ZnCl_4$ crystal; a, b — $E=15$ V/cm, $\sigma=0$ (*1*), 7.5 (*2*), 12 (*3*), 15 (*4*), 20 bar (*5*); c — $\sigma=0$, $E=5.5$ (*1*), 15 (*2*), 20 (*3*), 25 V/cm (*4*); $t_0=1$ min, $T=+5.85$ °C.

$$f(\tau)=[a^n/\Gamma(n)](1/\tau)^{n+1}\exp(-a/\tau), \tag{3}$$

where $\Gamma(n)$ is the gamma function. Sometimes it is more convenient to use the dimensionless function $g(\tau)=\tau\cdot f(\tau)$, characterizing the distribution density of $\ln\tau$, or the distribution of the potential barriers U for centers, since according to the Arrhenius law $\ln\tau$ and U are related linearly as $\ln(\tau/\tau_0)=U/kT$ (τ_0 is the kinetic constant).[5] The functions $f(\tau)$ and $g(\tau)$ are bell-shaped with maxima at $\tau_m=a/(1+n)$ and $\tau_m=a/n$, respectively.

TABLE I. Relaxation parameters a and n as a function of the electric field E and uniaxial mechanical stress σ.

E, V/cm ($\sigma=0$)	5.5	15	20	25		
a	20.3±0.6	5.76±0.17	3.1±0.1	2.64±0.08		
n,10^{-2}	2.96±0.03	4.19±0.04	4.71±0.05	7.5±0.1		
σ, bar ($E=15$ V/cm)	0	7.5	10	12	15	20
a	24.7±0.7	8.5±0.3	7.6±0.2	6.8±0.2	10.8±0.3	15.4±0.5
n, 10^{-2}	7.43±0.07	5.35±0.05	4.23±0.04	7.93±0.08	4.94±0.05	4.56±0.04

Figure 2 shows spectra of the distribution $f(\tau)$ for various values of σ with $E=15$ V/cm (b) and for various values of E with $\sigma=0$ (c). The variation in $f(\tau)$ as a function of the field E is standard:[5] As E increases, the spectra shift in the direction of lower values of τ. The variation in $f(\tau)$ with pressure is anomalous: As σ increases, the spectra shift nonmonotonically to smaller and then larger values of τ. A plot of $\tau_m=a/(1+n)$, determined from the spectra $f(\tau)$, as a function of σ (Fig. 3) gives a clear picture of this anomaly. It is seen that τ_m has a deep minimum (the reciprocal $1/\tau_m$ has a maximum) for the same values $\sigma^*=10$–12 bar as the anomalies in P_s and E_c in Fig. 1. The quantity τ_m corresponds to the most likely (with maximum distribution density $f_{\max}(\tau)$) energy barrier $U_m=kT\ln(\tau_m/\tau_0)$. According to Eq. (1), the quantity $U_m=(U_0)_m-2V_aP_sE$ and, correspondingly, τ_m can initially decrease with increasing σ if

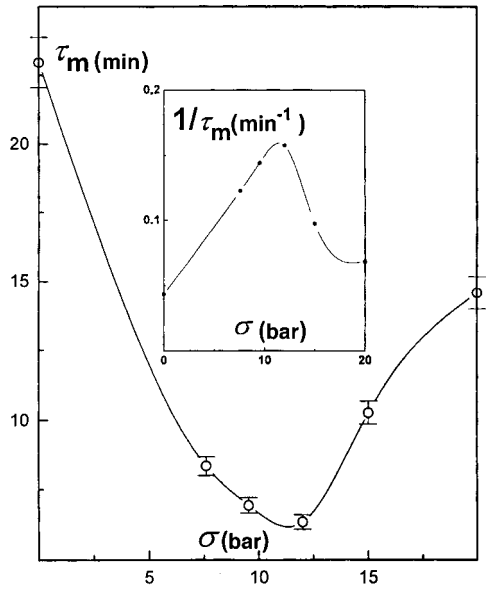

FIG. 3. The relaxation time τ_m, corresponding to the maximum of the distribution $f(\tau)$, versus the uniaxial pressure σ for a TMA-$ZnCl_4$ crystal; $T=+5.85$ °C. Inset: The reciprocal quantity $1/\tau_m$ proportional to the relaxation rate.

the first term $(U_0)_m$ makes the dominant contribution to U_m. This decrease of $(U_0)_m$ (and all U in the spectrum) is much larger in a weak field E, in which the relaxation was recorded, than in a strong field $E > E_c$ (Figs. 1 and 3).

In summary, the structural transformation of the polar phase of a crystal, with P_s decreasing monotonically all the way to zero under uniaxial compression, occurs in the following order. Compression at first decreases the potential barriers U for centers of polarization, and the rate of relaxation of the polarization in a field E increases. At a pressure $\sigma = \sigma^*$ the barrier energy U reaches a minimum, and new waves of structural modulation appear. Under further compression U once again increases, specifically, because of a decrease in the electrostatic interaction PE [see Eq. (1)], and the relaxation rate drops continuously. Such a transformation of the crystal structure under compression is like a phase transition to a different nonuniform state, this transition occurring at the pressure $\sigma = \sigma^*$ for which the energies of the barriers separating different metastable states are minimum. The transition is accompanied by sharp anomalies of the kinetic properties of the crystal. These anomalies are observed only in slowly varying or static electric fields.

This work was supported by the Russian Fund for Fundamental Research (Project No. 99-02-17303).

[1] H. Z. Cummins, Phys. Rep. **185**, (5,6), 211 (1990).
[2] S. N. Kallaev, V. V. Gladkiĭ *et al.*, Zh. Éksp. Teor. Fiz. **96**, 1804 (1990) [Sov. Phys. JETP **71**, 1013 (1990)].
[3] V. V. Gladkii, S. N. Kallayev, and V. A. Kirikov, Ferroelectrics **125**, 171 (1992).
[4] B. Sh. Bagautdinov, V. V. Gladkiĭ, S. N. Kallaev *et al.*, JETP Lett. **59**, 119 (1994).
[5] V. V. Gladkiĭ, V. A. Kirikov, S. V. Nekhlyudov, and E. S. Ivanova, Fiz. Tverd. Tela (St. Petersburg) **39**, 2046 (1997) [Phys. Solid State **39**, 1829 (1997)].
[6] A. K. Tagantsev and A. E. Glasounov, Phase Transit. **65**, 117 (1998).

Translated by M. E. Alferieff

Weak-field Hall resistance and effective carrier density measurements across the metal–insulator transition in Si-MOS structures

V. M. Pudalov*)
P. N. Lebedev Physics Institute Russian Academy of Sciences, 117924 Moscow, Russia

G. Brunthaler, A. Prinz, and G. Bauer
Institut für Halbleiterphysik, Johannes Kepler Universität, Linz, A-4040, Austria

(Submitted 3 June 1999)
Pis'ma Zh. Éksp. Teor. Fiz. **70**, No. 1, 48–52 (10 July 1999)

The weak-field Hall voltage in Si-MOS structures with different mobility is studied on both sides of the metal–insulator transition. In the vicinity of the critical density on the metallic side of the transition, the Hall voltage is found to deviate by 6–20 % from its classical value. The deviation does not correlate with the strong temperature dependence of the diagonal resistivity $\rho_{xx}(T)$. In particular, the smallest deviation in R_{xy} is found in the highest-mobility sample, which exhibits the largest variation in the diagonal resistivity ρ_{xx} with temperature.
 [S0021-3640(99)00913-5]

PACS numbers: 71.30.+h, 73.40.Qv, 73.50.Jt

In the framework of the quasiclassical description of Si-MOS structures,[1] the charge of the inversion layer $Q_{\rm inv}$ is proportional to V_g, as in a plain capacitor formed by the metallic gate and the 2D layer. This prediction was confirmed by the measurements of the Shubnikov–de Haas effect in a perpendicular field.[2] At low temperatures, when the bulk conductance is frozen out and the charge in the depletion layer does not vary with gate voltage, the variation of the capacitor charge with V_g is related to the inversion layer charge only:

$$Q_{\rm inv}=C(V_g-V_t). \tag{1}$$

Here $C=dQ/dV_g$ is the geometric capacitance between the gate and the 2D carrier layer, V_t is determined by the difference in work functions of the Al gate film and the 2D carrier layer, by the energy of the bottom of the lowest subband in the confining potential well, and by the charge trapped in the depletion layer and at the interface.[1] The charge in the Si-MOS structure $Q_{\rm inv}$ was measured directly[3] and was found to be equal (within 2 % uncertainty) to the charge of the 2D carrier layer $Q_{\rm 2D}=e\times n_{\rm ShdH}$, where $n_{\rm ShdH}$ is the density of carriers participating in the Shubnikov–de Haas or Quantum Hall effect (QHE), $n_{\rm ShdH}=(eB/h)\times i$, and i is the number of filled quantum levels in a given magnetic field B.

The issue of the carrier density was raised recently again in connection with the metal–insulator (M–I) transition in 2D carrier systems at $B=0$. The transition occurs at

a critical gate voltage V_{gc} (where $V_{gc}>V_t$).[4] The critical gate voltage is interpreted as corresponding to a critical carrier density $n_c=(dn/dV_g)(V_{gc}-V_t)$. Recently an alternative interpretation was put forward[5] wherein it was supposed that the density of carriers participating in transport at $B=0$ is equal to $n_{\rm eff}=(dn/dV_g)V_g-n_c$, so that $n_{\rm eff}=0$ at the transition, i.e., at $V_g=V_{gc}$.

The effective number of carriers is not a well-defined parameter close to the M–I transition, and may, *a priori*, turn out to be different in different effects. In a weak magnetic field, the Hall resistance in the single-particle approximation[6] is inversely proportional to the number of carriers:

$$R_{xy}\approx\frac{\omega_c\tau}{\sigma_0}\left[1-\frac{1}{(\omega_c\tau_0)^2}\frac{\Delta G(\epsilon_F)}{G}\right]. \tag{2}$$

Here $\sigma_0=ne^2\tau/m^*$ is the diagonal conductivity at $B=0$, $\omega_c=eB/m^*$ is the cyclotron frequency, and τ is the transport scattering time at $B=0$. G and ΔG are the monotonic and oscillatory parts of the density of states. According to the theory,[7,8] electron–electron interaction affects R_{xy} in the same order as σ_{xx}, and thus $\delta R_{xy}/R_{xy}\approx 2(\delta\rho_{xx}/\rho^0_{xx})$.

The Hall resistance was measured earlier in low-mobility *p*- and *n*-type Si-MOS structures[9,10,1] and was found to remain *finite and nonactivational through the transition to the temperature-activated conduction regime*. In high-mobility *n*-type Si-MOS samples the Hall resistance was measured across the QHE–insulator transition[11–13] and was also found to be close to its classical value[12] $R_{xy}=B/ne$, with n given by Eq. (1). Low frequency (~ 3 Hz) ac measurements of the ''gate–2D layer'' capacitance[11] have shown that the capacitance remains unchanged, within a few %, across the QHE–insulator transition. With such a precision, the number of carriers participating in charging–discharging is described by the same Eq. (1) in both the insulating and metallic phases. This observation also sets an estimated upper bound on the possible variation of the trapped charge in the vicinity of the M–I transition: $dV_t/dV_g<10\%$.

The above measurements of R_{xy} and of the capacitance, however, were done in *quantizing magnetic field*. In this paper we report measurements of R_{xy} performed in such *weak magnetic fields*, where Landau levels are not resolved, $\Delta G/G\ll 1$. We found that the *weak-field Hall voltage remains finite across the M–I transition*. Deviation of R_{xy} from the quasiclassical value is within 6–20% for different samples. Under the assumption that the inverse Hall voltage is a measure of the effective number of carriers $n_{\rm eff}$, the latter does not decrease to zero at the M–I transition.

We studied three samples from different wafers: Si22 (with a peak mobility $\mu=33.000\,{\rm cm^2/V\cdot s}$ at $T=0.3$ K), Si4/32 ($\mu=8.000\,{\rm cm^2/V\cdot s}$) and Si-46 ($\mu=1.350$ ${\rm cm^2/V\cdot s}$). All samples had oxide thickness of 200 ± 30 nm, and, correspondingly, $dn/dV_g=(1.05\pm 0.15)\times 10^{11}\,{\rm V^{-1}cm^{-2}}$. The samples had potential probes lithographically defined with an accuracy of 1 μm. The top view of the samples is shown in the inset to Fig. 1, where $w=800\,\mu$m and $l=1250\,\mu$m are the channel width and intercontact distance, and $d=25\,\mu$m is the width of the bulk diffusion area contacting the 2D layer. For Hall voltage measurements at low density, we used battery-operated electrometric amplifiers with input current $<10^{-14}$ A. Four-probe measurements were taken by an ac lock-in technique at 3–7 Hz and also, partly, by a dc technique.

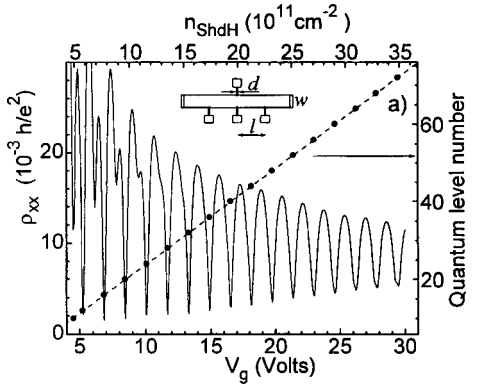

FIG. 1. Shubnikov–de Haas oscillations in ρ_{xx} versus gate voltage at $T=0.29$ K and $B=2$ T. The dashed line and filled dots demonstrate a linear relation between the number of the quantum level and the gate voltage, from which the n_{ShdH} density is calculated. The inset shows the sample geometry.

Figure 1 demonstrates that the minima of the Shubnikov–de Haas oscillations in ρ_{xx} are equidistant on the gate voltage scale. The carrier density calculated from the minima is independent of magnetic field (in the range 0.5 to 5 T) and of temperature (for 0.3 to 1.4 K), within an uncertainty of 1–2%. The Hall voltage was measured in a field of 0.2–0.3 T, which is large enough to suppress the quantum interference corrections to conductivity[14] and low enough to keep the oscillatory part in the density of states small, for all gate voltages and temperatures down to 30 mK.

For the samples Si22 and Si4/32, the resistivity exhibited an exponential decline for $V_g > V_{gc}$ as the temperature decreased.[4,15] For the most disordered sample, Si46, the resistivity $\rho(T)$ is activational in the insulating state (for $V_g < V_{gc}$) and has a weak, almost linear, ''metallic'' temperature dependence for $V_g > V_{gc}$ (Ref. 15), as demonstrated in Fig. 2. The effective ''Hall density'' $n_{\mathrm{Hall}} = B/eR_{xy}$, calculated from R_{xy} at $T=0.29$ K is shown in Fig. 2. The dashed line depicts n_{ShdH} versus gate voltage, calculated from the period of oscillations. As V_g decreases, the effective Hall density deviates from the classical linear dependence, and then falls quickly to zero, deep in the insulating

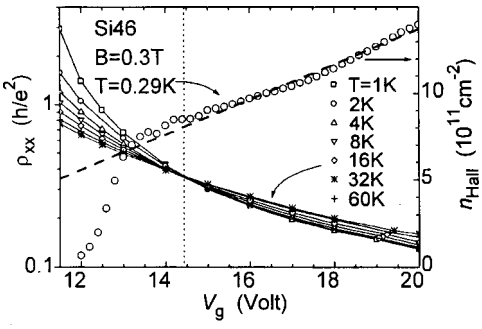

FIG. 2. Resistivity at $B=0$ (left Y axis) versus gate voltage for the sample Si46 for seven temperature values. Hall density (right Y axis) as a function of gate voltage at $B=0.3$ T and $T=0.29$ K. The dotteded line depicts V_{gc}; the dashed line is for the density n_{ShdH}.

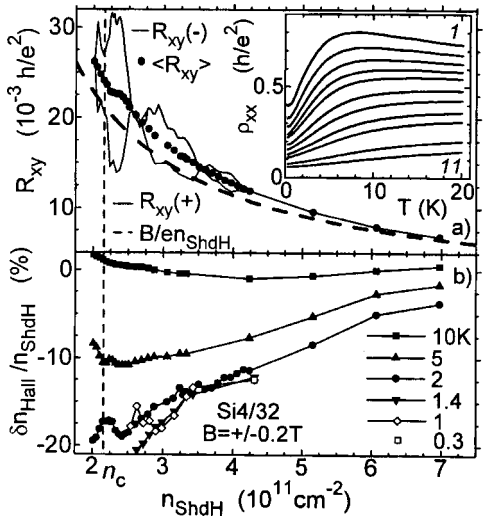

FIG. 3. a) Hall resistance versus carrier density, measured at two opposite field directions at $T=2$ K and $B=\pm 0.2$ T. Dotted curve represents an averaged resistance, $\langle R_{xy}\rangle=(R_{xy}(+B)-R_{xy}(-B))/2$. The bold dashed curve is the classical dependence B/ne. b) Deviation in the ''Hall density,'' $\delta n_{\rm Hall}$, measured at $B=\pm 0.2$ T for six temperatures. The vertical dashed lines mark the critical density n_c. The inset shows ρ_{xx} versus temperature for 11 densities, 2.4, 2.5, 2.6, 2.7, 2.8, 3, 3.2, 3.4, 3.7, 4.7, 5.7, in units of 10^{11} cm^{-2}.

state. This is consistent with the earlier results of Ref. 10. Right at the critical gate voltage, $V_{gc}=14.4$ V, the Hall density is 5% *larger* than the classical value given by Eq. (1).

For samples with higher mobility, the critical density n_c is lower and the critical resistivity ρ_c is higher.[15] For this reason, the admixture of longitudinal voltage produces large distortions of the measured Hall voltage. As Fig. 3a shows, the admixture can be reduced substantially by subtracting the results taken for opposite magnetic field directions. The Hall resistance for sample Si4/32 at low density is larger than the quasiclassical value $B/en_{\rm ShdH}$. The deviation in the effective Hall density, $\delta n_{\rm Hall}=n_{\rm Hall}-n_{\rm ShdH}$, calculated from the measured R_{xy} values for six temperatures is plotted in Fig. 3b. At high density and high temperature, the deviation in the Hall density tends to zero. As temperature decreases to 0.3 K, the deviation rises to almost 20%, and seems to saturate.

Finally, as shown in Fig. 4, the deviation in the Hall density for the high mobility sample Si22 has a 3 times weaker dependence on gate voltage and temperature than for Si4/32. As V_g increases, the disagreement between $n_{\rm Hall}$ and $n_{\rm ShdH}$ becomes less than the measurement uncertainty. It should be noted that the absolute value of $n_{\rm ShdH}$ and the true position of the ''zero'' on the vertical scales in Figs. 4 and 3b have an uncertainty of $\sim 1-2\%$ for Si22 and 4% for Si4/32. Although the deviation of the Hall density is small for all samples, $\delta n_{\rm Hall}/n_{\rm ShdH}\ll 1$, it is much larger than the error bars. Due to the charge neutrality in Si-MOS structure [Eq. (1)], the nonzero value of the $\delta n_{\rm Hall}$ indicates either a departure from the Drude–Boltzmann interpretation of the Hall voltage in the vicinity of V_{gc} or a noticeable contribution from carrier exchange between the 2D layer and shallow potential traps at the Si/SiO_2 interface.[16,17]

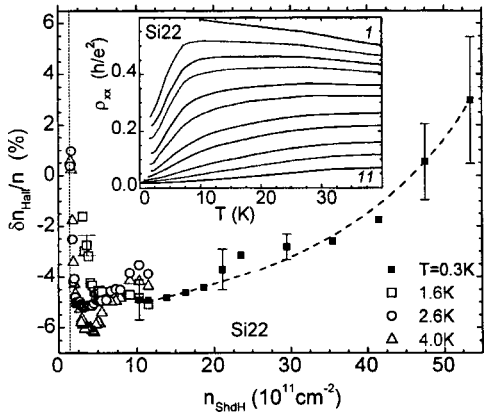

FIG. 4. Deviation in the ''Hall density,'' δn_{Hall} measured at $B=\pm 0.2$ T on sample Si22 for four temperatures. The dashed line is a guide to the eye. Dotted vertical line marks the critical density n_c. The inset shows ρ_{xx} versus temperature for 11 densities, 1.5, 1.7, 1.8, 1.9, 2.1, 2.4, 2.9, 3.34, 4.3, 5.5, 7.9, in units of 10^{11} cm^{-2}.

In the framework of the Drude–Boltzmann model, the effective carrier density n_{Hall} for all samples remains close to the classical value over the metallic range of densities $V_g > V_{gc}$, where ρ_{xx} strongly varies with temperature. We conclude, in the same framework, that the strong exponential decline in $\rho_{xx}(T)$ with decreasing T (Ref. 4) is associated with an anomaly in the scattering time or in the transport mechanism, rather than with carrier density. The insets to Figs. 3a and 4 show that the variations of the diagonal resistivity with temperature are much larger than those in R_{xy}, over the same range of density and of temperature. The lack of a linear relationship between δR_{xy} and $\delta \rho_{xx}$ in the vicinity of V_{gc}, indicates that at least one of these two quantities is not related to the interaction quantum corrections[7] (with the reservation that the theory may be not valid for the strong interaction case, $r_s \sim 3-10$).

In conclusion, we have measured the weak-field Hall resistance in *n*-Si-MOS samples across the metal–insulator transition. We found no signatures of a complete carrier freeze-out at $V_g = V_{gc}$. However, for low density and low temperatures, the Hall voltage in different samples was found to deviate from the classical value by about 6–20%. The deviation in R_{xy} does not correlate with the strong temperature dependence of $\rho_{xx}(T)$. In particular, the smallest value of the deviation in R_{xy} (6 %) was measured in the high mobility sample Si22, where the diagonal resistivity ρ_{xx} varies most strongly (by 5.5 times) in the same temperature range.

V. P. acknowledges help by M. D'Iorio and E. M. Goliamina in sample processing, and acknowledges discussions with B. Altshuler and D. Maslov. The work was supported by the RFBR, by the Programs ''Physics of Solid-State Nanostructures'' and ''Statistical Physics,'' by INTAS, NWO, and by FWF P13439, ÖNB 6333 and GME, Austria.

*)e-mail: pudalov@sci.lebedev.ru

[1] For a review see: T. Ando, A. B. Fowler, and F. Stern, Rev. Mod. Phys. **54**, (1982).
[2] A. B. Fowler *et al.*, Phys. Rev. Lett. **16**, 901 (1966).

[3] V. M. Pudalov, S. G. Semenchinskii, and V. S. Edel'man, JETP Lett. **39**, 576 (1984).
[4] S. V. Kravchenko *et al.*, Phys. Rev. B **50**, 8039 (1994). S. V. Kravchenko *et al.*, Phys. Rev. B **51**, 7038 (1995).
[5] S. Das Sarma and E. H. Hwang, http://xxx.lanl.gov/abs/cond-mat/9812216 http://xxx.lanl.gov/abs/cond-mat/9901117.
[6] L. Smrĉka and A. Isihara, J. Phys. C **19**, 6777 (1986).
[7] B. L. Altshuler, and A. G. Aronov, in *Electron-Electron Interaction in Disordered Systems*, edited by A. L. Efros and M. Pollak, North-Holland, Amsterdam, 1985.
[8] A. Houghton, J. R. Senna, and S. C. Ying, Phys. Rev. B **25**, 2196 (1982). S. M. Girvin, M. Johnson, and P. A. Lee, Phys. Rev. B **26**, 1651 (1982).
[9] E. Arnold and J. M. Shannon, Solid State Commun. **18**, 1153 (1976).
[10] M. Pepper, Philos. Mag. B **38**, 515 (1978).
[11] S. V. Kravchenko, J. A. A. Perenboom, and V. M. Pudalov, Phys. Rev. B **44**, 13513 (1991).
[12] V. M. Pudalov, M. D'Iorio, and J. W. Campbell, JETP Lett. **57**, 608 (1993).
[13] S. V. Kravchenko, J. E. Furneaux, and V. M. Pudalov, Phys. Rev. B **49**, 2250 (1994); S. V. Kravchenko *et al.*, Phys. Rev. B **51**, 7038 (1995).
[14] V. M. Pudalov, G. Brunthaler, A. Prinz, and G. Bauer, JETP Lett. **65**, 932 (1997); Physica B **249-251**, 697 (1998).
[15] V. M. Pudalov, G. Brunthaler, A. Prinz, and G. Bauer, Physica E **3**, 79 (1998); JETP Lett. **68**, 442 (1998).
[16] T. M. Klapwijk and S. Das Sarma, http://xxx.lanl.gov/abs/cond-mat/9810349.
[17] B. L. Altshuler and D. L. Maslov, Phys. Rev. Lett. **82**, 145 (1999).

Published in English in the original Russian journal. Edited by Steve Torstveit.

Optical nutation at a Raman-active transition

S. V. Anikeev, V. B. Morozov,*) A. N. Olenin, and V. G. Tunkin
M. V. Lomonosov Moscow State University, 119899 Moscow, Russia

V. N. Kulyasov
S. I. Vavilov State Optics Institute, 194100 St. Petersburg, Russia

(Submitted 19 May 1999)
Pis'ma Zh. Éksp. Teor. Fiz. **70**, No. 1, 7–12 (10 July 1999)

Optical nutation at the Raman-active transition $6P_{1/2}-6P_{3/2}$ of thallium atoms ($\omega_R/2\pi c=7793\,\mathrm{cm}^{-1}$) under resonant Raman excitation by a biharmonic picosecond pulsed field, giving rise to substantial motion of the population, is detected. Optical nutation appears as an oscillatory behavior of the energy of the anti-Stokes scattering of probe pulses, which follow with a fixed delay, as a function of the product of the energies of the excitation pulses. As a result of the dynamic Stark effect, which decreases the frequency of the transition under study, resonance excitation conditions are satisfied for negative initial detunings of the Raman excitation frequency from resonance. The Raman scattering cross section for the transition under study is estimated by comparing the experimental data with the calculations. © *1999 American Institute of Physics.* [S0021-3640(99)00213-3]

PACS numbers: 42.50.Md, 42.50.Hz

1. For fast (relative to the relaxation times) excitation of optical transitions by a resonant or nearly resonant field, the temporal evolution of a two-level system has the character of regular oscillations of the population difference and polarization (optical nutation). For dipole-forbidden transitions, excitation can be accomplished by a two-photon ($\omega_1+\omega_2=\omega_R$) or a Raman ($\omega_1-\omega_2=\omega_R$) scheme, where ω_1 and ω_2 are laser frequencies and ω_R is the frequency of the transition under study.

In Ref. 1, for two-photon excitation of the $3S-4D$ transition of sodium atoms, optical nutation was observed by detecting the modulation of the luminescence from the $4D$ level with a nonzero detuning from resonance, so that the nutation period was shorter than the relaxation times. In Ref. 2 nutation was observed with excitation of a two-photon vibrational–rotational transition of the NH_3 molecule by pulses with close frequencies and different intensities. The 294 MHz detuning from the resonance frequency was compensated by the dynamic Stark effect. It was asserted by the author that the observed beats in the intensity of the weaker beam, passing through a cell containing NH_3 molecules, corresponded to periodic modulation of the inversion. It is important to note that in Refs. 1 and 2 the excitation beams propagated in opposite directions, which made it possible to compensate the Doppler shift.

The Doppler shift is not compensated for Raman excitation. For relatively high-

frequency transitions the Doppler dephasing time T_2^* can be quite short, down to ~ 1 ns. A universal method in which the conditions for coherence of excitation in detection of nutation are certainly satisfied, is to use excitation pulses with duration shorter than the times T_1, T_2, and T_2^*. The possibility of an experimental arrangement in which the dependence of the energy of coherent anti-Stokes (Stokes) scattering of a probe pulse, following through the medium with a fixed delay, would be measured as a function of the product of the energies of the excitation pulses is discussed in Ref. 3.

In gases the conditions for coherence of excitation are satisfied, as a rule, for picosecond pulses. Since the Raman scattering cross section is small, quite powerful picosecond pulses must be used to obtain substantial motion of the population. Then the dynamic Stark effect becomes substantial. The spectral manifestations of this effect with the excitation of Raman-active transitions have been investigated in Refs. 4 and 5.

In the present work optical nutation was detected at a Raman-active transition of thallium atoms under conditions of resonant biharmonic excitation with picosecond pulses, accompanied by a considerable motion of the population. The dynamic Stark effect was manifested as a strong ''asymmetry'' of the nutation under a change in sign of the initial detuning of the Raman excitation frequency $\omega_1 - \omega_2$ from resonance ω_R.

2. Single picosecond pulses of a dye laser (30 ps, $\lambda_1 \approx 0.582\,\mu$m, energy 0.75 mJ) and an Nd:YAG laser (30 ps, $\lambda_2 = 1.064\,\mu$m, maximum energy 5 mJ) were used as excitation pulses, and single second-harmonic pulses (25 ps, $\lambda_p = 0.532\,\mu$m, 0.5 mJ), following with a fixed delay, were used as probe pulses. The radiations of the excitation and probe pulses were collimated into ≈ 1 mm diameter beams (at the $1/e$ intensity level) and directed into a 15 mm long cell containing thallium vapor heated to 950 K. The cell was filled with neon as a buffer gas to a pressure of 3 Torr at room temperature.

To decrease the effect of the averaging of the signal over the profile of the excitation beams, which smooths the nutations, a diaphragm 0.3 mm in diameter was placed on the axis of the beams 6 cm from the exit window of the cell. After passing through the diaphragm, the radiation of the excitation pulses was separated from the anti-Stokes signal ($\lambda_A \approx 0.376\,\mu$m), and the energies W_1 and W_2 of these pulses were measured with photodetectors. In the process of detecting nutation, the energy W_1 of the excitation pulse with $\lambda_1 \approx 0.582\,\mu$m was fixed, and the energy W_2 of the excitation pulse with $\lambda_2 = 1.064\,\mu$m was varied using a polarization rotator and a Glan prism. The polarization rotator, which did not cause beam drift, consisted of a fused-quartz plate, compressed in a direction perpendicular to the axis of the beams. After passing through the double diffraction monochromator the anti-Stokes radiation was detected with a photomultiplier.

The fixed delay of 140 ps was chosen on the basis of the following considerations. First, it must be greater than the duration of the excitation pulses. Second, no appreciable decrease of the coherent signal should occur over the delay time. For a fixed neon buffer gas density, the collisional dephasing time is 9.3 ns,[6] and it can be neglected in the calculations. Larger decays of the signal come as a result of Doppler dephasing, with a dephasing time of 1.1 ns at 950 K,[6] and as a result of interference of the hyperfine components of the $6P_{1/2}-6P_{3/2}$ transition under study, which differ in frequency by $0.0175\,\mathrm{cm}^{-1}$, which leads to quantum beats with period 1.9 ns in the pulsed response.[6] Thus the factors enumerated above are negligible with a 140 ps delay time and were neglected.

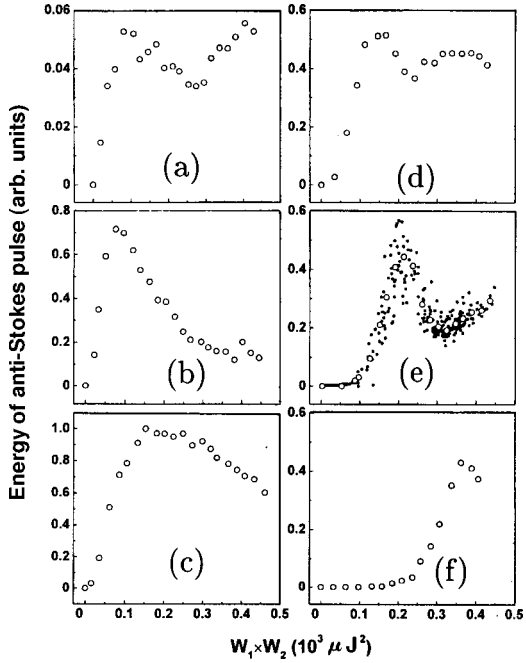

FIG. 1. Experimental dependence of the anti-Stokes scattering energy W_A on the product W_1W_2 of the energies of the excitation pulses for different initial detunings $\Delta\omega_0$: a) $\Delta\omega_0=0\ \mathrm{cm}^{-1}$; b) $-1.4\ \mathrm{cm}^{-1}$; c) $-2.4\ \mathrm{cm}^{-1}$; d) $-3.2\ \mathrm{cm}^{-1}$; e) $-4.2\ \mathrm{cm}^{-1}$; f) $-5.6\ \mathrm{cm}^{-1}$.

3. The experimentally measured dependence of the anti-Stokes radiation energy W_A on the product W_1W_2 of the energies of the excitation pulses are shown in Fig. 1 for different initial detunings $\Delta\omega_0$. The range of values of W_1W_2 corresponds to W_2 in the range $0-400\,\mu$J with the fixed average value $W_1=10\,\mu$J. The curves in Fig. 1 are normalized to the maximum value of W_A in Fig. 1c. The initial detuning is determined as $\Delta\omega_0=(\omega_1-\omega_2)-\omega_R$, i.e., this is the detuning for small values of W_1 and W_2, for which the Stark shift can be neglected. The circles indicate the average values of the anti-Stokes signal.

It should be noted first that the amplitude of the signal increases as the detuning $\Delta\omega_0$ varies from the initial zero value (Fig. 1a) to $\Delta\omega_0=-1.4\,\mathrm{cm}^{-1}$ (Fig. 1b) and then to $\Delta\omega_0=-2.4\,\mathrm{cm}^{-1}$ (Fig. 1c). The characteristic rise and fall of the signal, which are most clearly seen in Fig. 1b, form simultaneously. As $|\Delta\omega_0|$ increases, the maximum in Figs. 1b, and 1c shifts to larger values of W_1W_2. As $|\Delta\omega_0|$ increases further, the apex becomes almost flat ($-2.4\,\mathrm{cm}^{-1}$, Fig. 1c), after which a dip appears at the center ($-3.2\,\mathrm{cm}^{-1}$, Fig. 1d), the minimum of the dip also shifting in to larger values of $W_1W_2(-4.2\,\mathrm{cm}^{-1})$ with increasing $|\Delta\omega_0|$. As $|\Delta\omega_0|$ increases, a signal appears with an increasing shift on the W_1W_2 scale (Figs. 1e and 1f). As $\Delta\omega_0$ varies from zero in the direction of positive values, however, the signal drops off rapidly.

As an example, the results of the unaveraged measurements in each laser shot are shown in Fig. 1e (dots) together with the average values. A number of circumstances make it difficult to detect a larger number of nutation periods. The variance of the

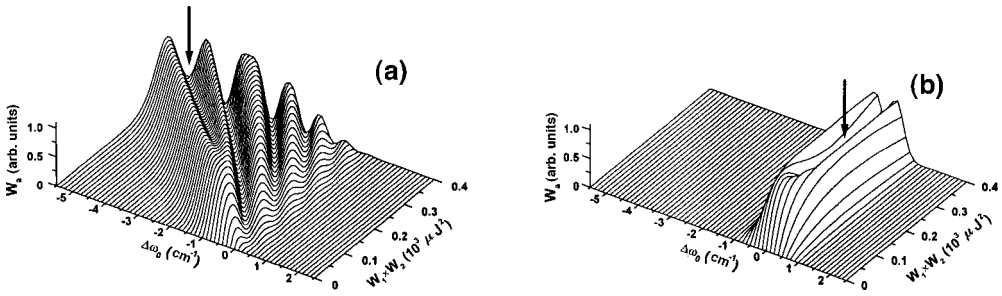

FIG. 2. Calculation of the anti-Stokes scattering energy W_A as a function of the initial detuning $\Delta\omega_0$ and the product W_1W_2 of the energies of the excitation pulses on the basis of the model in Eqs. (1) and (2), with (a) and without (b) the dynamic Stark effect.

experimental points, which is due to fluctuations of the pulses, decreases the contrast in observing the nutation. This effect becomes more pronounced with increasing phase of the nutation. The smoothing of the nutation as a result of averaging over the area of the diaphragm is also more pronounced here. Moreover, the power density attained in the experiments corresponded to electric fields of the light up to 2.5×10^6 V/cm. At these fields self-action appears in the optical components, and other nonlinear optical effects that distort the nutation picture also cannot be ruled out.

4. The Bloch equations for a generalized two-level system in a biharmonic pump field are, in a rotating coordinate system and in neglect of dephasing,[7,8]

$$d\boldsymbol{\rho}/dt=\boldsymbol{\Omega}\times\rho, \tag{1}$$

where $\boldsymbol{\rho}=(u,v,w)$ is the Bloch vector, u and v are the in-phase and quadrature components of the polarization, w is the normalized population difference between the lower and upper levels, $\boldsymbol{\Omega}=(-\gamma A_1,A_2,0,\Delta\omega)$, where $\Delta\omega$ is the detuning of the excitation frequency from the Raman resonance frequency, and γA_1A_2 is the Rabi frequency for Raman excitation with $\Delta\omega=0$ (there is no phase modulation of the excitation pulses and the slowly varying amplitudes A_1 and A_2 are real).

The motion of the Bloch vector under the influence of the excitation pulses is complicated by the dynamic Stark effect, which shifts the resonance frequency ω_R by $\Delta\omega_{\mathrm{St}}=(\Delta\alpha_1A_1^2+\Delta\alpha_2A_2^2)/4\hbar$ (Ref. 9), where $\Delta\alpha_1$ and $\Delta\alpha_2$ are the differences of the polarizabilities of the upper and lower levels for the waves ω_1 and ω_2. Therefore the total detuning from Raman resonance is

$$\Delta\omega=\Delta\omega_0+\Delta\omega_{\mathrm{St}}=(\omega_1-\omega_2)-\omega_R+\Delta\omega_{\mathrm{St}}. \tag{2}$$

The pulses were assumed to be Gaussian: $A_{1,2}=A_{1,2}^0\exp(-4t^2/\tau_P^2)$, where τ_P is the pulse duration with respect to the $1/e$ level. Calculations were performed for plane waves with the obvious initial conditions: $u_0=0$, $v_0=0$, and $w_0=-1$.

5. In accordance with the experimental arrangement, the position of the Bloch vector after the passage of excitation pulses was calculated, taking account of the experimentally measured Stark shift, using the model (1) and (2). The pulse energy W_A at the anti-Stokes frequency was found as the quantity proportional to the squared projection of the Bloch vector on the $w=0$ plane. Figure 2a shows the calculations of W_A as a function of W_1W_2

for different values of $\Delta\omega_0$. This shows the general character of the nutation under Stark shift conditions. Since the polarizability of an atom in the upper level is greater than the polarizability in the lower level, the frequency of the transition investigated shifts to lower values in accordance with the temporal form of the excitation pulses. The additive contribution, which we measured experimentally, to the shift of the transition frequency by each excitation pulse was $0.32\,\mathrm{cm}^{-1}$ ($W_1=8\,\mu$J) and $0.67\,\mathrm{cm}^{-1}$ ($W_2=70\,\mu$J), which corresponds to polarizability differences $\Delta\alpha_1=100(30)\times10^{-24}\,\mathrm{cm}^3$ and $\Delta\alpha_2=25(8)\times10^{-24}\,\mathrm{cm}^3$.

The experimentally measured dependence of the anti-Stokes signal energy W_A on the product W_1W_2 of the energies of the excitation pulses with fixed initial detunings $\Delta\omega_0$ correspond to a $\Delta\omega_0=\mathrm{const}$ section through the three-dimensional dependence presented in Fig. 2a. Figure 2b shows the computational results with the same scale as in Fig. 2a but neglecting the Stark effect. In this case, the nutation picture is symmetric with respect to the $\Delta\omega_0=0$ plane: For $\Delta\omega_0=0$, as the product W_1W_2 increases, the system successively passes through a state of maximum polarization (the Bloch vector lies in the horizontal plane), maximum inversion (the Bloch vector points upwards along the w axis), then once again maximum polarization, and finally back to the initial state. The region of maximum polarization corresponds to the apex of the three-dimensional dependence, and its total width is determined by the doubled Rabi frequency.[10,11] The region marked by the arrow in Fig. 2b is the inversion region.

The Stark shift introduces characteristic features in the nutation. Even with exact tuning to resonance ($\Delta\omega_0=0$), for small W and W_2 the dye-laser pulse with energy $W_1=10\,\mu$J leads to a detuning because of the Stark shift $\Delta\omega\approx0.4\,\mathrm{cm}^{-1}$, as a result of which the signal amplitude is small. For $\Delta\omega_0>0$ the Stark shift increases the detuning $\Delta\omega$ even more and the signal drops off rapidly, which experiment confirms. For $\Delta\omega_0<0$, satisfaction of the condition $\Delta\omega_0+\Delta\omega_{\mathrm{St}}=0$ for the corresponding amplitudes A_1 and A_2 means that the Stark shift compensates the negative initial detuning and brings the system to resonance. The larger the value of $|\Delta\omega_0|$, the larger the resonance field amplitudes are. The nutation picture is ''skewed'' with respect to the $\Delta\omega_0$ axis, extending along the axis, given by the condition $\Delta\omega_0+\Delta\omega_{\mathrm{St}}=0$; in addition, as $|\Delta\omega_0|$ increases, a signal appears with increasing shift on the W_1W_2 scale. In the range of $\Delta\omega_0$ from 0 to approximately $-2\,\mathrm{cm}^{-1}$ the nutation amplitude increases, reaching the region of maximum polarization $u^2+v^2=1$. However, as $|\Delta\omega_0|$ increases, the maximum shifts to larger values of W_1W_2. The system still does not enter the inversion region, marked by the arrow in Fig. 2a (the Bloch vector, having reached an almost horizontal position, then moves downwards). As $|\Delta\omega_0|$ increases further, a dip (marked by the arrow in Fig. 2a) appears at the apex of the three-dimensional dependence; this dip corresponds to a transition of the system into the inversion region, where the Bloch vector lies in the upper hemisphere. The depth of the dip increases with $|\Delta\omega_0|$, but for the values of W_1W_2 reached in the experiment it does not reach the bottom. The experimentally observed dependences also demonstrated nutation of a similar character.

Computer simulation of the nutation shows that the above-described features of optical nutation are very sensitive to the parameters of the model: the polarization differences $\Delta\alpha_1$ and $\Delta\alpha_2$ and the coefficient γ in the expression for the Rabi frequency, proportional to the Raman scattering cross section.[12] This enabled us to estimate, by comparing the experimental and computed dependences, the Raman scattering cross sec-

tion for the experimental transition as $d\sigma/do = 1.5(0.6) \times 10^{-27}\,\mathrm{cm}^2/\mathrm{sr}$. It should be noted that while it describes the basic qualitative features of the observed nutation, the model employed does not give complete agreement, specifically, it gives a larger delay of the signal on the $W_1 W_2$ scale. This is probably due to the simplicity of the model.

6. In summary, we have detected optical nutation upon the resonant biharmonic excitation of a Raman-active transition, leading to a substantial, even inverted, population of the upper level. The form of the nutation depended on the initial detuning of the biharmonic excitation frequency from Raman resonance; the resonance excitation range is shifted to negative values of the initial detuning on account of the dynamic Stark effect.

We thank K. N. Drabovich for fruitful discussions and valuable remarks during the preparation of this letter and A. V. Andreev, T. M. Il'inova, and S. Yu. Nikitin for a discussion of the results. This work was supported by the Russian Fund for Fundamental Research (Grant 96-02-18837-a).

*)e-mail: morozov@picar1.ilc.msu.su

[1] M. Bassini, F. Biraben, B. Gagnac, and C. Crynberg, Opt. Commun. **21**, 263 (1977).
[2] M. M. T. Loy, Phys. Rev. Lett. **36**, 1454 (1976).
[3] K. N. Drabovich, L. M. Kocharyan, and G. N. Slepchenko, Izv. Akad. Nauk SSSR, Ser. Fiz. **45**, 1532 (1981).
[4] L. A. Rahn, R. L. Farrow, M. L. Koszykowski, and P. L. Mattern, Phys. Rev. Lett. **45**, 620 (1980).
[5] M. Pealat, M. Lefebre, J.-P. Taran, and P. L. Kelley, Phys. Rev. A **38**, 1948 (1988).
[6] F. Sh. Ganikhanov, V. N. Kulyasov, I. G. Konovalov *et al.*, Opt. Spektrosk. **70**, 483 (1991) [Opt. Spectrosc. **70**, 283 (1991)].
[7] L. Allen and J. H. Eberly, *Optical Resonance and Two-Level Atoms* (Wiley, New York, 1975) [Russian translation, Mir, Moscow, 1978, p. 62].
[8] V. I. Anikin, K. N. Drabovich, and A. N. Dubovik, Zh. Éksp. Teor. Fiz. **72**, 1727 (1977) [Sov. Phys. JETP **45**, 906 (1977)].
[9] V. S. Butylkin, A. E. Kaplan, Yu. G. Khronopulo, and E. I. Yakubovich, *Resonant Interactions of Light with Matter* [in Russian] (Nauka, Moscow, 1977, p. 24).
[10] N. B. Delone and V. P. Kraĭnov, *Atoms in Strong Light Fields* (Springer-Verlag, New York, 1985) [Russian original, Énergoatomizdat, Moscow, 1984, p. 51].
[11] V. M. Akulin and N. V. Karlov, *Intense Resonant Interactions in Quantum Electronics* (Springer-Verlag, New York, 1991) [Russian original, Nauka, Moscow, 1987, p. 210].
[12] S. A. Akhmanov and N. I. Koroteev, *Methods of Nonlinear Optics in Light Scattering Spectroscopy* [in Russian] (Nauka, Moscow, 1981, p. 225).

Translated by M. E. Alferieff

The Einstein–Podolsky-Rosen effect and causality

S. N. Molotkov and S. S. Nazin
Institute of Solid-State Physics, Russian Academy of Sciences, 142432 Chernogolovka, Moscow Region, Russia

(Submitted 25 May 1999)
Pis'ma Zh. Éksp. Teor. Fiz. **70**, No. 1, 53–58 (10 July 1999)

It is shown for a simple example that the formalism of quantum field theory and the requirement of microcausality do not forbid complete correlation of the results of measurements performed by two observers separated by a spacelike interval.
 [S0021-3640(99)01013-0]

PACS numbers: 03.65.Bz

Quantum mechanics admits so-called entangled states, which became widely known after the work of Einstein, Podolsky, and Rosen (EPR),[1] who examined the question of whether or not a wave function gives a complete description. The ''nonlocality'' of the correlations of two particles in an entangled state has no classical analog.[2] In nonrelativistic quantum mechanics such nonlocality leads to a correlation between the results of measurements performed by two spatially separated observers. Since in nonrelativistic physics there are no limits on the propagation velocity of the interaction, a correlation of the results of simultaneous measurements performed by two observers at spatially separated points does not lead to any contradictions. We also note that the statistics of measurements performed on entangled states leads to violation of the Bell inequalities.[2] At the same time the special theory of relativity imposes a limit on the propagation velocity of an interaction. A causal relation between points of space–time can exist only if the points are located inside the light cone (they are separated by a timelike interval). For this reason, in quantum field theory, at first glance, it would be natural to assume that the results of measurements performed by two observers separated by a spacelike interval cannot be correlated, i.e., they must be statistically independent. It turns out, however, that in reality in the formalism of the relativistic theory there are no restrictions on the correlation of the results of measurements at two points separated by a spacelike interval. The point is that such a correlation is not equivalent to the existence of a causal link and does not permit the transmittal of information faster than the speed of light.

An example of an entangled state of a composite system consisting of two nonrelativistic particles is a wave function of the type

$$|\psi\rangle=\int |\mathbf{p}\rangle_1|-\mathbf{p}\rangle_2 d\mathbf{p}, \quad \text{or in the coordinate representation} \quad |\psi\rangle=\int |\mathbf{x}\rangle_1|\mathbf{x}\rangle_2 d\mathbf{x}. \quad (1)$$

In the state (1) neither particle has a completely determined momentum (coordinate). Only the total momentum of the particles (difference of coordinates), which is zero (the particles are ''located'' the same distance from the coordinate origin), is determined. If

measurements of the coordinates of the particles are performed by two spatially separated observers, then if the result of a measurement by the first observer gives the value $\mathbf{x}_1$, the result of the second observer is $\mathbf{x}_1$ with certainty. A similar situation occurs in measurements of the momenta of the particles. If the result of a measurement by the first observer is $\mathbf{p}_1$, then the result of measurement by the second observer is $-\mathbf{p}_1$ with certainty. In addition, measurements of the coordinates, for example, can be performed at the same time at two points separated by a spacelike interval. In this sense the results of the measurements are ''instantaneously'' correlated.

One of the basic postulates of relativistic quantum field theory is the requirement of microcausality, which can be expressed formally as vanishing of the commutator of two field operators at points separated by a spacelike interval.[3] It is postulated that the commutator (anticommutator) of two field operators is a *c*-number function

$$[u(\hat{x}),u(\hat{x}')]_{\pm}=iD(\hat{x}-\hat{x}').$$

A very important feature of the function $D(\hat{x}-\hat{x}')$ is that it is zero for spacelike intervals $(\hat{x}-\hat{x}')^2=c^2(x^0-x^{0'})^2-|\mathbf{x}-\mathbf{x}'|^2<0$. The latter is interpreted as the absence of correlations between the values of the fields at two points separated by a spacelike interval (see, for example, Ref. 4, where no distinctions are made between the correlation and the causal link).

It will be shown below for a simple example that the formalism of quantum field theory admits correlations between the values of a field at points separated by a spacelike interval. The result of a measurement at one point can completely determine the outcome of a measurement at a second point, and nonetheless such a correlation between the two outcomes of the measurements does not signify the existence of a causal link between them. For measurements performed on an entangled state of a field a causal link exists, conventionally speaking, between the point of ''creation'' of a two-particle entangled state of the field and the two points where the measurements are performed. For this reason, the violation of the Bell inequalities in the experiments of Ref. 5 in measurements performed at two points separated by a spacelike interval on a biphoton state of a field obtained with parametric conversion is unsurprising. Therefore microcausality does not imply the absence of correlations between physical quantities characterizing the state of a field at two points separated by a spacelike interval.

The amplitude Φ of an arbitrary state of a field in the Fock representation can be obtained as the action of field creation operators $u_i^+(\hat{x})_i$ on the vacuum state of the field Φ_0 as[3]

$$\Phi=\int\ \ldots\int \tilde{F}(\hat{k}_1,\ldots,\hat{k}_n)\,\delta(\hat{k}_1^2-m_1^2)\ldots\delta(\hat{k}_n^2-m_n^2)u_1^+(\hat{k})_1\ldots u_n^+(\hat{k})_n d\hat{k}_1\ldots\hat{k}_n\Phi_0. \tag{2}$$

The integration in Eq. (2) extends over states on the mass shell.

In what follows we shall work with massless particles, e.g., photons. The four-dimensional vector potential operators $A_n^{\pm}(\hat{x})$ are required to satisfy the Bose commutation relations[3]

$$[A_n^-(\hat{x}),A_m^+(\hat{x}')]_-=ig^{nm}D_0^-(\hat{x}-\hat{x}'),$$

where g^{nm} is the metric tensor ($g^{00}=-g^{11}=-g^{22}=-g^{33}=1$) and $D_0^-(\hat{x}-\hat{x}')$ is the negative-frequency part of the commutation function:

$$D_0^-(\hat{x})=\frac{i}{(2\pi)^{3/2}}\int d\hat{k}\,\delta(\hat{k}^2)\,\theta(-k^0)\exp(i\hat{k}\hat{x})=\frac{1}{4\pi}\varepsilon(x^0)\,\delta(\lambda),$$

$$\varepsilon(x^0)=\theta(x^0)-\theta(-x^0),\quad \lambda^2=(x^0)^2-\mathbf{x}^2,$$

which is nonzero and possesses a singularity on the light cone. The four-dimensional vector potential operators have the form

$$A_n^{\pm}(\hat{x})=\frac{1}{(2\pi)^{3/2}}\int\frac{d\mathbf{k}}{\sqrt{2k^0}}\exp(\pm i\hat{k}\hat{x})A_n^{\pm}(\mathbf{k})=\frac{1}{(2\pi)^{3/2}}\int\frac{d\mathbf{k}}{\sqrt{2k^0}}e_n^m(\mathbf{k})\exp(\pm i\hat{k}\hat{x})a_m^+(\mathbf{k}),$$

where $a_m^{\pm}(\mathbf{k})$ are creation and annihilation operators for four types of photons — two transverse, one ''timelike,'' and one longitudinal). The latter are fictitious and are introduced to preserve the four-dimensional structure of the vector potential, and

$$[a_m^-(\mathbf{k}),a_n^+(\mathbf{k}')]_-=-g^{nm}\delta(\mathbf{k}-\mathbf{k}'),\quad (\mathbf{e}^{\alpha}\cdot\mathbf{e}^{\beta})=\delta_{\alpha,\beta}\,(\alpha,\beta=1,2,3),$$

$$e_0^{\alpha}=0,\quad \mathbf{e}^3=\frac{\mathbf{k}}{|\mathbf{k}|}.$$

For what follows it is convenient to switch to two transverse polarizations of the photons. The vector-potential operator in such a gauge acquires the form

$$\mathbf{A}(\hat{x})=\frac{1}{2(2\pi)^{3/2}}\int\frac{d\mathbf{k}}{\sqrt{2k^0}}\sum_{\lambda=1,2}\{\mathbf{e}(\mathbf{k},\lambda)a^-(\mathbf{k},\lambda)\exp(-i\hat{k}\hat{x})+\mathbf{e}(\mathbf{k},\lambda)a^+(\mathbf{k},\lambda)\exp(i\hat{k}\hat{x})\},$$

$$[\mathbf{e}(\mathbf{k},1)\times\mathbf{e}(\mathbf{k})]=-\mathbf{e}(\mathbf{k},2),\quad \mathbf{e}(\mathbf{k})=\frac{\mathbf{k}}{|\mathbf{k}|},\quad [a^-(\mathbf{k},\lambda),a^+(\mathbf{k}',\lambda')]_-=\delta_{\lambda,\lambda'}\delta(\mathbf{k}-\mathbf{k}').$$

To perform the integration over k_i^0 in Eq. (2), it is convenient to make a change of variables. In this case the relativistic analog of the EPR pair (1) is a field state of the form

$$\Phi=\int\int\delta(\mathbf{k}_1+\mathbf{k}_2)[a^+(\mathbf{k}_1,1)a^+(\mathbf{k}_2,2)+a^+(\mathbf{k}_1,2)a^+(\mathbf{k}_2,1)]\frac{d\mathbf{k}_1d\mathbf{k}_2}{\sqrt{2k_1^0}\sqrt{2k_2^0}}\Phi_0. \qquad (3)$$

This field state is entangled with respect to momenta and polarizations of the photons. The coefficient singular function $\delta(\mathbf{k}_1+\mathbf{k}_2)$ in Eq. (3) should be interpreted as the improper limit of the coefficient functions from the principal space ($F(\mathbf{k}_1,\mathbf{k}_2)\to\delta(\mathbf{k}_1+\mathbf{k}_2)$). In what follows it will be more convenient to work with the normalized states of the type (3), i.e., with the substitution $\delta(\mathbf{k}_1+\mathbf{k}_2)\to F(\mathbf{k}_1,\mathbf{k}_2)$.

The propagation amplitude of the field in the case of creation at the points $(\hat{x}_1,\hat{x}_2)$ and annihilation at the points $(\hat{y}_1,\hat{y}_2)$ satisfies the causality condition, and it is nonzero for points lying on the light cone. Indeed, changing to operators in the $\hat{x}$ representation, we have

$$a^+(\hat{x},\lambda)=\int a^+(\mathbf{k},\lambda)\exp(i\hat{k}\hat{x})\frac{d\mathbf{k}}{\sqrt{2k^0}}.$$

In an entangled state the creation operator of the field can be represented as

$$\Psi^+(\hat{x}_1,\hat{x}_2)=F\left(i\frac{\partial}{\partial \mathbf{x}_1},i\frac{\partial}{\partial \mathbf{x}_2}\right)\int\int [a^+(\mathbf{k}_1,1)a^+(\mathbf{k}_2,2)$$

$$+a^+(\mathbf{k}_1,2)a^+(\mathbf{k}_2,1)]\exp[i(\hat{k}_1\hat{x}_1+\hat{k}_2\hat{x}_2)]\frac{d\mathbf{k}_1 d\mathbf{k}_2}{\sqrt{2k_1^0}\sqrt{2k_2^0}}.$$

Derivative operators can be substituted for the numbers $\mathbf{k}_i$ in the arguments of F if F is a sufficiently smooth function.

The propagation amplitude of the field is given by the expression

$$\Phi_0^*\Psi^-(\hat{y}_1,\hat{y}_2)\Psi^+(\hat{x}_1,\hat{x}_2)\Phi_0$$

$$=F^*\left(i\frac{\partial}{\partial \mathbf{y}_1},i\frac{\partial}{\partial \mathbf{y}_2}\right)F\left(i\frac{\partial}{\partial \mathbf{x}_1},i\frac{\partial}{\partial \mathbf{x}_2}\right)\{D_0^+(\hat{x}_1-\hat{y}_1)D_0^+(\hat{x}_2-\hat{y}_2)$$

$$+D_0^+(\hat{x}_1-\hat{y}_2)D_0^+(\hat{x}_2-\hat{y}_1)\}.$$

For bosons the propagation amplitude is a symmetrized combination of positive-frequency commutation functions. The amplitude itself is nonzero and singular on the light cone. On going over to an ideal EPR pair the limit of the amplitude ($F\to\delta$) becomes an improper limit. For any coefficient function from the principal space ($F\to\delta$) the amplitude is always nonzero only on the light cone[1)] $[(\hat{x}_i-\hat{y}_i)^2=0]$.

We shall now discuss measurements on an EPR state. In contrast to nonrelativistic quantum mechanics, there is no systematic and complete theory of measurements in relativistic quantum field theory.

In nonrelativistic quantum mechanics any measurement on a system can be described by a mapping of a convex set of states of the system, which is described by positive operators with unit trace (density matrices), into a distribution of probabilities on some measurable set of results. Such mappings can be described by operator expansions of unity on the measurable set of results (see, for example, Ref. 6). Working with field states with a fixed number of particles (in a subspace of Fock states), a measurement can be constructed by analogy with the expansion of unity for the nonrelativistic case. We introduce the local detection operators

$$M(\hat{x}_1)=\sum_{\lambda=1,2}\left(\int a^+(\mathbf{k},\lambda)\exp(i\hat{k}\hat{x}_1)d\mathbf{k}\right)\left(\int a^-(\mathbf{k}',\lambda)\exp(-i\hat{k}'\hat{x}_1)d\mathbf{k}'\right), \qquad (4)$$

and similarly for the second observer at the point $\hat{x}_2$. A given measurement can be interpreted as a measurement of the number of photons, irrespective of the polarization, at the points $\hat{x}_1$ and $\hat{x}_2$, respectively. In nonrelativistic quantum mechanics this measurement would correspond to an expansion of unity of the form

$$M(d\mathbf{x})=\sum_{s=\uparrow,\downarrow}\left(\int |\mathbf{k},s\rangle\exp(i\mathbf{k}\cdot\mathbf{x})d\mathbf{k}\right)\left(\int \langle\mathbf{k}',s|\exp(-i\mathbf{k}\cdot'\mathbf{x})d\mathbf{k}'\right)d\mathbf{x}, \qquad \int M(d\mathbf{x})=I,$$

where $|\mathbf{k},\mathbf{s}\rangle$ is a state of a nonrelativistic particle with momentum $\mathbf{k}$ and spin s.

A calculation of the commutator of the detection operators shows that

$$[M(\hat{x}_1),M(\hat{x}_2)]=2(2\pi)^3 i\sum_{\lambda}\left(B^+(\hat{x}_1)B^-(\hat{x}_2)\frac{\partial}{\partial x_2^0}D_0^+(\hat{x}_2-\hat{x}_1)\right.$$

$$\left.-B^+(\hat{x}_2)B^-(\hat{x}_1)\frac{\partial}{\partial x_2^0}D_0^-(\hat{x}_2-\hat{x}_1)\right),$$

$$B^{\pm}(\hat{x}_i)=\int a^{\pm}(\mathbf{k},\lambda)\exp(\pm i\hat{k}\hat{x}_i)d\mathbf{k},$$

i.e., $[M(\hat{x}_1),M(\hat{x}_2)]\neq 0$ only on the light cone, $(\hat{x}_1-\hat{x}_2)^2=0$. Therefore it would be natural to conjecture that the results of measurements of the operators $M(\hat{x}_1)$ and $M(\hat{x}_2)$ can be correlated only if $(\hat{x}_1-\hat{x}_2)^2=0$ (for massive particles, if $(\hat{x}_1-\hat{x}_2)^2\geqslant 0$). In reality, however, it turns out that for certain states of the field (including EPR states) a correlation can also exist if $(\hat{x}_1-\hat{x}_2)^2<0$.

Because of the singularity of the functions in quantum field theory it makes sense to talk only about relative probability in measurements. The joint probability of detecting photons with polarization λ_1 at the point $\hat{x}_1$ and λ_2 at the point $\hat{x}_2$ has the form (the detection operators are taken in normal form, where the annihilation operators stand to the left of the creation operators)

$$\Pr(\hat{x}_1,\lambda_1;\hat{x}_2,\lambda_2)=\boldsymbol{\Phi}^*:M(\hat{x}_1)M(\hat{x}_2):\boldsymbol{\Phi}=\boldsymbol{\Phi}_0^*\boldsymbol{\Psi}^-:M(\hat{x}_1)M(\hat{x}_2):\boldsymbol{\Psi}^+\boldsymbol{\Phi}_0.$$

Here

$$\Phi=\Psi^+\Phi_0=\int\int F(\mathbf{k}_1,\mathbf{k}_2)[a^+(\mathbf{k}_1,1)a^+(\mathbf{k}_2,2)+a^+(\mathbf{k}_1,2)a^+(\mathbf{k}_1,2)]\frac{d\mathbf{k}_1 d\mathbf{k}_2}{\sqrt{2k_1^0}\sqrt{2k_2^0}}\Phi_0,$$

and we find (omitting inconsequential numerical factors)

$$\Pr(\hat{x}_1,\lambda_1;\hat{x}_2,\lambda_2)=(\delta_{\lambda_1,1}\delta_{\lambda_2,2}+\delta_{\lambda_1,2}\delta_{\lambda_2,1})\left|F\left(i\frac{\partial}{\partial\mathbf{x}_1},i\frac{\partial}{\partial\mathbf{x}_2}\right)D_0^+(\hat{x}_1)D_0^-(\hat{x}_2)\right|^2. \quad (5)$$

A complete correlation exists in polarization measurements performed by two observers, and the probability is nonzero, as follows from Eq. (5), even if the observers are separated by a spacelike interval. In the limit of ideal EPR correlations ($F\to\delta$) the expression for the probability reduces to the following (we omit a factor containing the polarizations):

$$\Pr(\hat{x}_1;\hat{x}_2)=-D_0^+(-\hat{\mathcal{X}})D_0^-(\hat{\mathcal{X}})=[D_0^-(\hat{\mathcal{X}})]^2,\quad \mathcal{X}=(x_1^0+x_2^0,\mathbf{x}_1-\mathbf{x}_2). \quad (6)$$

The probability is given by the product of two singular generalized functions. Even though each cofactor is singular at $\hat{\mathcal{X}}^2=0$, this product and its Fourier transform nonetheless exist as generalized functions.[7] This is because the carrier of the function D^- lies in the forward part of the light cone. We note that the singularity in the D^- functions in Eq. (6) lies on the surface $\hat{\mathcal{X}}^2=0$ (for other entangled states the singularity can occur for a different combination of arguments) and not on the light cone, where $(\hat{x}_1-\hat{x}_2)^2=0$.

The Fourier transform of Eq. (6) has the form

$$\mathcal{F}[D_0^+(-\hat{\mathcal{X}})D_0^-(\hat{\mathcal{X}})]=\int D_0^+(-\hat{\mathcal{X}})D_0^-(\hat{\mathcal{X}})\exp(i\hat{k}\hat{\mathcal{X}})d\hat{\mathcal{X}}=\frac{1}{8\pi}\theta(k^0)\theta(\hat{k}^2).$$

Since the integration extends only over the front part of the light cone, the probability (6) is determined as a generalized function

$$\Pr(\hat{x}_1;\hat{x}_2)=\frac{1}{8\pi}\int\theta(k^0)\theta(\hat{k}^2)\exp(-i\hat{k}\hat{\mathcal{X}})d\hat{k}=-\frac{1}{2r}\varepsilon(\mathcal{X}^0)\frac{\partial}{\partial r}\delta(\hat{\mathcal{X}}^2)+\frac{2}{\pi}\mathcal{P}\left[\frac{1}{\hat{\mathcal{X}}^2}\right],$$

$$\varepsilon(\mathcal{X}^0)\delta(\hat{\mathcal{X}}^2)=\frac{\delta(\mathcal{X}^0-r)-\delta(\mathcal{X}^0+r)}{2r},\quad r^2=(\mathbf{x}_1-\mathbf{x}_2)^2.$$

The requirement of microcausality in quantum field theory does not forbid complete correlations in measurements performed by two observers separated by a spacelike interval on an entangled EPR state of the field. Such a correlation in the results of measurements does not signify the existence of a causal link, because even though the outcome of a measurement at one point predetermines the outcome of a measurement performed at a second point, such correlations in themselves do not permit transmitting information between two observers faster than the speed of light. Indeed, information transmission and a causal link between two points imply that the first observer can prepare *at his own volition* at least two different quantum states of the field, which then reach the second observer. A change in the state of the field cannot propagate to the second observer faster than the speed of light; this is a consequence of the requirement of microcausality (locality of commutation relations).

For measurements on a two-particle EPR state of the field, the result obtained by the first observer is unknown to him beforehand, and this circumstance makes it impossible for him to transmit information (to realize a causal link with the second observer). A causal link exists between *one* ''source'' (cause) EPR state of the field and *two* results of measurements (effects). The propagation amplitude of the field from the source to each observer is not faster than light.

This work was supported by the Russian Fund for Fundamental Research (Project No. 99-02-18127).

[1)]We note that for massive particles, because of the exponential ''tails'' of the functions $D^{\pm}$, the propagation amplitude of the field is nonzero outside the light cone at the Compton length, but this does not destroy causality (see Ref. 4 for details).

[1] A. Einstein, B. Podolsky, and N. Rosen, Phys. Rev. **47**, 777 (1935).
[2] J. S. Bell, *Speakable and Unspeakable in Quantum Mechanics* (Cambridge University Press, New York, 1987).
[3] N. N. Bogoliubov and D. V. Shirkov, *Introduction to the Theory of Quantized Fields*, 3rd edition (Wiley, New York, 1980) [Russian original, Nauka, Moscow, 1973].
[4] D. I. Blokhintsev, *Space and Time in the Microworld* (Reidel, Dordrecht, 1973) [Russian original, Nauka, Moscow, 1982].
[5] G. Weihs, T. Jennewein, C. Simon *et al.*, Phys. Rev. Lett. **81**, 5039 (1998).
[6] A. S. Kholevo, *Probabilistic and Statistical Aspects of Quantum Theory* [in Russian] (Nauka, Moscow, 1980).
[7] N. N. Bogoliubov, A. A. Logunov, and I. T. Todorov, *Introduction to Axiomatic Quantum Field Theory* (Benjamin, New York, 1975) [Russian original, Nauka, Moscow, 1969].

Translated by M. E. Alferieff

Multiqubit spin

A. R. Kessel' and V. L. Ermakov*)
Kazan Physicotechnical Institute, Kazan National Science Center of the Russian Academy of Sciences, 420029 Kazan, Russia

(Submitted 29 April 1999; resubmitted 2 June 1999)
Pis'ma Zh. Éksp. Teor. Fiz. **70**, No. 1, 59–63 (10 July 1999)

It is proposed that the state space of quantum objects with a complicated discrete spectrum be used as a basis for multiqubit recording and processing of information in a quantum computer. As an example, nuclear spin 3/2 is considered. The possibilities of writing and reading two quantum bits of information, preparation of the initial state, and the implementation of the operations ''rotation'' and ''controlled negation,'' which are sufficient for constructing complex algorithms, are demonstrated. © *1999 American Institute of Physics.*
[S0021-3640(99)01113-5]

PACS numbers: 03.67.Lx, 03.67.Hk, 03.65.Bz

We shall consider a nucleus with spin $I=3/2$ and with an electric quadrupole moment in an axisymmetric crystalline electric field and a constant magnetic field parallel to the symmetry axis. We assume that the Zeeman energy is greater than the quadrupole energy, so that the nucleus possesses four nonequidistant spin energy levels E_m and eigenfunctions χ_m $(m=\pm 3/2, \pm 1/2)$, which are eigenfunctions of the z component $\mathbf{I}_z$ of the nuclear spin $\mathbf{I}$.

Let a radio frequency (rf) field $2H_a\cos\Omega_a t$, polarized along the y axis and resonant for a certain pair of energy levels $\hbar\Omega_a=E_m-E_n$, act on the spin. The interaction operator H_a with the field in the interaction representation contains a time-independent term $H_{a,\mathrm{eff}}=\hbar\gamma H_a[\langle m|I_Y|n\rangle\mathbf{P}_{mn}+\langle n|I_Y|m\rangle\mathbf{P}_{nm}]$ and rapidly oscillating (at frequencies which are multiples of Ω_a and $(E_k-E_1)/\hbar$) terms, whose role in the evolution of the spin states is negligible. (Here and below, to simplify the notation we use a 4×4 matrix representation of the projection operators $\mathbf{P}_{mn}$ for which all of the matrix elements p_{kl} are zero except $p_{mn}=1$. Projection operators are very convenient because of their very simple properties: $\mathbf{P}_{kl}\mathbf{P}_{mn}=\delta_{lm}\mathbf{P}_{kn}$ and $\mathbf{P}_{mn}\chi_k=\delta_{nk}\chi_m$. In addition, 1, 2, 3, and 4 will stand for the indices $-3/2$, $-1/2$, $+1/2$, and $+3/2$, respectively.)

The evolution operator of the spin states under the interaction $H_{a,\mathrm{eff}}$ is

$$\mathbf{U}(\varphi_a)=[\mathbf{P}_{mn}+\mathbf{P}_{nn}]\cos(\varphi_a/2)+[\mathbf{P}_{kk}+\mathbf{P}_{ll}]+[\mathbf{P}_{nm}-\mathbf{P}_{mn}]\sin(\varphi_a/2), \tag{1}$$

where $\varphi_a=2(\gamma H_a t)|\langle m|\mathbf{I}_Y|n\rangle|$, $E_m>E_n$, and the indices $k,l\neq m,n$. If the rf field $2H_f\cos\Omega_{mn}t$ is polarized along the x axis, the evolution operator is

$$U_f(\varphi_f)=[\mathbf{P}_{mm}+\mathbf{P}_{nn}]\cos(\varphi_f/2)+[\mathbf{P}_{kk}+\mathbf{P}_{ll}]+i[\mathbf{P}_{nm}+\mathbf{P}_{mn}]\sin(\varphi_f/2), \tag{1a}$$

where $\varphi_f = 2(\gamma H_f t)|\langle m|\mathbf{I}_X|n\rangle|$.

In the currently accepted NMR model of a quantum computer two *real* exchange-coupled spins $R=1/2$ and $S=1/2$ are considered as a basis for constructing quantum logic elements.[1–4] In the formalism of quantum mechanics the states of such a system and the operations on them are written in an *abstract* four-dimensional space, which is a direct product $\Gamma_R \otimes \Gamma_S$ of the two-dimensional spaces of eigenstates of the *real* spins **R** and **S**. In our case, to clarify the information aspect of the proposed logical operations it is convenient to perform the inverse procedure: to represent the four-dimensional space Γ_I, corresponding to *real* spin 3/2, as a direct product $\Gamma_R \otimes \Gamma_S$ of two *abstract* two-dimensional states spaces of *fictitious* spins **R** and **S**. Then any operator **P** in the four-dimensional basis can be expressed as a linear combination of the direct products $\mathbf{R}\otimes\mathbf{S}$ of operators given in the subspaces Γ_R and Γ_S. The following isomorphic correspondence exists between the basis $|m\rangle$ of the space Γ_I and the basis $|m_1\rangle\otimes|m_2\rangle$ of the direct product $\Gamma_R\otimes\Gamma_S$:

$$|\chi_1\rangle \propto |-1/2\rangle|-1/2\rangle \equiv |11\rangle, \quad |\chi_3\rangle \propto |+1/2\rangle|-1/2\rangle \equiv |01\rangle,$$

$$|\chi_2\rangle \propto |-1/2\rangle|+1/2\rangle \equiv |10\rangle, \quad |\chi_4\rangle \propto |+1/2\rangle|+1/2\rangle \equiv |00\rangle,$$

where $|10\rangle$ and so on are the notations adopted in information theory for states of two quantum bits (qubits). The energies corresponding to these states satisfy $E_1 > E_2 > E_3 > E_4$.

As is well known, the initial state for quantum algorithms developed on an abstract quantum computer is the state $|00\rangle \propto |\chi_4\rangle$. From the standpoint of subsequent quantum calculations the spin density matrix

$$\rho_{\text{init}} = \text{const}[\mathbf{1} + \text{const}\cdot\mathbf{P}_{44}], \tag{2}$$

where **1** is the unit matrix in the space Γ_I, the equivalent of the state $|00\rangle$. It does not change under unitary computational transformations and does not contribute to the observed signal when the result is read.

In a sample of macroscopic size a collection of such nuclei forms an ensemble, whose spin levels in equilibrium are populated according to the Boltzmann distribution

$$\rho_{\text{eq}} = Z\exp(-\beta\mathbf{H}), \quad Z^{-1} = \text{Tr}[\exp(-\beta\mathbf{H})], \quad \beta = 1/kT, \tag{3}$$

and at room temperature the relative difference of the populations of the spin levels is ordinarily of the order of 10^{-5}–10^{-6} or less. Therefore, to obtain the state $\rho_{\text{init}} = \text{const}\cdot\mathbf{P}_{44}$ directly by cooling requires very low temperatures, which, besides presenting substantial technological difficulties, will affect the speed of the entire computational cycle.

A procedure whose idea goes back to Ref. 3 is proposed. Let the required calculation consist of performing the transformation $\mathbf{U}_{\text{comp}}$ of the state ρ_{init}, while the spin system is in a state given by the density matrix (3), which in the high-temperature approximation is

$$\rho_{\text{eq}} = Z[\mathbf{1} + \Sigma\lambda_m\mathbf{P}_{mm}], \quad \mathbf{1} = \Sigma\mathbf{P}_{mm}, \tag{4}$$

where $\lambda_m = E_m/kT$ and $m = 1,2,3,4$. We shall show that the sum of the results of three specially prescribed transformations of the state ρ_{eq} is equivalent to a transformation of the state ρ_{init}. Indeed, assume that we are required to perform a calculation which is a unitary transformation $\mathbf{U}_{\text{comp}}$ of the states of spin **I**. We define the unitary transformations

$$\mathbf{U}_1=\mathbf{U}_a(\pi)\mathbf{U}_b(\pi)=\mathbf{P}_{13}+\mathbf{P}_{21}+\mathbf{P}_{32}+\mathbf{P}_{44},$$

$$\mathbf{U}_2=\mathbf{U}_b(\pi)\mathbf{U}_a(\pi)=-\mathbf{P}_{12}-\mathbf{P}_{23}+\mathbf{P}_{31}+\mathbf{P}_{44},$$

where $\mathbf{U}_a(\pi)$ is the propagator (1) for a pulsed rf field at frequency $\Omega_a=(E_1-E_2)/\hbar$, which performs a rotation by the angle $\varphi=\pi$, and $\mathbf{U}_b(\pi)$ is the propagator for a resonant rf pulse at frequency $\Omega_b=(E_2-E_3)/\hbar$. It can be verified that the average of the three transformations $\mathbf{U}_{\text{comp}}$, $\mathbf{U}_{\text{comp}}\mathbf{U}_1$, and $\mathbf{U}_{\text{comp}}\mathbf{U}_2$,

$$(1/3)[\mathbf{U}_{\text{comp}}\rho_{\text{eq}}\mathbf{U}_{\text{comp}}^{\dagger}+\mathbf{U}_{\text{comp}}\mathbf{U}_1\rho_{\text{eq}}\mathbf{U}_1^{\dagger}\mathbf{U}_{\text{comp}}^{\dagger}+\mathbf{U}_{\text{comp}}\mathbf{U}_2\rho_{\text{eq}}\mathbf{U}_2^{\dagger}\mathbf{U}_{\text{comp}}^{\dagger}]$$
$$=(1/3)\mathbf{U}_{\text{comp}}(\rho_{\text{eq}}+\mathbf{U}_1\rho_{\text{eq}}\mathbf{U}_1^{\dagger}+\mathbf{U}_2\rho_{\text{eq}}\mathbf{U}_2^{\dagger})\mathbf{U}_{\text{comp}}^{\dagger}=\mathbf{U}_{\text{comp}}\rho_{\text{init}}\mathbf{U}_{\text{comp}}^{\dagger},$$

is a computation of $\mathbf{U}_{\text{comp}}$ on the density matrix

$$\rho_{\text{init}}=Z[\alpha\mathbf{1}+\beta\mathbf{P}_{44}], \tag{5}$$

where $\alpha=1+1/3[\lambda_1+\lambda_2+\lambda_3]$ and $\beta=\lambda_4-1/3[\lambda_1+\lambda_2+\lambda_3]$.

We shall specify the rotation by a certain angle in the space Γ_S under the condition that the space Γ_R is invariant. This can be done by acting on the spin I with a two-frequency rf pulse containing the resonance frequencies $\Omega_a=(E_1-E_2)/\hbar$ and $\Omega_c=(E_3-E_4)/\hbar$. The propagator of such a transformation in the space Γ_1 will be the sum of propagators of the form (1) which perform rotation by the same angle $\varphi_a=\varphi_c=\varphi$ at each transition:

$$\mathbf{U}_{a+c}(\varphi,\varphi)=\mathbf{1}\cos(\varphi/2)+[\mathbf{P}_{21}-\mathbf{P}_{12}+\mathbf{P}_{43}-\mathbf{P}_{34}]\sin(\varphi/2).$$

It can be expressed as follows in terms of the operators of the spaces Γ_R and Γ_S:

$$\mathbf{U}_{a+c}(\varphi,\varphi)=(\mathbf{R}_{11}+\mathbf{R}_{22})\otimes[(\mathbf{S}_{11}+\mathbf{S}_{22})\cos(\varphi/2)+(\mathbf{S}_{21}-\mathbf{S}_{12})\sin(\varphi/2)]$$
$$=\exp\{i(\varphi/2)\mathbf{1}_R\otimes\mathbf{S}_Y\}, \tag{6}$$

which proves the assertion made above (for fictitious spins 1/2 the indices 1 and 2 are used instead of $-1/2$ and $+1/2$, respectively; unit matrices are defined as $\mathbf{1}_R=\Sigma\mathbf{R}_{mm}$ and $\mathbf{1}_S=\Sigma\mathbf{S}_{mm}$, $m=1,2$). Similarly, the propagator for a two-frequency rf pulse with carrier (filling) frequencies $\Omega_d=(E_1-E_3)/\hbar$ and $\Omega_e=(E_2-E_4)/\hbar$ and angles $\varphi_d=\varphi_c=\varphi$, will equal, analogously,

$$\mathbf{U}_{d+e}(\varphi,\varphi)=[P_{22}+P_{44}]\cos(\varphi/2)+[P_{42}-P_{24}]\sin(\varphi/2)$$
$$+[P_{33}+P_{11}]\cos(\varphi/2)+[P_{31}-P_{13}]\sin(\varphi/2)$$

and can be expressed in terms of the spin operators of the spaces Γ_R and Γ_S as

$$\mathbf{U}_{d+e}(\varphi,\varphi)=[(\mathbf{R}_{11}+\mathbf{R}_{22})\cos(\varphi/2)+(\mathbf{R}_{21}-\mathbf{R}_{12})\sin(\varphi/2)]\otimes(\mathbf{S}_{11}+\mathbf{S}_{22})$$
$$=\exp\{i(\varphi/2)\mathbf{R}_X\otimes\mathbf{1}_S\}, \tag{7}$$

which is a rotation by the angle φ in the space Γ_R with Γ_S remaining unchanged. Generally speaking, the transitions at the frequencies Ω_d and Ω_e are forbidden in the initially adopted configuration of the magnetic and crystalline electric fields. In this case we shall assume that a small entanglement of the wave functions due to a deviation of η from zero (or for other reasons) allows these transitions, and a large amplitude of the ac

field provides the required rotation angle. All results of the present letter can also be obtained with an arbitrary configuration of fields, but this would unjustifiably complicate the exposition.

Next, the transformation $\mathbf{U}_f(\varphi_f)$ at $\varphi_f=\pi$, defined as

$$\mathbf{U}_f(\pi)=[\mathbf{P}_{33}+\mathbf{P}_{44}]+i[\mathbf{P}_{21}+\mathbf{P}_{12}],$$

performs the two-bit operation ''controlled negation'' CNOT — it performs the operation NOT on a spin S if the spin R is in state $|1\rangle$ and leaves the spin S unchanged if the spin R is in a state $|0\rangle$. Indeed, it is easy to check that

$$\mathbf{U}_f(\pi)|\chi_1\rangle\equiv\mathbf{U}_f(\pi)|11\rangle=|10\rangle,\quad \mathbf{U}_f(\pi)|\chi_2\rangle\equiv\mathbf{U}_f(\pi)|10\rangle=|11\rangle,$$

$$\mathbf{U}_f(\pi)|\chi_3\rangle\equiv\mathbf{U}_f(\pi)|01\rangle=|01\rangle,\quad \mathbf{U}_f(\pi)|\chi_4\rangle\equiv\mathbf{U}_f(\pi)|00\rangle=|00\rangle.$$

Hence one can see that the evolution operator $\mathbf{U}_f(\pi)$ can be represented in the basis $\Gamma_R\otimes\Gamma_S$ as

$$\mathbf{U}_f(\pi)=|0\rangle\langle 0|\otimes\mathbf{1}_S+|1\rangle\langle 1|\otimes\mathbf{S}_x\equiv\mathbf{R}_{22}\otimes\mathbf{1}_S+\mathbf{R}_{11}\otimes\mathbf{S}_x, \tag{8}$$

which proves the assertion made above.

To find the result of the computations it is necessary to read the state of the final density matrix $\rho_{\text{out}}=\mathbf{U}_{\text{comp}}\rho_{\text{init}}\mathbf{U}_{\text{comp}}^{\dagger}$. NMR methods make it possible to measure all elements of the density matrix by tomography of states.[4] As an illustration, we shall examine a variant of reading in the particular case of a diagonal density matrix

$$\rho_{\text{out}}=\mu_0\mathbf{1}+\Sigma\mu_m\mathbf{P}_{mm},\quad m=1,2,3,4 \tag{9}$$

in the important situation where the result of the computation is one of the states $|\chi_m\rangle$, i.e., when only one of the quantities μ_m can be nonzero. It is necessary to operate on the spin 3/2 under consideration with a pulsed two-frequency rf field, which generates a free-precession signal at the resonance frequencies Ω_{12} and Ω_{34} by rotating the density matrix elements by the angles $\varphi_a=\varphi_c=\pi/2$. Such a pulse corresponds to the evolution operator

$$\mathbf{U}_3=\mathbf{U}_a(\pi/2)\mathbf{U}_c(\pi/2)=(1/\sqrt{2})[\mathbf{1}+\mathbf{P}_{21}-\mathbf{P}_{12}+\mathbf{P}_{43}-\mathbf{P}_{34}]. \tag{10}$$

Under the evolution operator (10) the density matrix (9) in the Schrödinger representation assumes the form

$$\begin{aligned}\rho(\mathbf{t})=1/2\{&(\mu_1+\mu_2)(\mathbf{P}_{11}+\mathbf{P}_{22})+(\mu_4+\mu_3)(\mathbf{P}_{33}+\mathbf{P}_{44})\\&+(\mu_1-\mu_2)[\mathbf{P}_{21}\exp(-it\Omega_{12})+\mathbf{P}_{12}\exp(it\Omega_{12})]\\&+(\mu_3-\mu_4)[\mathbf{P}_{43}\exp(-it\Omega_{34})+\mathbf{P}_{34}\exp(it\Omega_{34})]\},\end{aligned} \tag{11}$$

where time is measured from the end of the computational cycle. In a state described by the density matrix (11), the quantum-mechanical averages of the transverse spin components become nonzero,

$$\begin{aligned}\langle I_+(t)\rangle\equiv\langle I_x+iI_y\rangle&=\langle\sqrt{3}(P_{43}+P_{21})+2P_{32}\rangle=\mathrm{Tr}[\rho(t)(I_x+iI_y)]\\&=\sqrt{3}(\mu_3-\mu_4)\exp(-it\Omega_{34})+\sqrt{3}(\mu_1-\mu_2)\exp(-it\Omega_{12}),\end{aligned} \tag{12}$$

and a precession of the nuclear spin, inducing in the detection coil a periodic voltage at the two resonance frequencies Ω_{12} and Ω_{34} with Fourier components $\sqrt{3}(\mu_3-\mu_4)$ and $\sqrt{3}(\mu_1-\mu_2)$, arises in a plane perpendicular to the constant magnetic field. We note that an identical pulse acting on the equilibrium density matrix (4) would have produced a similar precession but with Fourier components $\sqrt{3}Z(\lambda_3-\lambda_4)$ and $\sqrt{3}Z(\lambda_1-\lambda_2)$. A measurement of the sign of the ratios

$$b_{34}\equiv(\mu_3-\mu_4)/(\lambda_3-\lambda_4) \quad \text{and} \quad b_{12}\equiv(\mu_1-\mu_2)/(\lambda_1-\lambda_2)$$

of the corresponding Fourier components before and after the computation permits determining the final state of two fictitious spins:

if $b_{34}<0$ and $b_{12}=0$, then the result of the computation is $|00\rangle$,

if $b_{34}>0$ and $b_{12}=0$, then the result of the computation is $|01\rangle$,

if $b_{34}=0$ and $b_{12}<0$, then the result of the computation is $|10\rangle$,

if $b_{34}=0$ and $b_{12}>0$, then the result of the computation is $|11\rangle$.

Nuclear spin 3/2 is not rare. Nuclei with such spin appear in the most diverse and easily accessible materials. Writing of two qubits on discrete levels of a single quantum particle obviates the need for an exchange interaction between the carriers of the qubits, which in existing schemes for implementing quantum gates must be suppressed by special methods, complicating the implementation of algorithms. The scheme described above applies to quantum systems of arbitrary physical nature. In principle, the same purpose can be served by using nuclear spins of large magnitude (after choosing four suitable energy levels), ESR spectra with effective spin $S^*\geqslant 3/2$, and optical energy levels. Only the expressions for the resonance frequencies and the matrix elements of the operators will change. Specifically, one can use a nuclear quadrupole resonance energy spectrum, split (or not split) by the interaction with a static magnetic field is suitable. The use of effective spins $S^*\geqslant 3/2$ and therefore a large number of discrete energy levels gives, generally speaking, additional possibilities, which are not discussed in the present work.

*)e-mail: ermakov@sci.kcn.ru

[1] N. A. Gershenfeld and I. L. Chuang, Science **275**, 350 (1997).
[2] D. G. Cory, M. D. Price, and T. F. Havel, Physica D **120**, 82 (1998).
[3] E. Knill, I. L. Chuang, and R. Laflamme, Phys. Rev. A **57**, 3348 (1998).
[4] R. Laflamme, E. Knil, W. H. Zurek *et al.*, Philos. Trans. R. Soc. London, Ser. A **356**, 1941 (1998).

Translated by M. E. Alferieff